2-13-2014

DEVELOPMENT OF SYNTHETIC POLYMERS FOR BONE TISSUE ENGINEERING: ENGINEERING THE DEGRADATION RATE

Kirsten Cicotte

Kirsten N. Cicotte
Candidate

Biomedical Engineering
Department

This dissertation is approved, and it is acceptable in quality and form for publication:

Approved by the Dissertation Committee:

Elizabeth L. Hedberg-Dirk, Ph.D., Chairperson

Shawn M. Dirk, Ph.D.

David G. Whitten, Ph.D.

Mahmoud Reda Taha, Ph.D.

Thomas R. Howdieshell, M.D.

DEVELOPMENT OF SYNTHETIC POLYMERS FOR BONE TISSUE ENGINEERING: ENGINEERING THE DEGRADATION RATE

by

KIRSTEN N. CICOTTE

BS., Biomolecular Science and Chemistry,
Clarkson University, 2005

DISSERTATION

Submitted in Partial Fulfillment of the
Requirements for the Degree of

Doctor of Philosophy
Engineering

The University of New Mexico
Albuquerque, New Mexico

December 2013

DEDICATION

For my loving and supporting parents, Warren and Janet Cicotte, who encouraged me early on to strive for happiness, believed in my choices and nurtured my passion to succeed in what brings me joy. As well as my second biggest supporters, John and Gertrude Weir, although I lost you both during this journey, I know your still supporting me, Dude and Gram.

ACKNOWLEDGMENTS

I would like to thank my advisor Dr. Elizabeth Hedberg-Dirk and co-mentor Dr. Shawn M. Dirk for their unceasing support throughout my doctoral studies. I was honored to take advantage of each of your areas of expertise and further my knowledge in many research areas. I would also like to thank my committee members, Dr. David Whitten, Dr. Mahmoud Reda Taha and Dr. Thomas Howdieshell, for taking the time to have thoughtful discussions and collaborations that are directly reflected in this work.

I have also been fortunate to receive excellent training and guidance from various experts due to my employment at Sandia while obtaining my doctorate. Their feedback and actions as sounding boards helped greatly throughout the journey as well as continue to have an impact. Thank you!

I was also lucky to have a support team, those who kept me sane during the process. For this I would like to take the opportunity to thank Jamie Reed, Ross Johnson and Michele Denton. You have been much more than my co-workers, offering an ear when needed, as well as offering inspiration and direction in my research. I am grateful to be able to call each of you a friend.

Lastly, and most importantly, I cannot thank my family enough for their love, encouragement and continual support. I'd like to thank my sister and brother, Britney and Warren Cicotte, for always bragging about my accomplishments, whether big or small. I must also thank my niece, Brynn Cicotte, for the FaceTime® chats and taking my mind away from the stress of it all. And I'd like to thank my

parents, Warren and Janet Cicotte, for never doubting my decisions and being my most loyal fans.

Development of Synthetic Polymers for Bone Tissue Engineering: Engineering the Degradation Rate

By

Kirsten N Cicotte

B.S., Biomolecular Science and Chemistry, Clarkson University, 2005

Ph.D., Engineering, University of New Mexico, 2013

ABSTRACT

In this work the development, synthesis, and characterization of biodegradable synthetic polymers, poly (butylene fumarate) (PBF) and the copolymer poly (butylene fumarate)-*co*-(butylene maleate) (PBFcBM) is described. The unsaturated linear polyesters were synthesized via two synthetic routes, including an acid catalyzed transesterification reaction of (Z)-4-((4-hydroxybutan-2-yl)oxy)-4-oxobut-2-enoic acid which was formed via a ring opening reaction of maleic anhydride with 1,3-butylene glycol (BG) and reacting the acid chlorides, maleoyl chloride (MCl) and fumaryl chloride (FCl) with BG. Both methods introduce the *cis* (maleate) functionality into the polymer backbone, however a controlled fumarate to maleate ratio was only obtained via the acid chloride starting monomers.

The PBF polymer differs from the previously examined PPF polymer through an additional methylene (CH_2) unit in the polymer backbone. This methylene unit increases the chain length between the crosslinkable fumarate (C=C) double bond. Because of this, It was hypothesized that PBF allow for a greater water ingress and

therefore an increased rate of degradation relative to PPF. Results from *In vitro* accelerated degradation studies confirmed our hypothesis.

An *in vitro* cytocompatibility study with the murine cell line MC3T3-E1 demonstrated that there were no cytotoxic components that leached from crosslinked PBF networks. In addition, the PBF crosslinked networks were assessed for the ability to support mesenchymal stem cell (MSC) differentiation down the osteogenic lineage. Cellular adhesion and proliferation as well as the presence of alkaline phosphatase and extracellular calcium of MSCs cultured under osteogenic medium conditions on crosslinked PBF networks were evaluated.

Methodology to fabricate highly interconnected porous mats comprised of nano to micro sized fibers was developed using the photo initiator bis(2,4,6-trimethybenzoyl) phenoylphosphine oxide (BAPO) to crosslink the fumarate-based fibers *in situ* while electrospinning. Characterization showed that the alterations to the general electrospinning technique could be used to spin polymers with glass transition (T_g) temperatures below room temperature without the use of a sacrificial polymer.

Table of Contents

Approval Page		i
Title Page		ii
Dedication		iii
Acknowledgements		iv-v
Abstract		vi-vii
Chapter I:	Introduction	1
Chapter 2:	Specific Aims	12
Chapter 3:	Synthesis and Characterization of Novel Fumarate-based Polymeric System	
	Introduction	14
	Materials and Methods	16
	Results and Discussion	28
	Conclusions	33
	Schemes, Tables and Figures	35
Chapter 4:	Crosslinked Network Characterization and *In Vitro* Degradation of Photo Crosslinked Poly(Propylene Fumarate) and Poly(Butylene Fumarate)	
	Introduction	40
	Materials and Methods	42
	Results and Discussion	51
	Conclusions	57
	Schemes, Tables and Figures	58
Chapter 5:	Cytotoxicity Evaluation of Crosslinked Poly(Butylene Fumarate) Networks and their Osteoconductive Potential	
	Introduction	64
	Materials and Methods	66
	Results and Discussion	74
	Conclusions	79
	Schemes, Tables and Figures	81

Chapter 6: Method Development for Fabricating 3D Crosslinked Polymer Networks via Electrospining and Projection MicroStereolithography

Introduction	87
Materials and Methods	90
Results and Discussion	93
Conclusions	97
Schemes, Tables and Figures	98

Chapter 7: Part I: Potential Neural Interface Material Printed via Projection Micro-StereoLithography

Introduction	105
Materials and Methods	107
Results and Discussion	113
Conclusions	116
Schemes, Tables and Figures	118

Chapter 7: Part II: Printed Poly(Dimethyl Siloxane) Substrates with Controlled Pore Size: Studying Flap Revascularization in and Ischemic Mouse Model

Introduction	124
Materials and Methods	126
Results and Discussion	129
Conclusions	133
Schemes, Tables and Figures	134

Chapter 8: Summary and Future Directions 138

Chapter 9: References 143

Chapter 1. Introduction

Bone undergoes maintenance, resorption and rearrangement through the interaction of osteoblasts (bone forming), osteocytes (bone maintaining) and osteoclasts (bone resorbing) cells. This remodeling cycle allows for repair and regeneration following most injuries, such as small-scale fractures.[1-3] However, each year up to 15 million people receive traumatic bone injuries and 1.5 million bone fractures occur which cannot be remedied by the intrinsic capacity for bone to self-repair, leaving a non-union which requires surgical intervention.[4, 5]

Non-union defects in bone arise from diseases, traumatic injuries as well as tumor resection.[6-8] In order to heal this non-union defect a material must be used to fill the defect. The current standard followed to do this is through bone grafting. Bone grafting inserts harvested bone in a defect area; sources include: 1) autografts, or donor bone removed from the patient 2) allografts, or bone from another human, typically a cadaver and 3) xenografts, or bone from a different species.[4, 9]

Of these sources, autografting is the gold standard and preferred over the other options due to the inherent structural stability and osteogenic (bone producing) ability.[10] Regardless, both allograft and autograft options are accompanied by severe limitations due to limited supply of donor bone,as well as the significant risks associated with the surgery itself.[11] These risks include infection at the grafting site, formation of a seroma, and development of a hematoma or disease transmission.[12, 13] Due to the risks associated with grafting, alternative approaches are gaining much attention, as there is an obvious clinical need. One such approach is tissue engineering (TE), involving biology, engineering, materials and medicine to

accommodate the shift in healthcare from replacement to towards repair/regeneration.

Tissue Engineering

Tissue engineering (TE) uses engineered materials with complex architectures to mimic the 3D cellular microenvironment, thereby providing suitable mechanical properties for the tissue environment that is being mimicked (NIH).[14] This interdisciplinary approach combines: 1) cells isolated from a patient source, allowing seeding of specific cell populations, 2) a matrix (scaffold) capable of providing appropriate mechanical and structural support, and finally 3) biomolecular cues, such as growth factors to promote tissue formation with the appropriate function.[15] The TE paradigm is depicted in Figure 1.1.

Scaffold Material Selection

There is a need to identify, develop and broaden materials for use in TE scaffolds beyond the options currently under development or commercially available options. At a minimum, scaffold materials must be biocompatible, biodegradable and be capable of having sufficient mechanical properties for use in orthopedic (bone) applications. Many materials, including ceramics, metals and polymers have been evaluated as a scaffolding material. Drawbacks associated with ceramics and metals include being non degradable (both), brittle (ceramics) and mismatched in mechanical properties compared to bone (metals).[16, 17] Polymeric biomaterials, either natural or synthetic in origin, have shown initial success in orthopedic tissue

engineering. Natural polymers offer inherent biocompatibility, but lack suitable mechanical properties, while synthetic polymeric materials can be more easily tailored to fit the specific needs required by the tissue environment.[18, 19] Synthetic polymers for bone tissue engineering (BTE) which are subject to hydrolytic degradation due to the functionality in the polymer backbone include poly α-hydroxyesters[20-27], poly(orthoesters)[28-30], polyanhydrides[31-34], polyhydroxyalkanoates[35-41](Figure 1.2). These synthetic polymers have not been limited to use for BTE applications, poly α-hydroxyesters including poly(glycolic acid) (PGA), poly(lactic acid) (PLA) and the copolymer poly(lactic)-*co*-(glycolic acid) (PLGA) are approved for use by the Federal Drug Administration (FDA). These esters have a tunable degradation rate, dependent on the ratio of lactic acid:glycolic acid, and are seen in clinical application as dissolvable sutures.

Although many polymers offer biodegradability, several of the aforementioned polyester classes lack the appropriate mechanical properties to match native bone (Table 1.1). Mechanical properties of bone span a large range, this is due to the location, age and overall health of the bone. The tensile strength and modulus range from 3.1 - 180 GPa and 3.9 – 71 GPa, for dense bones (cortical), respectively.[3, 9] Where compressive strength and modulus for less dense bone (trabecular/cancellous) can be seen in the range from 0.2 – 300 MPa and 1.5 – 9500 MPa (with midrange of 5-10 MPa and 50-100 MPa), respectively.[9] Therefore, these are the ranges in mechanical properties, which need to be achieved for optimal repair and use in BTE applications. The polymer poly(propylene fumarate) (PPF) is being extensively researched due to the ability to achieve high compressive

strengths which are inline with native bone, and are still able to undergo biodegradation.

Poly(Propylene Fumarate) (PPF)

The unsaturated linear polyester, PPF has been synthesized via poly condensation reactions from the monomers of propylene glycol (PG) and a variety of fumarate derivatives, including diethyl fumarate (DEF)[42-45], fumaryl chloride[44, 46, 47], fumarate dicarbodiimide[44], fumaric acid[44, 48, 49](Figure 1.3). The PPF polymeric backbone contains both ester linkages, which are susceptible to hydrolysis as well as a carbon-carbon double bond. After synthesis, PPF can be covalently crosslinked either thermally[50] or photochemically[51] through the carbon- carbon double bond of the fumarate functional group.

The choice of synthetic route as well as the choice of initiator system leads to crosslinked networks that display varying mechanical properties. Fisher *et al* [52] synthesized PPF (high and low molecular weight, MW) from monomers DEF and propylene glycol (PG), followed by crosslinking with the photoinitiator . Measured compressive moduli were in the range of bone with a modulus of 195.3 ± 17.5 MPa and fracture strength of 68.8 ± 9.4 MPa. To increase mechanical properties, composite of PPF crosslinked networks with the inclusion of beta tricalcium phosphate (β-TCP) were prepared. Inclusion of β-TCP yielded a crosslinked polymer network whose modulus and yield strength were increased to ~1200 MPa and ~300 MPa.[3] These experimental values demonstrate that PPF crosslinked networks have sufficient mechanical properties and display similar properties to

bone (trabecular/cancellous). As PPF has been synthesized and researched to display high mechanical properties over the other materials used in BTE applications, a consideration also has to be the effect of increased mechanical properties and how that modulates ester hydrolysis.

High modulus PPF materials such as those fabricated by Fisher et al have been evaluated both *in vitro* and *in vivo*. Although the polymer displayed mechanical properties similar to that of bone, the rate of bone growth was greater than that of scaffold degradation. The material displayed little to no degradation after 50 weeks *in vitro*[53] and 18 weeks *in vivo*.[54] To try and address this, PPF copolymers have been synthesized, including poly(ε-caprolactone) (PPF-PCL),[55, 56] poly(ethylene glycol) (PPF-PEG) and oligo(polyethylene glycol) fumarate (OPF).[57, 58] These crosslinked polymeric networks display mechanical properties in the range of 1.8-145 MPa

Scaffold Requirements

Material selection is not the only factor that has to be considered when designing a synthetic replacement to autologous bone grafting. Besides the scaffold needing to be mechanically suitable, the key factors to an ideal scaffold for bone tissue engineering applications are: 1) it is comprised of macro (pore size > 100 μm) and micro (pore size < 20 μm) architecture, 2) highly interconnected pores with a large surface area to volume ratio, allowing for cellular infiltration, integration and vascularization, 3) favorable chemical environment to promote cellular attachment,

growth and differentiation, 4) controlled degradation kinetics, with out compromising the mechanical suitability and 5) a sterile environment for cells.[4, 59]

Again, PPF has been shown in many publications to be biocompatible and biodegradable. The degradation products that result from ester hydrolysis of PPF are PG and fumaric acid, a commonly used diluent in drug formulations and a naturally occurring substance found in the Krebs cycle.[60] In addition, it has also been shown both *in vitro*[61, 62] and *in vivo*[63, 64] to be osteoconductive (ability to provide the appropriate scaffold or template for bone formation), by providing a scaffold for osteoblasts to infiltrate, lay down extracellular matrix (ECM) and generate new bone.

Scaffold Fabrication

As synthesized, PPF has a glass transition temperature (T_g) below room temperature (RT), making it a liquid at room temperature (RT). This characteristic allows for either pre-fabrication of scaffolds for implant and well as an injectable system which can be crosslinked *in-situ*.[65-68] Porous PPF and PPF composite scaffolds have been fabricated using solvent casting/leaching[69-71], stereolitography[72-75] and high internal phase emulsions (polyHIPEs).[76] All of these techniques are capable of making highly porous structures, yet each has some potential drawbacks and limitations. Solvent casting involves incorporation of particles (ie. sodium chloride, NaCl) prior to crosslinking followed by leaching using solvent, creating a network with controlled porosity and pore size, but random spatial organization.[77] Stereolithography, a term that broadly describes rapid prototyping (RP) or solid free form (SFF), allows computer aided generation of more complex architecture

scaffolds, but fabrication is both costly and time consuming.[77] Although overcoming some of the limitations seen in other processing techniques, the technique has many advantages and disadvantages including fine structure control and cost. More recently gaining attention is polyHIPEs, or high internal phase emulsions, due to the ability to create highly porous interconnected scaffold. However, these scaffolds do not include the complex micro and macro structure that is needed to mimic the native ECM.

Conclusions

There is an apparent clinical need for an alternative to current bone grafting with over 500,000 grafting procedures being performed yearly in the United States alone.[78] The interdisciplinary field of tissue engineering (TE) can provide a possible solution through the use of a patient's own cells, a synthetic scaffolding material and various signaling molecules (ie. growth factors).

Focus on polymeric materials that undergo degradation, provide biocompatibility, serve as an osteoconductive matrix and are mechanically suitable are being widely explored. Extensive research is being carried out on the fumarate-based unsaturated polyester poly(propylene fumarate) (PPF) due to the initial *in vitro* and *in vivo* success. This polymer system also is attractive due to the ability to form crosslinked polymeric networks either pre-implantation or as an injectable. Although PPF has moved the field of bone tissue engineering (BTE) forward in the last 20 years, there are still properties that are non-ideal. Primarily, the mismatch of

scaffold degradation and bone formation being at the forefront of properties that needs to be addressed.

Further bridging the scientific, engineering and clinical disciplines will allow for movement towards an ideal scaffold with mechanical suitability, biocompatibility with the desired degradation profile. This task is non-trival, there are many factors such as robustness, reproducibility and standardization that must be addressed before a product is approved by the Federal Drug Adminstration (FDA) for clinical use.

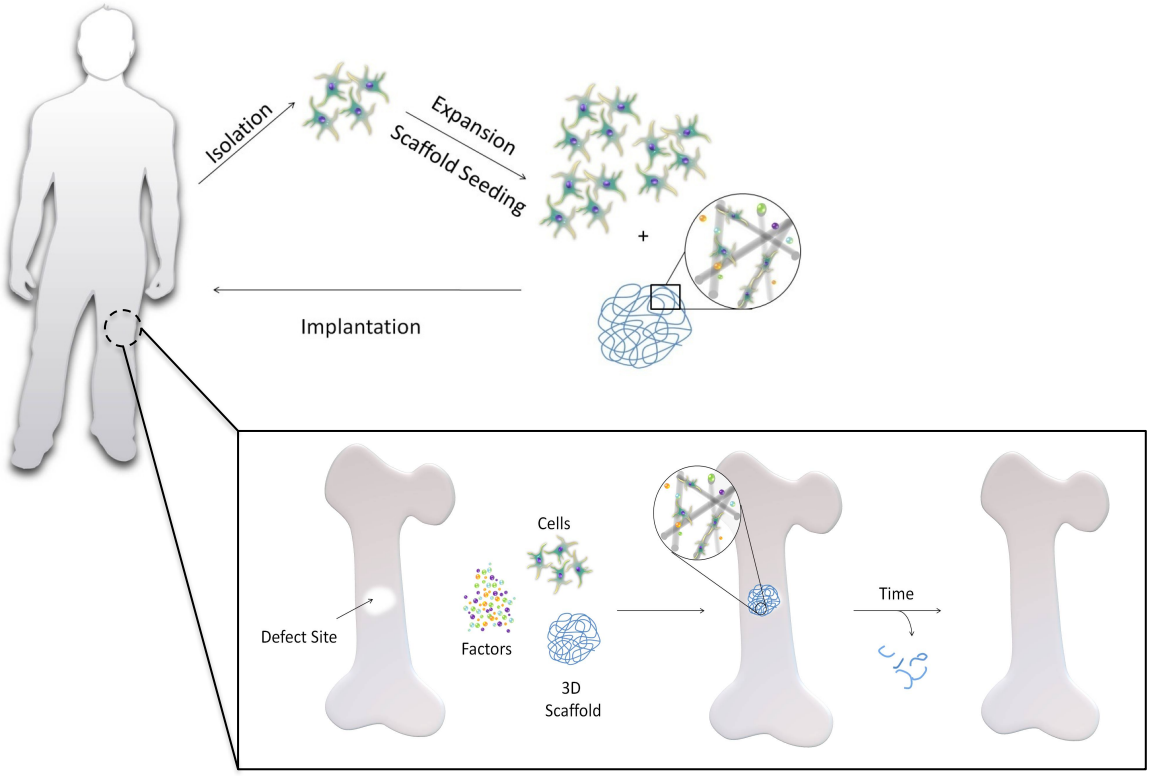

Figure 1.1. Schematic representation of the tissue engineering (TE) paradigm, involving isolation of cells from the patient, followed by expansion *ex vivo* , scaffold seeding where cells and growth factors are loaded on a three dimensional porous scaffold and implanted. In the case of bone, the 3D scaffold is placed in the non-union. Over time, bone formation occurs within the defect area and the temporary scaffold degrades, resulting in complete repair/regeneration of functional bone.

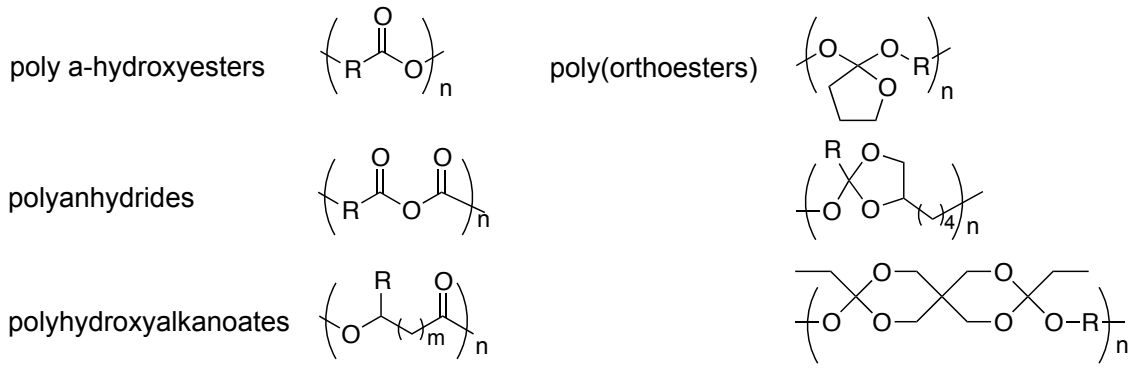

Figure 1.2. Representative classes of hydrolytically degradable synthetic polymers currently being explored for use as biodegradable scaffolding materials in orthopedic tissue engineering.

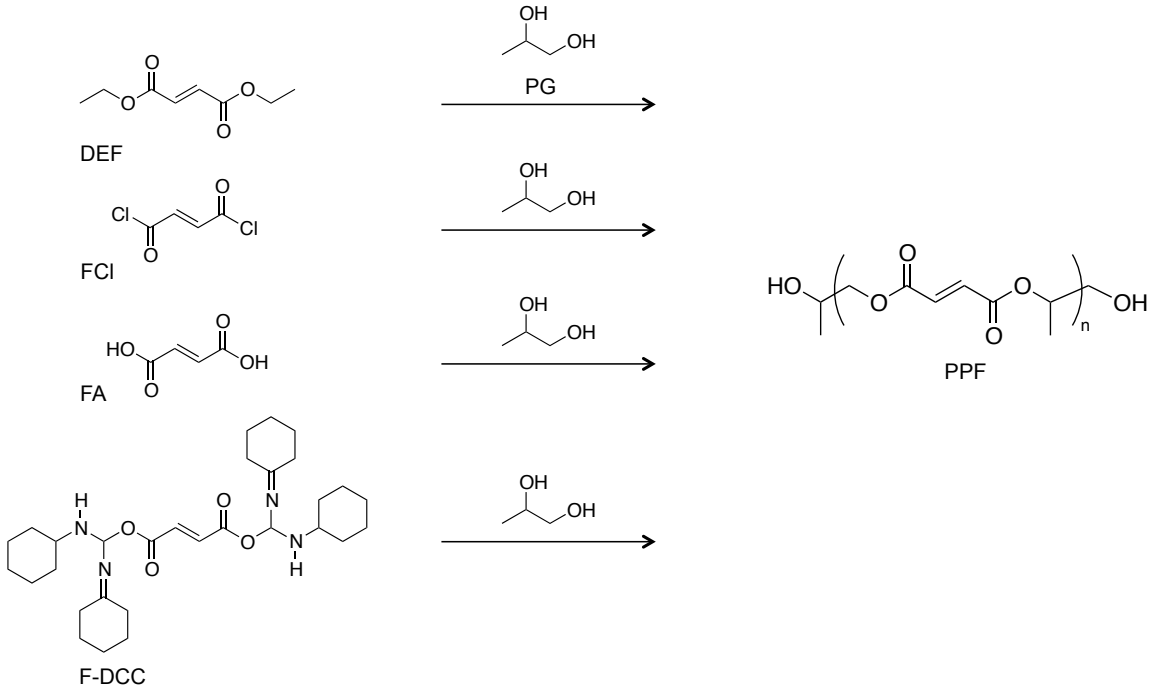

Figure 1.3. Fumarate derivative monomers diethyl fumarate (DEF), fumaryl chloride (FCl), fumaric acid (FA) and fumarate dicarbodiimide (F-DCC) used as starting monomers with propylene glycol (PG) to form poly(propylene fumarate) (PPF). (Adapted from Ibay, 1987, # 43)

Table 1.1. Summary of bones (cortical and cancellous) mechanical properties. (Adapted from Porter, 2009, #9)

Property	Cortical bone	Cancellous bone
Compressibe strength (MPa)	100-230	2-12
Tensile strength (Mpa)	50-150	10-20
Strain to toughness (%)	1-3	5-7
Fracture toughness (Mpa $m^{1/2}$)	2-12	--
Young's modulus (Mpa)	7-30	0.5-0.05

Chapter 2. Specific Aims

The overall objectives of this research are to development and characterize a crosslinkable, biocompatible polymeric system with tunable degradation for use in the fabrication of scaffolds to be used in bone tissue engineering (BTE). The worked described herein leverages the extensive prior research on the fumarate-based poly(propylene fumarate) (PPF) to develop a biocompatible and biodegradable polyester through modifications in the polymer backbone. Engineering of the backbone will alter the degradation kinetics of the crosslinked networks without compromising the polymers workability (ease of processing), crosslinkability or the crosslinked networks mechanical suitability.

In the course of this work, the following specific aims were identified and investigated:

1. Synthesize and characterize a novel fumarate-based polymer system (Chapter 3).
2. Characterize network structures of the crosslinked polymer network, both initially and during degradation. (Chapter 4)
3. Validate cytocompatibility and the ability to support bone formation (osteoconductivity)(Chapter 5).
4. Develop inexpensive techniques for the fabrication of 3D polymeric scaffolds (Chapter 6).

The results obtained through the proposed specific aims will contribute to the current class of synthetic biocompatible polymers being used in orthopedic or, more

generally, tissue engineering applications and drug delivery. The synthesis of new fumarate-based synthetic polyesters with “tunable” degradation rates will lead to a better understanding of how polymer composition can be tailored to achieve a better match of bone formation and scaffold degradation.

Initial broader impacts can be seen in the form of established collaborations. These collaborations look at using our inexpensive polymer processing techniques in a pre-clinical setting (*in vivo* animal models).

1. Development and evaluation of polydimethylsiloxane (PDMS) and PBF as potential peripheral nerve interface (PNI) materials (Chapter 7 Part I).

2. Development and evaluation of PDMS scaffolds with controlled pore size for implantation in an ischemic mouse model to evaluate neovascularization (Chapter 7 Part II).

Chapter 3. Synthesis and Characterization of Novel Fumarate-based Polymeric System

1. *Introduction*

Poly(propylene fumarate) (PPF) is an unsaturated linear polyester, which has been extensively studied for use as a degradable biomaterial for orthopedic tissue engineering applications. PPF degrades through hydrolysis of the ester linkages yielding biocompatible degradation products.[1] Since the introduction of PPF in 1987[2, 3], it has been synthesized from various fumarate derivatives including diethyl fumarate (DEF)[4-7], fumaryl chloride (FCl)[5, 8], fumarate dicarbodiimide[5], and fumaric acid.[5, 9, 10] The resulting polymers have been shown to form crosslinked networks which are both biocompatible and promote bone formation *in vitro* and *in vivo* regardless of the synthetic methodology used to create the unsaturated polyester.[2, 11-13] Crosslinked PPF has been shown to be a suitable biomaterial as it is easy to process and it degrades into non-cytotoxic products. However, a drawback is that the degradation rate is slow relative to the rate of bone formation. *In vitro* studies show little or no degradation of PPF up to 50 weeks,[14-16] while *in vivo* studies have shown little or no degradation up to 18 weeks. The *in vivo* degradation studies used porous PPF scaffolds placed in a critical sized defect rabbit radii model, where initial bone growth into the scaffold was observed at the scaffold/defect edges however scaffold infiltration was not observed. This observation suggests that the degradation rate of the scaffold was sufficiently slow to impede bone formation.[13]

Attempts to increase the rate of ester hydrolysis of PPF by chemical alterations to the fumarate-based polymer have included altering the molecular

weight[14, 17], introducing more hydrolytic groups[18, 19], modifying the crosslinked polymer network via surface modification after the crosslinking event[20-22] and introducing porosity.[23] Our interest and the current work has focused on increasing the degradation rate of crosslinked unsaturated fumarate-based polyesters via modification of the polymer backbone. To introduce these modifications we have substituted the biocompatible butylene glycol (BD) has been substituted in place of propylene glycol (PD) as a starting material, providing an extra methylene group in the resulting polymer.[24, 25] In addition to a diol substitution, two synthetic routes have been identified to incorporate *cis* (maleate) along with the *trans* (fumarate) functionality. *We hypothesize that these modifications will increase ester hydrolysis by either 1) increasing the distance between hydrolysable esters and reduce steric hindrance, or 2) introduce chain "kinks" resulting in void spaces that will increase the ability of water infiltration into crosslinked networks.*

Herein we have identified synthetic routes to yield the homopolymers of poly(propylene fumarate) (PPF) and poly(butylene fumarate) (PBF) as well as the copolymers of poly(propylene fumarate)-*co*-(propylene maleate) (PPFcPM) and poly(butylene fumarate)-*co*-(butylene maleate) (PBFcBM). PPF and PBF were made from maleic anhydride (MA) over the more expensive DEF and FCl starting monomers which are currently used.[26, 27] Selection of MA allows for ring opening polymerization (ROP) to yield the copolymer or homopolymer by controlling the *cis* to *trans* isomerization of the more energetically favorable fumarate functionality.[28, 29] However, this route can produce polymers with various material properties based on the catalyst selected and the feed ratio of MA and either PD or BD.[30] The

copolymers of PPFcPM and PBFcBM as well can vary greatly due to reaction conditions, resulting in various maleate:fumarate (M:F) ratios in the resulting polymer. Leading to the identification and development of a novel controlled synthetic route where the F:M ratio in the resulting copolymer will be dictated by the starting ratio of monomers used. To do this the acid chlorides of FCl and maleyol chloride (MCl) are used with the diol (BD) and the reaction kept at low temperatures in order to limit the *cis* to *trans* isomerization, offering control over F:M based on MCl:FCl starting ratios.

2. Materials and Methods

2.1. Chemicals and Reagents

p-Toluensulfonic acid (TsOH), monohydrate 99%, extra pure was purchased from Acros. Anhydrous magnesium sulfate ($MgSO_4$), certified ACS plus sulfuric acid (H_2SO_4), silica gel sorbent (200-425 mesh), HPLC grade ethyl acetate (EtOAc), reagent grade triethylamine (TEA), and potassium hydroxide (KOH) were purchased from Fisher. Maleic anhydride (briquettes 99%, MA), 1,2-propanediol (99%, PD), 1,3-butanediol (Reagent Plus®, 99%, BD), Zinc chloride (anhydrous powder 99.995% trace metals, $ZnCl_2$), Iron (III)Chloride (reagent grade 97%), potassium bromide (KBr) and anhydrous dichloromethane (DCM) were purchased from Aldrich. Chlorofom, (for HPLC, $CHCl_3$) and fumaryl chloride (95%, FCl) were purchased from Acros Organics. Thionyl chloride ($SOCl_2$) was purchased from Alfa Aesar. All chemicals were used as received from suppliers.

2.2. Equipment

Nuclear magnetic resonance (NMR) was carried out on a 400 MHz Bruker DRX-AVANCE. Proton chemical shifts (δ) are reported as shifts from the internal standard tetramethylsilane (TMS). Infrared Spectroscopy (IR) was carried out on a Nicolet 6700 FTIR equipped with a continuum microscope. Gel Permeation Chromatography (GPC) molecular weight determinations were performed by GPC using a Polymer Labs 220 PL-GPC equipped with a UV-Vis detector. Two columns (PLgel 5 µm MiniMIX-C, 250 × 4.6 mm) and a guard column (PLgel 5 µm MiniMIX-C, 50 × 4.6 mm) were used in series with a flow rate of 0.4 mL/min and a run pressure of 6.0 MPa. Relative molecular weights were determined using polystyrene standards with a narrow molecular weight distribution (Fluka ReadyCal 400-2,000,000). Chloroform was used as the eluent (0.4 mL/min), and measurements were performed at 35°C. Differential Scanning Calorimetry (DSC) was carried out on TA Instruments DSC Q100.

2.3. Polymer Synthesis: Ring Opening Polymerization (ROP) from MA

2.3.1. Homopolymer Synthesis

2.3.1.1. Poly(1,2-Propylene fumarate) (PPF) Synthesis from MA

To a 100 ml round bottom flask equipped with a stir bar and distillation head, MA (10.0 g, 102 mmol), PD (7.8 g, 102 mmol), and TSOH (0.02 g, 0.1 1 mmol) were added. The reaction mixture was heated to 250°C with stirring. After 3 hr, the reaction was allowed to cool to RT. The resulting viscous crude polymer was

dissolved in ethyl acetate (50 mL) and washed with distilled water (50 ml, 3×). The organic layer was dried over anhydrous $MgSO_4$, filtered and solvent removed *in vacuo* to yield a slightly yellow viscous polymer.

IR (neat) 2984.1, 1714.7, 1645.4, 1454.7, 1379.0, 1290.2, 1255.5, 1153.4, 1116.2, 1075.9, 1022.5, 979.1, 837.3, 753.5, 666.4cm^{-1}. ^{1}H-NMR (400MHz, CDCl3) δ 6.88–6.78 (m, -CH=CH-), 5.25–5.2 (m, -CH(CH_3)), 4.68–2.8 (m,-OCO-CH_2-), 1.43–1.15 (m, (CH_3)CH_2). GPC (1 mg/ml,$CHCl_3$) Mw 949 Mn 473.

Tg (°C) -15.24.

2.3.1.2. Poly(1,3-Butylene Fumarate) (PBF) Synthesis from MA

To a 100 ml round bottom flask equipped with a stir bar and distillation head, MA (10.0 g, 102 mmol), BD (9.2 g, 102 mmol), and TSOH (0.02 g, 0.1 1 mmol) were added. The reaction mixture was heated to 250°C with stirring. After 3 hr, the reaction was allowed to cool to RT. The resulting viscous crude polymer was dissolved in ethyl acetate (50 mL) and washed with distilled water (50 mL, 3×). The organic layer was dried over anhydrous $MgSO_4$, filtered and solvent removed *in vacuo* to yield a slightly yellow viscous polymer. IR (neat) 3430.5, 3231.7, 3081.2, 3027.5, 2979.1, 2937.7, 2684.8, 1743.8, 1696.8, 1646.1, 1456.4, 1382.9, 1356.2, 1317.9, 1277.1, 1189.5, 1107.7, 1046.1, 989.1, 877.4, 850.8, 756.6 and 665.7 cm^{-1}. ^{1}H NMR (400 MHz, $CDCl_3$) δ 6.91-6.73 (m, 2H), 5.13-5.07 (m, 1H), 4.32-4.15 (m, 2H), 2.05-1.77 (m, 2H), 1.32-1.10 (m, 3H). Mw 1777, PDI 1.78. T_g (°C) -21.64.

2.3.2. Copolymer Synthesis

2.3.2.1. General One-Step Aziotropic Distillation: Method A

Monomers, toluene, and catalyst were added to a round bottom flask equipped with stir bar and Dean-Stark (DS) trap for azeotropic distillation. The reaction was allowed to proceed at a maximum temperature 110°C, until no more distillate (water) was collected. The reaction mixture was cooled to RT and the toluene was removed *in vacuo*. The crude polymer was then dissolved in EtOAc and washed with distilled water (dH_2O) (3×). The organic layer was then dried over anhydrous MgSO4 and solvent again removed *in vacuo*.

2.3.2.1.1. Poly(1,2-Propylene Fumerate)-co-(1,2-Propylene Maleate) (PPFcPM)

MA (10.0 g, 102 mmol), PD (7.8 g, 102 mmol), toluene(30–50 mL), and the appropriate catalyst, TsOH (0.2g, 1.0 mmol), H2SO4 (1 drop, 18N), ZnCl2 (0.14 g, 1.0mmol) or FeCl3 (0.17 g, 1 mmol), were added to a 100mL round bottom flask equipped with stir bar along with DS trap and condenser. The reaction mixture was allowed to progress overnight. The reaction was ended and brought to RT, upon cooling toluene was removed *in vacuo*. The crude polymer was then dissolved in ethyl acetate (50 mL) and washed with water (50 ml, 3x). The organic layer was dried over MgSO4 with filtration and the solvent was removed *in vacuo* to yield a clear viscous polymer.

PPFcPM synthesized with TsOH:

IR (neat) 3490.0, 3058.6, 2983.4, 1711.9, 1643.6, 1455.3, 1384.2, 1252.6, 1077.7,

983.6, 828.7, 777.3 cm^{-1}. ^{1}H-NMR (400 MHz,CDCl3) δ 7.17–7.14 (m, Ar), 7.09–7.03 (m, Ar), 6.83–6.76 (m, trans -CH1=CH), 6.27–6.13 (m, cis –CH=CH-),5.19–5.17 (bs, -CH(CH_3)), 4.34–3.61 (m, -OCO-CH_2-), 2.26 (s, CH_3-Ar), 1.25–1.03 (m, (CH_3)CH_2-). GPC (1 mg/ml, $CHCl_3$) Mw 995 Mn728. Tg (°C) -40.38.

PPFcPM synthesized with $ZnCl_2$:

IR (neat) 3516.3,3079.6, 2984.3, 2943.7, 2883.4, 1711.1, 1644.0, 1452.5,1381.1, 1356.2, 1289.2, 1251.9, 1224.0, 1149.6, 1116.0,1075.9, 1019.6, 978.3, 835.7, 773.5, 668.1 cm^{-1}.^{1}HNMR(400 MHz, CDCl3) δ 7.22–7.20 (m, Ar), 7.14–7.10 (m, Ar), 6.90–6.76 (m, trans –CH=CH-), 6.23–6.20 (m, cis –CH=CH-), 5.27–5.07 (m, -CH(CH_3)), 4.40–4.02 (m, -OCO-CH_2-), 2.32 (s, CH_3-Ar), 1.51–1.23 (m, (CH_3)CH_2=). GPC (1 mg/ml, $CHCl_3$) Mw 1297 Mn 824. Tg (°C) -18.66.

PPFcPM synthesized with $FeCl_3$:

IR (neat) 3445.0,3235.5, 3081.1, 2985.9, 2661.0, 2362.5, 1716.2, 1751.0,1700.4, 1646.7, 1455.9, 1386.3, 1355.4, 1324.4, 1279.4,1190.8, 1121.8, 1080.2, 990.2, 838.6, 775.3 cm^{-1}. ^{1}HNMR (400 MHz, $CDCl_3$) δ 6.93–6.83 (m, trans –CH=CH), 6.33–6.23 (m, cis –CH=CH-), 5.27–5.10 (m, -CH(CH_3)), 4.40–4.10 (m, -OCO-CH_2-), 1.44–1.23 (m, (CH_3)CH_2-). GPC (1 mg/ml, $CHCl_3$) Mw1871 Mn 1043. Tg (°C) -37.58.

PPFcPM synthesized with H_2SO_4:

IR (neat) 3526.2, 3079.3, 2984.1, 1716.1, 1645.5, 1558.5, 1541.9, 1508.1,1456.2, 1379.8, 1253.1, 1217.4, 1150.1, 1113.8, 1074.7,977.1, 833.2, 773.2 cm^{-1}. ^{1}H-NMR

(400 MHz, $CDCl_3$) δ 7.23–7.20 (m, Ar), 7.15–7.10 (m, Ar), 6.88–6.82 (m, trans –CH=CH), 6.34–6.24 (m, cis –CH=CH-), 5.24 (bs, -CH(CH_3)), 4.77–4.00 (m, -OCO-CH_2-), 2.32 (s, CH_3-Ar), 1.44–1.21 (m, (CH_3)CH_2-). GPC (1 mg/ml, $CHCl_3$) Mw 672 Mn 330. Tg (°C) -12.86.

2.3.2.1.2. Poly(1,3-Butylene Fumerate)-co-(1,3-Butylene Maleate) (PBFcBM)

MA (10.0 g, 102 mmol), BD (9.2 g, 102 mmol) toluene (30-50 ml) TsOH (0.2 g, 1.0 mmol), were added to a 100 ml round bottom flask equipped with stir bar along with Dean Stark trap and condenser. The reaction mixture was allowed to progress overnight. The reaction was ended and brought to RT. Upon cooling toluene was removed *in vacuo*. The crude polymer was then dissolved in ethyl acetate and washed with water (3×). The organic layer was dried over $MgSO_4$ and solvent removed *in vacuo,* resulting in a clear viscous polymer.

2.3.2.2. General Two-Step Aziotropic Distillation: Method B

Monomers and toluene were added to a round bottom flask. The reaction mixture was heated to 50°C and stirred overnight. The reaction mixture was allowed to cool to RT and the toluene was removed *in vacuo*. The reaction flask was then equipped with a DS trap and condenser to collect water through azeotropic distillation during the second reaction. Next, a protic acid catalyst was added to the product of the first reaction, and the mixture heated to a maximum temperature of 110°C, until the appropriate volume of water was collected. The reaction mixture was allowed to cool to RT, the solvent was removed *in vacuo*, and the crude

polymer was dissolved in EtOAc and washed with distilled water (3×). Finally, the organic layer was dried over anhydrous $MgSO_4$ and solvent removed *in vacuo*.

2.3.2.2.1. Poly(1,2-Propylene Fumerate)-co-(1,2-Propylene Maleate) (PPFcPM)

MA (10.0 g, 102 mmol), PD (7.8 g, 102 mmol) and toluene (15 mL) were added to a 100mL round bottom flask equipped with a stir bar. Under a nitrogen (N_2) blanket, the reaction heated to 50°C with stirring was allowed to run overnight. The next day, the reaction mixture was cooled to RT and the solvent removed *in vacuo*. The reaction flask was then equipped with a DS trap and condenser. Toluene and either tosic acid (0.2 g, 1 mmol) or sulfuric acid (1 drop, 18 N) was added to the product of the first reaction. The reaction was allowed to run until the expected amount of distillate (water) was collected via the DS trap. The reaction was allowed to come to RT and the solvent was removed *in vacuo*. The crude polymer was then dissolved in EtOAc (50 mL) and washed with water (50 mL, 3×). The organic layer was dried over MgSO4 with filtration and the solvent was removed *in vacuo* to yield a slightly yellow viscous polymer.

PPFcPM synthesized with TsOH:

IR (neat) 2985.9,1721.6,1691.3,1644.4,1454.6,1381.1, 1289.9, 1252.0, 1215.8, 1152.4, 1116.1, 1075.4, 979.0, 838.2, 774.3,736.5, 669.0 cm^{-1}. ^{1}H-NMR (400 MHz, $CDCl_3$) δ 6.86–6.83 (m, trans –CH=CH-), 6.29–6.23 (m, cis –CH=CH-), 5.24 (bs, -CH(CH_3)), 4.78–3.44 (m, -OCO-CH_2), 1.32–1.17 (m, (CH_3)CH_2-). GPC (1 mg/ml, $CHCl_3$) Mw 11,388 Mn 2347. Tg (_C) -13.78.

PPFcPM synthesized with H2SO4:

IR (neat) 2985.7, 1717.7, 1643.6, 1454.7, 1382.5, 1253.8, 1151.8, 1116.5,1075.3, 978.7, 889.8, 838.1, 7775.0, 734.6, 694.8 cm^{-1}. ^{1}H-NMR (400 MHz, CDCl3) δ 7.24–7.21 (m, Ar), 7.16–7.11 (m, Ar), 6.83 (s, trans –CH=CH-), 6.25 (s, cis –CH=CH-) , 5.26 (bs, -CH(CH_3)), 4.78–2.75 (m, -OCO-CH_2-), 2.33 (s, CH_3-Ar), 1.33–1.17 (m, (CH_3)CH_2-). GPC (1 mg/ml, $CHCl_3$) Mw 5520 Mn 739. Tg (°C) -13.78

2.3.2.2.2. Poly(1,3-Butylene Fumerate)-co-(1,3-Butylene Maleate) (PBFcBM)

MA (10.0 g, 102 mmol), BD (9.2 g, 102 mmol) and toluene (15 ml) were added to a 100 ml round bottom flask equipped with a stir bar. Under a nitrogen blanket, the reaction heated to 50°C with stirring was allowed to run overnight. The next day, the reaction mixture was allowed to cool to RT and the solvent was removed *in vacuo*. The reaction flask was then equipped with a Dean Stark trap and condenser. TsOH (0.2g, 1mmol) was added to the product of the first reaction and the reaction was allowed to run until appropriate amount of distillate was collected via the Dean Stark trap. The reaction was allowed to come to RT and the solvent was removed *in vacuo*. The crude polymer was dissolved in ethyl acetate (50 mL) and washed with water (50 mL, 3×). The organic layer was dried over $MgSO_4$ with filtration and the solvent was removed *in vacuo* to yield a slightly yellow viscous polymer.

2.4. Polymer Synthesis: Controlled Synthesis from Acid Chlorides

2.4.1. Monomer Synthesis

2.4.1.1. Synthesis of Maleic Acid (MAc)

MA (0.25 mol, 25 g) and H_2O (0.25 mol, 4.6 g) were added to 100 ml round bottom flask equipped with a stir bar and allowed to react overnight under N_2. Upon completion, the product was filtered and washed with $CHCl_3$ and dried yielding 25 g (87% yield). ^{1}H NMR (400 MHz, $CDCl_3$) δ 6.08 (2H, s), 4.80 (2H, s).

2.4.1.2. Synthesis of Maleoyl Chloride (MCl) (3)

MAc (69 mmol, 8.0 g) was added to a round bottom flask equipped with stir bar. The atmosphere was removed and replaced with N_2 (3×) and the flask was cooled in an ice water bath. $SOCl_2$ (138 mmol, 16.4 g) was added and the reaction was stirred overnight. Upon completion of the reaction, excess $SOCl_2$ was removed *in vacuo* producing a white powder. Anhydrous $CHCl_3$ was added and the residual acid was removed by filtration through a schlenk filter. Solvent was removed *in vacuo* to yield a white powder, which was carried on to the next step without further purification. Melting Point (°C) 54-55; ^{1}H NMR (400 MHz, $CDCl_3$) δ 7.03 (2H, s).

2.4.2. Homopolymer Synthesis

2.4.2.1. General Synthesis with no Proton Scavenger

MCl was added to a 250 ml 3-neck round bottom flask, equipped with stir bar, addition funnel, N_2 sparge and hose inlet/outlet adapter. Atmosphere was removed and replaced with N_2 (3×), DCM (30 ml) was added to the round bottom containing

MCl and FCl, to the addition funnel was added BD and DCM (10 ml) under nitrogen. Upon addition of both dichloride monomers (FCl and MCl), BD and 20 ml DCM were added drop wise to the reaction (at 0°C), sweeping away the HCl (gas) from the reaction flask via the hose inlet/outlet adapter to a beaker containing a KOH (aq) base trap. Each of the PBFcBM copolymers where synthesized using this general setup.

2.4.2.1.1. Poly(1,3-Butylene Fumarate) (PBF) Synthesis from FCl

FCl (65.4 mmol, 10 g) was added to a 250 ml 3-neck round bottom flask equipped with a stir bar, addition funnel, and a N_2 sparge adapter. Atmosphere was removed and replaced with N_2 (3×) and DCM (30 ml) was added and the flask was cooled to 0°C. BD (65.4 mmol, 5.9 g) and DCM (10 ml) were added to the addition funnel. The solution of BD was added drop wise to the MCl/DCM solution. The evolved HCl(g) was swept using a N_2 sparge to a KOH(ag) base trap. The reaction was washed with dH_2O (3×) dried over $MgSO_4$ and solvent removed *in vacuo*.
IR (neat) 2980.2, 2935.2, 2362.3, 2335.6, 1724.1, 1646.3, 1558.7, 1456.5, 1380.9, 1356.6, 1300.9, 1261.5, 1225.3, 1163.1, 1105.0, 983.0, 872.5, 773.8, 668.6 cm^{-1}; ^1H NMR (400 MHz, $CDCl_3$) δ 6.89-8.80 (m, 2H), 5.10 (bs, 1H), 4.68-4.10 (bm, 2H) 2.06-2.00 (bm, 2H) 1.30-1.19 (m, 3H); Mn 834 PDI 1.89. T_g (°C) -34.67.

2.4.2.1.2. Poly (1,3-Butylene Maleate) (PBM)

MCl (65.4 mmol, 10 g) was added to a 250 ml 3-neck round bottom flask equipped with a stir bar, addition funnel, and a N_2 sparge adapter. Atmosphere was

removed and replaced with N_2 (3×) and DCM (30 ml) was added and the flask was cooled to 0°C. BD (65.4 mmol, 5.9 g) and DCM (10 ml) were added to the addition funnel. The solution of BD was added drop wise to the MCl/DCM solution. The evolved HCl(g) was swept using a N_2 sparge to a KOH(ag) base trap. The reaction was washed with dH_2O (3×) dried over $MgSO_4$ and solvent removed *in vacuo*.

IR (neat) ; 2978.9, 1726.6, 1637.9, 1413.9, 1215.9, 1168.8, 1042.2, 982.4, 821.3, 484.4, 411.0 (Fumarate:Maleate, 9:91) T_g (°C) -29.31

2.4.2.2. Copolymer Synthesis

2.4.2.2.1. Synthesis of 75/25 PBFcBM

MCl (16.34 mmol, 2.5 g) was added to a 250 ml 3-neck round bottom flask equipped with a stir bar, addition funnel, and a N_2 sparge adapter. Atmosphere was removed and replaced with N_2 (3×), FCl (51.5 mmol, 7.9 g) was added to the round bottom containing MCl. DCM (30 ml) was added to the round bottom containing MCl and FCl, to the addition funnel was added BD (67.84 mmol, 6.11 g) and TEA (74.6 mmol, 7.55 g), under nitrogen and on ice/water bath BD was slowly added to the round bottom and the reaction was allowed to progress overnight. Upon completion the reaction was washed with dH_2O (3×) dried over MgSO4 and solvent removed *in vacuo*, resulting in a yellow viscous polymer.

IR (neat) 3506.1, 2976.8, 1719.8, 1644.4, 1457.3, 1383.0, 1356.3, 1300.7, 1162.9, 1102.0, 981.6, 911.5, 850.3, 821.5, 757.8, 668.5, 418.4 cm^{-1}; ^1H NMR (400 MHz, $CDCl_3$) δ 6.87-6.76 (m, 2H), 6.43-6.28 (m, 2H), 5.13 (bs, 1H), 4.43-3.65 (bm, 2H)

2.05-1.74 (bm, 2H) 1.37-1.20 (m, 3H); (Fumarate:Maleate, 78:22); Mn 804 PDI 1.67; T_g (°C) -35.39.

2.4.2.2.2. Synthesis of 50/50 PBFcBM

Synthesized following same procedure as 75/25 PBFcBM using the following amounts, MCl (32.7 mmol, 5 g), FCl (34.3 mmol, 5.25 g) and BD (67 mmol, 6.03 g). IR(neat) 2979.5, 2363.1, 1722.9, 1642.7, 1455.9, 1385.5, 1301.0, 1261.9, 1224.4, 1165.0, 1102.7, 1051.8, 980.7, 820.4, 756.8, 667.8 cm^{-1}; ^1H NMR (400 MHz, $CDCl_3$) δ 6.82-6.78 (m, 2H), 6.37-6.19 (m, 2H), 5.17-5.11 (bs, 1H), 4.29-4.06 (bm, 2H) 2.04-1.96 (bm, 2H) 1.34-1.20 (m, 3H); (Fumarate:Maleate, 51:49); Mn 697 PDI 1.58; T_g (°C) -37.68.

2.4.2.2.3. Synthesis of 25/75 PBFcBM

Synthesized following same procedure as 75/25 PBFcBM using the following amounts, MCl (49.0 mmol, 7.5 g), FCl (17.2 mmol, 2.6 g) and BD (66.2 mmol, 5.97 g). IR (neat) 3446.9, 2974.4, 1718.9, 1642.3, 1457.2, 1409.4, 1382.8, 1301.1, 1263.1, 1220.2, 1168.2, 1043.2, 982.7, 910.3, 821.5, 757.4, 668.0 cm^{-1}; ^1H NMR (400 MHz, $CDCl_3$) d 6.88-6.83 (m, 2H), 6.46-6.25 (m, 2H), 5.32-5.17 (m, 1H), 4.48-3.95 (bm, 2H) 2.05-1.78 (bm, 2H) 1.41-1.24 (m, 3H); (Fumarate:Maleate, 27 :73) ; Mn 746 PDI 1.30; T_g (°C) -39.12.

2.5. Polymer Characterization

2.5.1. Determination of Polymer Density

Density was measured in weight at room temperature (RT) using 1ml glass vials (Cole Parmer, Cat # WU-98815-00) relative to the same volume of distilled water in the glass vial (d= 1.0 g/ml).

2.5.2. Determination of Extinction Coefficients for Cis and Trans Double Bond Absorptions

FTIR was carried out by forming 1 wt% polymer/KBr pellets with a path length of 0.3105 mm, scanning from 1200-1300 wavenumbers/centimeter (resolution = 1, 64 scans). The IR Extinction coefficients were determined for each homopolymer (PBF and PBM) at 1215 and 1260 wavenumbers respectively. These extinction coefficients were used to quantify the amount of fumarate to maleate in each copolymer.

3. Results and Discussion

3.1. Polymer Synthesis: Ring Opening Polymerization (ROP) from MA

The homopolymers of poly(propylene fumerate) (PPF), poly(butylene fumarate) (PBF) as well as the accompanying copolymers of poly(propylene fumerate)-*co*-(propylene maleate) (PPFcPM) and poly(butylene fumerate)-*co*-(butylene maleate) (PBFcBM) were synthesized via step growth polycondensation reactions (Scheme 3.1). The glass transition temperatures of all polymers synthesized were below room temperature and ranged from -7°C to -40°C (Table 3.1). The neat polycondensation reaction at high temperatures yielded the all fumarate based homopolymers (PPF and PBF) were synthesized via the protic acid

catalyzed neat reaction of maleic anhydride (MA) with 1,2-propanediol (PD) or 1,3-butanediol (BD) at high temperatures (~250°C), whereas the copolymers (PPFcPM and PBFcBM) were obtained using a protic acid catalyst at lower temperatures (85–110°C).

3.1.1. Copolymers Synthesized via Method A and Method B

Synthesis of PPFcPM and PBFcBM was carried out via a one-step (Method A) and two-step (Method B) azeotropic distillation procedure (Scheme 3.2). The first method (Method A) used to synthesize the copolymer involved a protic acid or Lewis acid catalyzed polymerization reaction carried out at 85°C to 110°C to azeotropically remove water. The second method (Method B) involved an initial ring opening reaction carried out at 50°C without the use of a catalyst followed by an acid catalyzed condensation reaction in combination with azeotropic removal of water.

The ratio of fumerate to maleate (F:M) in the resulting polymer was influenced by both temperature and catalyst (Table 3.2). Polymer synthesized at high temperatures(neat) produced only PPF and PBF, however the molecular weight (MW) was low presumably due to side reaction products which changed the monomer stoichiometry. As the catalytic activities of each catalyst are slightly different, only direct comparison between polymerization techniques using the same catalyst can be made. For example, polymer synthesized at low temperatures according to Method A using TsOH yielded a polymer with 33% fumerate, whereas Method B yielded polymer that contained 55% fumerate (Table 3.1). Polymer formed with mostly maleate had a very low T_g when compared to polymer having a much

smaller amount of maleate. Furthermore, there appears to be no correlation between T_g and molecular weight as each polymer is a random copolymer. PPFcPM synthesized using sulfuric acid as the catalyst resulted in toluene inclusion due to Friedel-Craft alkylation.[4] The influence of temperature and catalyst was also observed in all of the one step azeotropic distillation scenarios, thus providing a system which has the ability to be adjusted.

The MW's of all polymers produced were determined through gel permeation chromatography (GPC) using narrow weight distribution polystyrene as the standards. PPF synthesized according to Method A had an average molecular weight (Mn) of 720, with PBF having an Mn of 536. The MW did not increase with longer reaction times (data not shown). The low MW is consistent with the initial production of PPFcPM and PBFcBM oligomers which thermally isomerizes to the more stable fumerate form. Presumably the high temperature results in both isomerization and side reactions that limit the polymer molecular weight by changing the step growth stoichiometry. PPF synthesized in this fashion is about 70% lower in molecular weight than other reported synthesis[26], however PPF is isolated via a two step synthesis in the previously reported synthesis. PPFcPM synthesized through one step synthesis (Method A) also resulted in polymers with low molecular weights (Table 3.1). To increase the Mn of our polyester, a two step synthesis (Method B) was developed. Method B again produced the copolymers PFcPM and PBFcBM, however in comparison to Method A the F:M ratio decreased. This decrease can be attributed to the initial ring opening of the MA at the lower temperature (50°C) prior to aziotropic distillation. The copolymer molecular weight were significantly higher

than the homopolymers (PPF,PBF) and are summarized in Table 3.2.

3.2 Polymer Synthesis: Controlled Synthesis from Acid Chlorides

Several ratios of fumaryl chloride to maleoyl chloride (FCl:MCl) (75:25, 50:50 and 25:75) were used with BD to yield PBFcBM with known F:M in the final polyester (Scheme 3.2). ^{1}H NMR was used to confirm the ratio of fumarate to maleate functionality through integration of the olefin peaks at 6.8-6.9 ppm (fumarate, F) and 6.2-6.3 ppm (maleate, M) (Figure 3.1). All of the polymers had slightly lower amounts of maleate functionality, which is consistent with a small amount of thermal isomerization to the more stable fumarate functional group. All of the PBFcBM copolymers synthesized here were evaluated using gel permeation chromatography (GPC) as well as differential scanning calorimetry (DSC) in order to determine molecular weight (Mn) and glass transition temperature (T_g) of the various fumarate:maleate (F:M) polymers synthesized (Table 3.2). The molecular weights were in the range of 746 to 834 with a PDI ranging from 1.30 to 1.89. The molecular weights of all the polymers were low, indicating oligomers and not polymers, which is not unexpected given that the reaction mechanism for the esterification reaction is step growth. Variation from a 1:1 ratio of reactants results in inhibition of high molecular weight polymers for step growth mechanisms. All of the oligomers had T_g values which were well below that of room temperature and as the maleate functionality was increased the T_g was shifted more negative from -34.67 (0% maleate) to -35.39°C (25% maleate) to -37.68°C (50% maleate) to -39.12°C (75% maleate).

3.3. Determination of Polymer Density

The density of each oligomer was determined and a clear trend was observed. As the amount of maleate increased relative to fumarate, the density of the polymer decreased (Table 3.2). This observation is consistent with a decrease in packing density as more maleate is included in the backbone of the polymer. As the amount of *cis* double bond incorporated into the backbone of the polymer increased more chain packing defects were induced.

3.4. Determination of Cis and Trans by FT-IR

Fourier transform infrared (FT-IR) data was collected in the spectral region ranging from 1200 to 1300 wavenumbers/cm to corroborate the ^{1}H NMR determinations of F:M ratio. It has been previously reported that the fumarate and maleate absorb at 1260 and 1215 wavenumber/cm, respectively. FTIR spectra were obtained for each of the fumarate-based oligomers, poly(butylene fumarate)(PBF) and poly(butylene maleate) (PBM), as well as all of the oligomers with varying F:M ratios (Figure 3.2 **).** Extinction coefficients were determined using Beers Law. The extinction coefficients (ε) for maleate and fumarate were calculated using the homopolymers of PBM and PBF, using the following equation:

$$\varepsilon = \frac{A - A_o}{cl}$$

Where *A* is the absorbance maximum of the peak (maleate or fumarate) and A_0 is the absorbance value at the baseline of the given peak, *c* is the molar concentration of polymer/sample and *l* is the path length. Solving the equation for $\varepsilon_{maleate}$ and $\varepsilon_{fumarate}$ yielded 7.56 x 10^3 $mol^{-1}cm^{-1}$ and 6.30 x 10^3 $mol^{-1}cm^{-1}$ respectively. The extinction coefficients were used to calculate the percentage of fumarate and maleate in all of the oligomer samples. The percentage of fumarate in each oligomer was determined by FTIR agreed closely with percent fumarate values determined by ^{1}H NMR analysis (Figure 3.3).

4. Conclusions

Poly(propylene fumarate) (PPF) and poly(propylene-fumarate)-co-poly(propylene-maleate) (PPFcPM) were successfully synthesized using maleic anhydride (MA) and 1,2-propanediol (PD),via a step growth polycondensation using the protic acid catalysts p-toluensulfonic acid (TsOH)and sulfuric acid (H2SO4) and Lewis acid catalysts ZnCl2 and FeCl3. In addition to PPF and PPFcPM, substituation of 1,3-butanediol (BD) for PD resulted in successful synthesis of poly(butylene fumarate) (PBF) and poly(butylene fumarate)-co-poly(butylene maleate) (PBFcBM) by transesterfication with TsOH as the catalyst.

Although successful maleate functionality was introduced in the polymer backbone via the ring opening polymerization (ROP) from MA, this synthetic route did not offer fine control over the resulting polymers fumarate:maleate (F:M) ratio. To address this, a novel synthetic route starting from the acid chlorides of fumaryl and meleoyl chloride was developed. We have demonstrated control over the F:M

ratio by carrying out the polymerization of PBFcBM at low temperatures in order to inhibit the thermal isomerization of the maleate to the more stable fumarate. The polymerization scheme is very versatile and can be used with any diol in order to produce a polyester copolymer with both maleate and fumarate functionality. Increasing the maleate concentration relative to the fumarate concentration in the backbone of the polymer resulted in polymers that contained kinks in the chain packing and thus lowered the density of the final polymers. Control of the *cis* to *trans* double bond ratio represents a novel methodology to control polymer degradation.

Scheme 3.1. Synthetic route followed in order to make the homopolymer (PPF and PBF), from MA (1) and PD (2a) or BD (2b). As well as the copolymers (PPFcPM and PBFcBM) using the same starting materials (1 and 2a,b) and forming the intermediate (3).

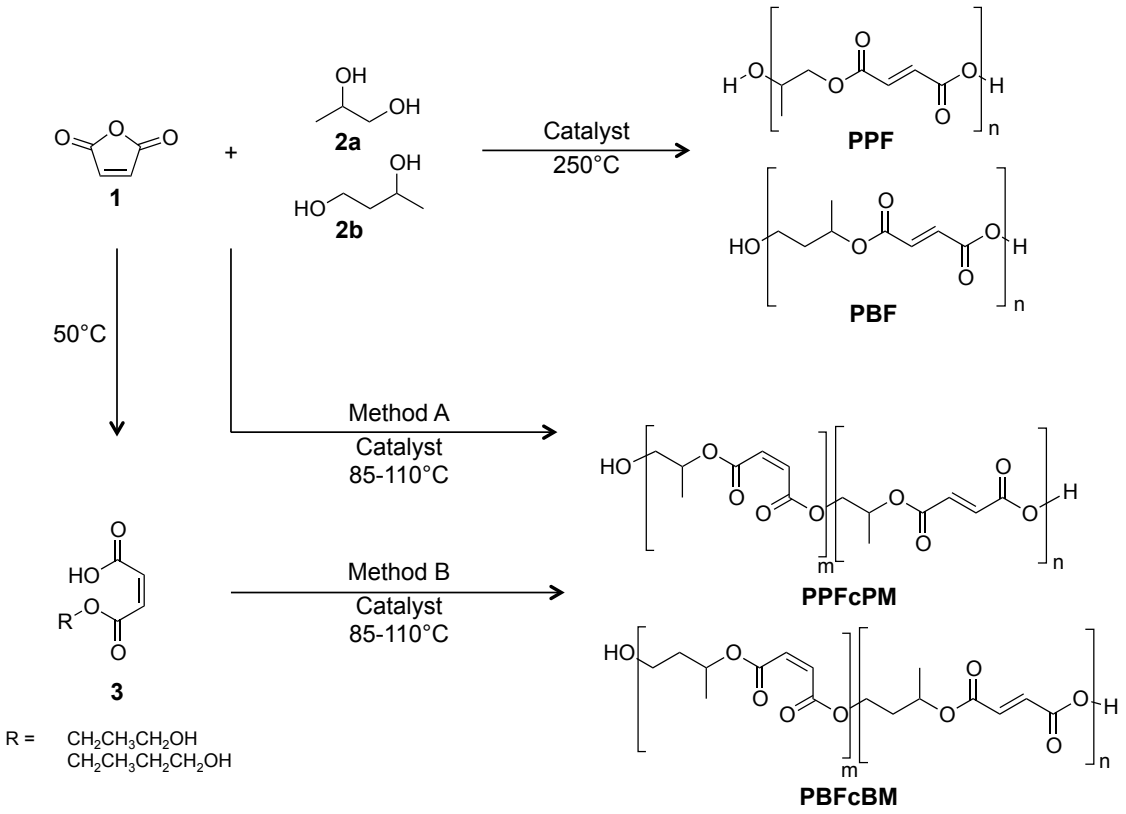

Scheme 3.2. Synthesis route followed in order to make MCl (1) from maleic acid, followed by copolymer synthesis of PBFcBM, from dichloride starting materials FCl (2) and MCl (1) with BD (3).

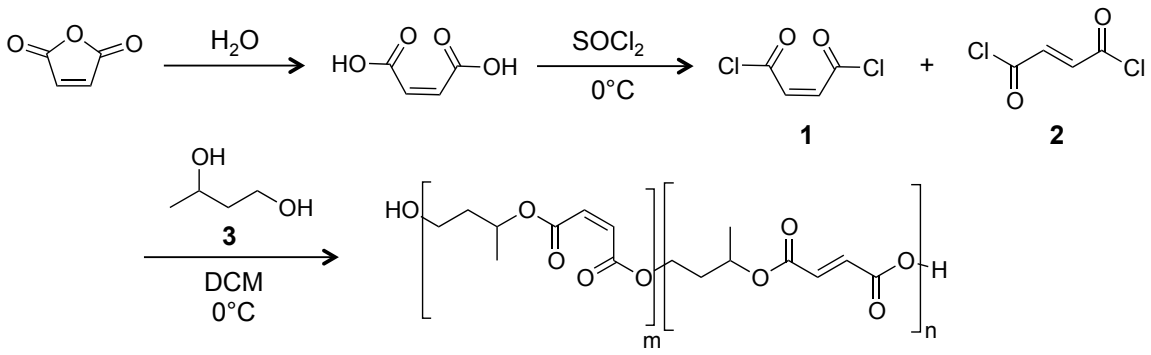

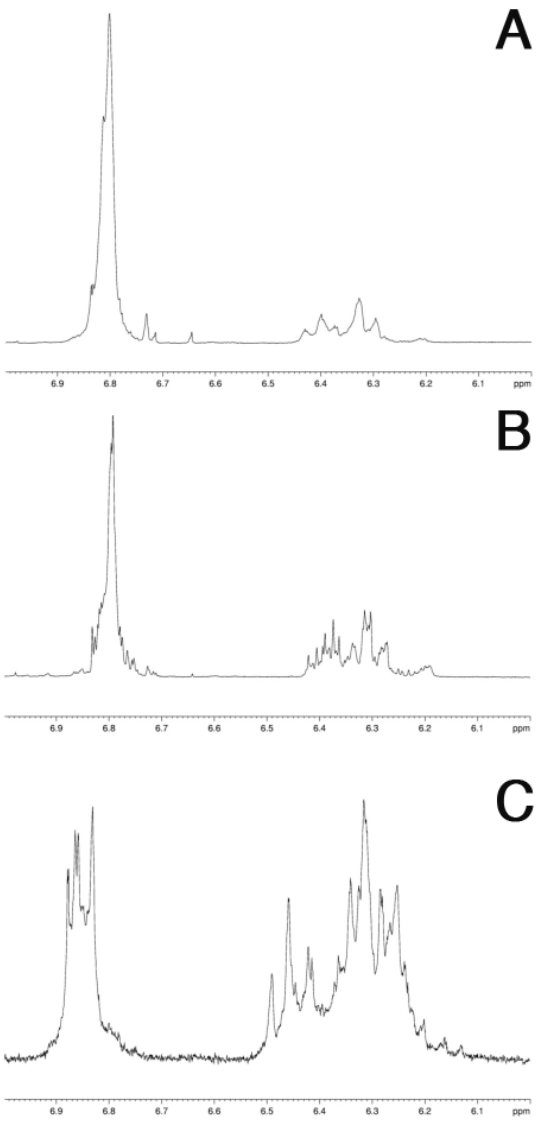

Figure 3.1. ^{1}H NMR of PBFcBM, where the peak at 6.8-6.9 ppm corresponds to the fumarate olefins and the peak at 6.1-6.3 indicates the olefins associated with the maleate. All reflect PBFcBM with varying fumarate:maleate ratios (A) 75:25, (B) 50:50 and (C) 25:75.

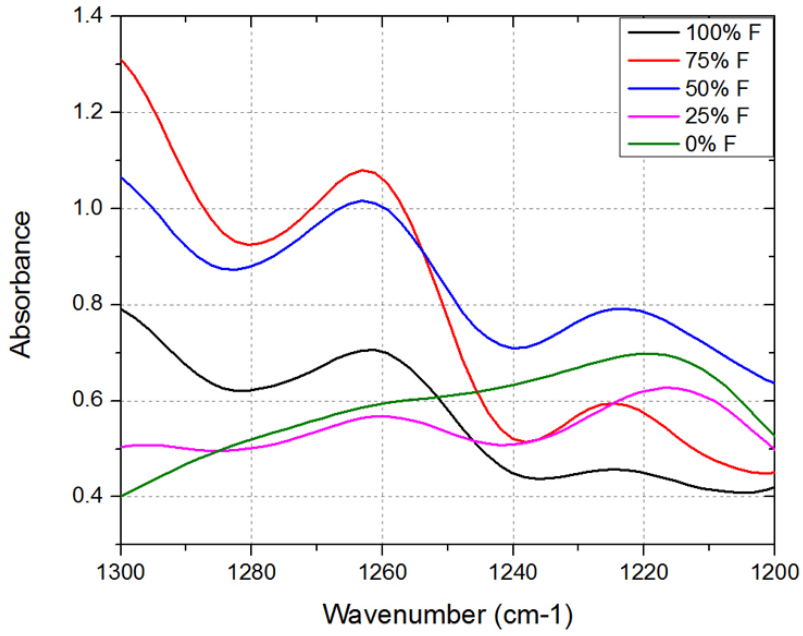

Figure 3.2. FTIR spectra for all homopolymers and copolymers in the region of 1200-1300 cm-1. The maleate absorption occurs at ~1220 cm^{-1} and fumarate absorption occurs at ~1260 cm^{-1}.

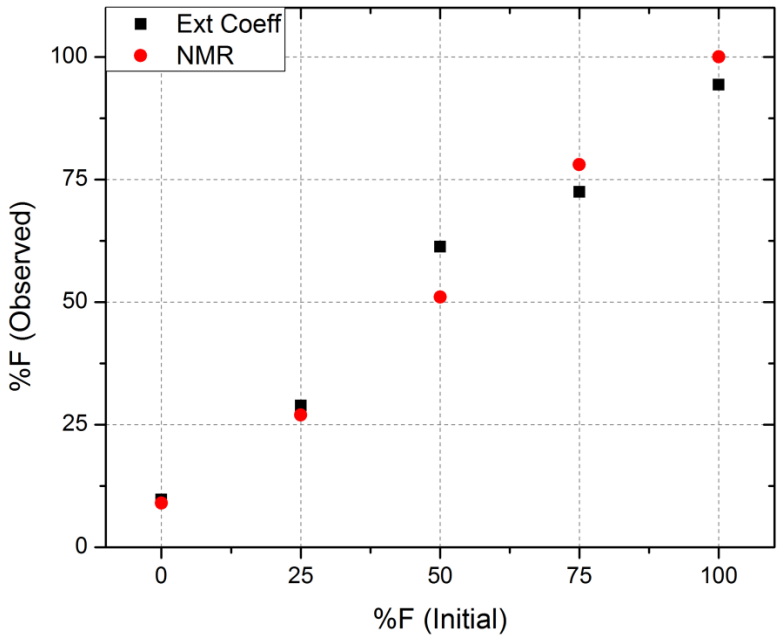

Figure 3.3. The observed percent fumarate in each polymer relative to initial stoichiometry as determined by FTIR (extinction coefficient) and ^{1}H NMR analysis (F:M olefin peak integration)

Table 3.1. Summary of PPF and PPFcPM reaction conditions and polymer characterization.

	Catalyst	Reaction Temperature (°C)	Fumarate:Maleate	Tg (°C)	Mn
Method A	TsOH	250	1	-15.24	473
	TsOH	85-110	0.5	-40.38	728
	H_2SO_4	85-110	3.82	-13.72	330
Method B	$ZnCl_2$	85-110	8.62	-18.66	824
	$FeCl_3$	85-110	6.54	-37.58	1043
	TsOH	50/85-110	1.25	-13.78	2347
	H_2SO_4	50/85-110	2.5	-13.65	1739

Table 3.2. Summary of PBF and PBFcBM polymer characterization.

Fumarate:Maleate (Starting Material)	Fumarate:Maleate (Product)	Tg (°C)	Mn	PDI	Density (g/ml)
100:0	100:0	-34.67	834	1.89	1.207
75:25	78:22	-35.39	804	1.67	1.175
50:50	51:49	-37.68	697	1.58	1.114
25:75	27:73	-39.12	746	1.3	1.077

Chapter 4. Crosslinked Network Characterization and *In Vitro* Degradation of Photo Crosslinked Poly(Propylene Fumarate) and Poly(Butylene Fumarate)

1. Introduction

The body is constructed of biodegradable materials, allowing cells to remove and replace old and defective tissue.[1] In addition, the ideal scaffold to be employed as a synthetic bone graft alternative would not only be biocompatible and osteoconductive, but also have mechanical suitability and controlled degradability. Ideal polymer degradation would occur in such a way that there would be gradual load transfer from the scaffold to the bone as well as increasing space for bone growth.[2, 3]

Major polymeric degradation mechanisms can be broken into four mechanism based on the processing conditions and environment. These mechanisms are: 1) hydrolytic, or degradation by water interaction, 2) oxidative, those polymers which interact with oxidant produced by the tissue, 3) enzymatic, and 4) physical degradation, due to mechanical loading or wear.[4, 5] Hydrolytic degradation, the primary form considered when developing biodegradable synthetic polymeric materials, can have different modes of degradation. These modes, surface erosion or bulk degradation, are determined by the rate of water diffusion into the bulk polymer and the rate of chain cleavage by water ions. Surface erosion displays exterior degradation with little to no ingress (penetration) into the bulk, where bulk degradation water penetrates the entire structure and degrades the entire polymeric network simultaneously (Figure 4.1).[6-8]

Bulk degradation is employed in bone tissue engineering (BTE) applications the scaffold must be osteoconductive, allowing the anchoring of cells (osteoblasts),

which would not occur with a material whose surface is continually eroding.[3] This mechanism of degradation has been displayed by the unsaturated linear polyester poly(propylene fumarate) (PPF) both *in vitro* and *in vivo*.[9, 10] The hydrolytic degradation of the ester functionality displayed in PPF can be altered based on polymer characteristic such as molecular weight, monomer selection and catalyst used during synthesis.[11, 12] PPF can be crosslinked using either thermally or photochemically initiated radicals polymerizing the carbon-carbon double bond. Selection of initiator system as well as crosslinking efficiency/density can alter the rate of degradation, or ester hydrolysis.[12]

A drawback is that the degradation rate is slow relative to the rate of bone formation. *In vitro* studies show little or no degradation of PPF up to 50 weeks,[9] while *in vivo* studies have shown little or no degradation up to 18 weeks. The *in vivo* degradation studies used porous PPF scaffolds placed in a critical sized defect rabbit radii model, where initial bone growth into the scaffold was observed at the scaffold/defect edges, however, scaffold infiltration was not observed. This observation suggests that the degradation rate of the scaffold was sufficiently slow to impede bone formation.[13] In order to address this, researchers have made copolymers of PPF with poly(e-caprolactone) (PPF-PCL)[14], poly(ethylene glycol) (PPF-PEG) and oligo(polyethylene glycol) fumarate (OPF).[15, 16] These crosslinked polymeric networks yielded compressive moduli from as low as 1.8 MPa[17], which is much lower than the 50- 100 MPa for trabecular bone.[18] Therefore a sacrifice in mechanical properties for increased rate of degradation is an area where development is needed.

Recently, we have developed another fumarate-based polymer poly(butylene fumarate) (PBF) and poly(butylene fumarate)-*co*(butylene maleate) (PBFcBM) as described in Chapter 3.[19] By substituting butylene glycol (BG) for the propylene glycol (PG), used to synthesize PPF, an additional methylene unit ($-CH_2$) is introduced between the crosslinkable carbon-carbon double bonds. We hypothesized that the rate of ester hydrolysis would increase due to the addition of a methylene unit in the polymer backbone. This increase in the rate of ester hydrolysis increases the rate of degradation over the currently well-explored PPF without compromising the mechanical properties.

2. Materials and Methods

2.1. Chemicals and Reagents

Tridecafluoro-1,1,2,2-tetrahydrooctyl trichlorosilane was purchased from Gelest. Phosphate buffered saline (10X, PBS) solution, sodium phosphate (monobasic anhydrous) and phosphoric acid (ACS grade) were purchased from Fisher. Ammonium hydroxide (ACS grade) was purchased from EMD Chemicals. Sodium hydroxide (1N, NaOH), dichloromethane (DCM), toluene, phenylbis(2,4,6-trimethylbenzoyl)-phosphine oxide (97%, BAPO) were purchased from Sigma. All chemicals were used as received from suppliers. Poly(propylene fumarate) (PPF) and poly(butylene fumarate) (PBF) were synthesized as previously described in Chapter 3.

2.2. Equipment

Polymer characterization was performed using the equipment detailed in Chapter 3. Glass molds (1 mL, Cat # WU-98815-00) were purchased from Cole Parmer. Ultra Violet (UV) dosages were supplied using a UV Fusion ® System (Fusion Inc.) and measured using a UV PowerPuck® (EIT). Differential Scanning Calorimetry (DSC) was carried out on TA Instruments DSC Q100. Pellets for IR were pressed using a manual pellet press (Carver). High Performance Liquid Chromatography (HPLC) was carried out on an Agilent 1200 (Agilent Technologies). Samples for degradation studies were cut to size using a wet saw (TechCut5™) from Allied High Tech, Inc. Compressive moduli were determined following ASTM D695-02a using an Instron 5500R with TestWorks 4 software. Accelerated degradation samples were incubated using a Major Scientific (MS) incubator equipped with temperature control and orbital shaker. Dimensional analysis was measured with digital calipers purchased from Flexbar®. Degradation samples masses were measured using a precision balance (Mettler-Toledo, #AB304-S/FACT).

2.3. Polymer Synthesis

Both PPF and PBF were prepared as previously reported and described in Chapter 3. In brief, MA, PD or BD and $ZnCl_2$ were added to a 250 mL round bottom flask equipped with a stir bar and distillation head. The reaction mixture was heated to ~250 °C through the use of a silicon oil bath with stirring, while distillate (water) was collected. Upon completion (distillate collection ceased), the reaction was allowed to come to room temperature (RT). The crude polymer was dissolved in

chloroform ($CHCl_3$) (250 mL) and washed with water (250 mL, 3×). The organic layer was dried over $MgSO_4$ and solvent removed *in vacuo,* resulting in a yellow viscous polymer.

GPC (1 mg/ml in $CHCl_3$) PPF: Mw 1851 repeat unit = 12; PBF: Mw 2213 repeat unit = 13

2.4. Network Characterization

2.4.1. Heat Capacity to Determine Crosslinking Efficiency

Differential scanning calorimetry (DSC) was used to measure heat capacity, a method to estimate the crosslinking density of a network due to changes in polymer degrees of freedom.[20, 21] Crosslinked PPF and PBF were compared to the non-crosslinked starting polymers and the change in heat capacities (Cp) was used to determine the degree of crosslinking. DSC thermograms were collected as a function of temperature on ~10 mg samples at a heating rate of 10°C/min from -90°C to 400°C followed by cooling from 400°C to -90°C at 10°C/min, this cycle was repeated 3× on the same polymer sample. Heat capacity (Cp), or specific heat capacity, was calculated by integration of the area under the curve, comparing crosslinked PPF and PBF with uncrosslinked PPF and PBF using the following equation:

$$\mathrm{Cp} = \frac{\text{Heat Flow}}{\text{Heating Rate}} \times \mathrm{K}$$

Where heat flow, or change in enthalpy of the sample is obtained in W/g for the specimen, heating rate is specific to the °C/min which is used and K is the calibration constant for the DSC instrument being used and is dimensionless.

2.4.2. Infrared Spectroscopy (FT-IR) to Determine Crosslinking Efficiency

To carry out FT-IR , 5.0 wt% polymer/KBr pellets with a path length of 0.32 mm were prepared using a pellet press (6,000 lbs for 1 min). The resulting sample pellet was then scanned from 1600-1800 wavenumbers/centimeter (resolution = 1, 64 scans). The IR extinction coefficients were determined for each uncrosslinked polymer (PPF and PBF, n = 3 for each) at ~1645 wavenumbers. The extinction coefficients (ε) for the fumarate peak was calculated using Beer's Law:

$$\varepsilon = \frac{\text{A-A}_\text{o}}{\text{cl}}$$

Where *A* is the absorbance maximum of the fumarate peak, A_0 is the absorbance value at the baseline of the given peak at 1645 cm^{-1}, *c* is the molar concentration of olefin/g sample (3.2 x 10^{-5} mol/g for PPF and 2.9 x 10^{-5} mol/g for PBF), and *l* is the path length (0.32 mm). These extinction coefficients were then used to quantify the concentration of double bonds which remained in the crosslinked PPF and PBF samples. To do this, 0.5 wt% crosslinked polymer/KBR pellets were prepared and FTIR was carried out in the same fashion as the uncrosslinked polymers. The crosslinking density (X) is then calculated by the following equation:

$$X = \frac{c_x}{c_0}$$

Where the concentration of remaining double bonds, as calculated by the crosslinked polymer samples (c_x) is divided by the initial concentration of double bonds in the uncrosslinked polymer samples (c_0).

2.4.3. High Performance Liquid Chromatography (HPLC) to Determine Crosslinking Efficiency

To carry out HPLC, uncrosslinked and crosslinked polymer samples of both PPF and PBF were degraded completely in basic conditions using a previously identified procedure. Briefly, 0.5 mg of polymer was placed in 10 ml of 1N NaOH in a 20 ml scintillation vial, followed by degradation at 60°C under gentle agitation. Prior to placement in degradative conditions, crosslinked PPF and PBF networks were ground using a mortar and pestle to increase the surface area and therefore increase the rate of degradation. The degradation product, fumaric acid (FA), was evaluated by HPLC equipped with a diode array detector. Analysis was carried out using 97:3 0.02M ammonium hydroxide: methanol as the mobile phase, the pH was adjusted to 2.35 with phosphoric acid and 0.03M ammonium acetate was added in order to avoid silonal effects with the column. The mobile phase was set to a flow rate of 0.25 ml/min. The degradation products of PPF and PBF crosslinked networks, were separated via a X Select HSS T3 column (35 μm × 100 mm) and chromatograms were acquired at a UV absorption of 200 nm.

First, to determine the retention time of FA under these conditions (ie. flow rate and column) a calibration curve was generated by preparing FA standards of 0,

0.05, 0.15, 0.25, 0.35 and 0.5 mg/ml in 1N NaOH (aq). Once the parameters were established, the degraded polymer samples were then run under the same HPLC conditions. Upon acquisition of chromatographs for uncrosslinked and crosslinked PPF and PBF, the degree of crosslinking for the network was calculated by the following:

$$X = \frac{A_x}{A_0}$$

Where X represents crosslinking density, A_x is the intensity of the FA peak in the crosslinked network and A_0 is the FA peak intensity in the uncrosslinked polymer.

2.4.4. Sol Fraction and Swelling Ratio Measurements

Solid samples were fabricated by dissolving 3 wt% BAPO/g polymer (PPF or PBF) in minimal dichloromethane (DCM) followed by solvent removal and placement in glass molds (diameter = 6mm). Polymers were then subjected to UV curing and crosslinked cylinders were removed from molds and cut into small discs (6 mm x 0.06-0.08 mm, diameter x thickness) (n = 3). Initial mass (M_i) was recorded and crosslinked polymer disks were immersed in toluene (~3 ml) for 48 hours. After soaking, discs were removed and lightly blotted to remove any attached solvent from the disks surface. The wet mass was measured (M_w). Excess solvent from the disks was removed *in vacuo* overnight and reweighed to determine a final or dry mass (M_d). The swell degree was calculated using the following equation:

$$\text{Swell} = \frac{(M_s\text{-}M_d)}{M_s}$$

The sol fraction, or the fraction of polymer following crosslinking that is not part of the crosslinked network was calculated via the following equation:

$$\text{Sol fraction} = 1 - \left(\frac{M_i - M_d}{M_i}\right)$$

2.5. Sample Preparation for Degradation of Crosslinked Networks

2.5.1. Silane Treatment of Glass Molds

Glass molds (diameter = 6 mm) were placed in a desiccator along with a beaker containing a few drops of tridecafluoro-1,1,2,2 tetrahydrooctyl)trichlorosilane. Vacuum (50 Torr) was applied to the desiccator for 30 minutes, followed by closure of the vacuum valve. The molds were allowed to sit overnight under vacuum.

2.5.2. Sample Fabrication for Degradation Studies

Polymer containing BAPO photoinitiator was prepared by dissolving 3% (w/w) BAPO/g polymer in a minimal amount of DCM. The solvent was removed *in vacuo* prior to filling the freshly silane treated glass molds. Initiator loaded polymer solution was delivered to the glass molds (diameter = 6mm) via a plastic syringe. The filled glass vials were subjected to centrifugation (3 minutes at 5000 rpm) in order to remove any air bubbles and/or defects. The polymer filled cylinders were than subjected to vacuum desiccation overnight, followed by centrifugation (5 min at 3000 rpm) before photo crosslinking. Polymers (PPF and PBF) were crosslinked using a UV Fusion ® System, for 15 passes at a belt speed of 15 at 25% power (43.133

mJ/cm^3). After the initial UV exposure, the vials were broken and the samples were exposed for 30 passes at belt speed of 15 @ 50% power (551.193 mJ/cm^3). All crosslinked samples were cut using a wet saw in order to achieve a height:diameter of 2:1 (12: 6 mm) (Figure 4.2).

2.6. Accelerated In Vitro Degradation

Sodium hydroxide (0.1N) was used to accelerate the hydrolysis reaction. Initial height, diameter and mass were recorded for each cylindrical sample prior to placement in a 20 mL scintillation vial. Accelerating solution, NaOH (0.1N, 10 mL) was added to each vial and tightly sealed. Vials were placed in an incubator equipped with shaker plate and maintained at 60°C under gentle agitation (~65 rpm). At each timepoint, five samples were pulled and wet dimensional measurements were recorded. Samples were then rinsed thoroughly with dH_2O and dried *in vacuo* for a minimum of 24 hours to ensure removal of any residual water. Upon drying samples were dimensionally analyzed for a final time in order to record dry height, diameter and mass changes. Control samples of PPF underwent the same procedures.

2.7. Mechanical Testing

Compression testing was performed on the dry cylindrical crosslinked networks using an Instron 5500R load frame equipped with TestWorks software, 10,000 lb load-cell in accordance with ASTM D695-02 for rigid plastics. Samples are compressed at 0.1 in/min, up to a strain of 0.5 with a data acquisition rate of 5

Hz. Stress-strain curves were than exported to Microsoft® Excel and were analyzed in the linear region (5 – 20% strain) to determine sample modulus.

2.8. Dimensional Analysis

Changes in mass and dimension and water adsorption were calculated for each time point using the initial mass (M_i), wet mass (M_w) and a dry mass (M_d). Mass loss and water adsorption (uptake) over the duration of the degradation study by the following equation:

$$\%\ \text{Mass loss} = \frac{(M_i - M_d)}{M_i} \times 100$$

$$\%\ \text{Water adsorption} = \frac{(M_w - M_d)}{M_d} \times 100$$

Fractional changes in height and diameter were calculated using the following, where the subscript d indicates dry and i indicates initial conditions:

$$\text{Fractional height change} = \frac{H_d}{H_i}$$

$$\text{Fractional diameter change} = \frac{D_d}{D_i}$$

2.9. Statistical Analysis

Network characterization and degradation were carried out on un-crosslinked and crosslinked PPF and PBF networks. Crosslinking density, sol fraction and degree of swelling determinations were carried out in triplicate (n = 3). Accelerated degradation determinations were carried out in quintet (n=5), including dimensional changes (height, diameter and mass) and compressive moduli. Results were compared by performing analysis of variance (ANOVA) with post hoc testing (ie. Tukey HSD) via statistical software (IBM SPSS®).

3. Results and Discussion

3.1. Network Characterization

This study aimed to evaluate the reduction of the fumarate carbon-carbon double bond (C=C) as a result of crosslinking. This was determined using differential scanning calorimetry (DSC) and Fourier transfer-infrared spectroscopy (FT-IR). First, chromatograms of un-crosslinked and crosslinked PPF and PBF were collected to experimentally determine the Cp values associated with each polymer (Figure 4.3). The Cp is calculated by evaluating the change in heat flow of a known polymer mass, this is calculated by integrating the area under the curve. The Cp values for un-crosslinked PPF and PBF were 41.87 J/g and 3.40 J/g and for the corresponding crosslinked networks was 6.9 J/g and 0.2 J/g, respectively. The reduction in Cp values of the crosslinked networks of PPF and PBF is attributed to the correlation of Cp to degrees of freedom in the polymer. Upon crosslinking of the

polymer network, fewer double bonds are present and therefore the polymer has less molecular mobility as compared to the un-crosslinked PPF and PBF samples.[20, 21] Crosslinking density was then determined to be 84% (PPF) and 94% (PBF) by calculating the percent change from the un-crosslinked samples (Table 4.1). This result provides a general idea of the network structure as indicated by the thermal changes compared to the un-crosslinked polymeric samples.

Second, FT-IR was used to evaluate the decrease in absorbance of the C=C bond at ~1645 cm^{-1}. The relative level of crosslinking was inspected by changes in absorbance due to the C=C stretching of crosslinked PPF and PBF networks as compared to the un-crosslinked networks (Figure 4.4). Molar absorptivity, or extinction coefficient (ε) of the un-crosslinked networks was determined to be 41,490 ± 2,099.6 $(mol \times mm/g)^{-1}$ for PPF and 30,170 ± 5,576.0. $(mol \times mm/g)^{-1}$ for PBF using Beer's Law. These values were than used to calculate the concentration of double bonds remaining in PPF and PBF networks relative to the absorbnce of the fumarate peak (1645 cm^{-1}). The concentration of remaining double bonds in crosslinked PPF and PBF networks was found to be $4.8 \times 10^{-6} \pm 2.4 \times 10^{-7}$ mol/g and $6.4 \times 10^{-7} \pm 1.3 \times 10^{-7}$ mol/g, resulting in a crosslinking efficiency of 85 ± 3 and 98 ± 2 % respectively (Table 4.1). Based on these results, the evaluation of crosslinking density by a thermal characterization (Cp) as well as spectral characterization (FT-IR), the effect of the fumarate C=C reduction and consumption due to crosslinking was found to be similar for each network using two different techniques.

In addition to DSC and FT-IR, In addition to evaluating crosslinking density via reduction of the double bond after crosslinking, polymer network degradation products were separated by high performance liquid chromatography (HPLC). The fumarate-based unsaturated PPF and PBF yield fumaric acid (FA) and the corresponding diol upon hydrolytic degradation of the ester group. Using the previously established HPLC technique, established by Timmer *et al*, the FA component was quantified for both un-crosslinked and crosslinked PPF and PBF networks. Verification of the technique was performed by first evaluating the performance of a FA by establishing a calibration curve using the aforementioned HPLC conditions (Figure 4.5). Chromatographs of FA standards in 1N NaOH supplied the retention time of ~11 minutes for FA and the peaks prior to 5 minutes being attributed to NaOH (Figure 4.5). Upon verification of the HPLC technique, accelerated PPF and PBF un-crosslinked and crosslinked samples were subjected to HPLC. The concentration of FA in crosslinked network as compared to un-crosslinked networks was used to determine crosslinking densities for PPF and PBF were calculated to be 76 ± 3 and 87 ± 1 %, respectively (Table 4.1).

These results, in contrast to the crosslinking densities determined previously by DSC and FT-IR, are significantly lower. This could be due to the assumption that degradation conditions would completely degrade the polymers as well as have no secondary reactions that take place by subjecting the uncrosslinked polymers to basic conditions. However, the same trend of PBF as compared to PPF is observed among all three characterization techniques evaluated in this study (Table 4.1).

In addition to quantifying the reduction in double bonds, network characterization was evaluated by sol fraction and degree of swelling (Table 4.2). Sol fraction, polymer chains that are not incorporated into the bulk crosslinked network, was evaluated by submersion in toluene. The crosslinked PPF and PBF networks were submerged in toluene, this solvent was chosen as the starting polymer is soluble and it will slightly swell the solvent versus other solvents such as dichloromethane (DCM), which is a harsher solvent and has destroyed networks in previous studies.[9] After 48 hours of solvent incubation and removal of excess solvent *in vacuo*, the sol fraction was calculated. This data indicates that there was 10 wt% (PPF) and 4 wt% (PBF) of the original polymer network mass that was not incorporated after crosslinking. Indicating that the PBF network is more crosslinked compared to the PPF. Following sol fraction analysis, the polymer discs were than placed in toluene for an addition 24 hrs to ensure all of the non-crosslinked polymer was removed from the crosslinked polymer by displaying no change in mass following removal of excess solvent *in vacuo*. Examination of swelling degree corroborated that the PBF networks were crosslinked more as compared to the PPF networks (Table 4.2). This trend was expected, as the swelling of PPF should be larger due to a less crosslinked network relative to PBF.

3.2. Degradation

3.2.1 Silane Treatment of Glass Vials for Sample Fabrication

The 1 ml glass via molds used as sample fabrication were silane treated prior to use in order to ease removal of the polymer upon crosslinking. Initial attempts

without silane treatment left crosslinked polymer samples that would adhere to randomly to the glass upon cooling after the crosslinking reaction. The adhesion to the glass mold produced stresses in the crosslinked network, thereby creating defects in the solid samples. Due to this observation, silane treatment of the glass vials was instituted as a necessary step for sample fabrication. Surfaces of the glass mold was modified with a fluorosilane in order for a highly hydrophobic surface to be presented. This barrier between the glass and polymer allowed for minimal wetting and adhesion of the polymer to the glass mold providing a more consistent crosslinked sample. [23]

3.2.2. Accelerated Degradation of Poly(Propylene Fumarate) and Poly(Butylene Fumarate) (PPF and PBF)

3.2.2.1. Mechanical Testing

Compressive properties of PPF and PBF crosslinked networks were evaluated under accelerated conditions (0.1 N NaOH at 60°C). Samples were evaluated after removal from basic solution, followed by soaking in water to remove excess NaOH and finally *in vacuo* removal of excess water. PPF degradation has been shown to degrade through bulk degradation[25], where the rate of water penetration is greater than the rate of ester hydrolysis and water enters the entire structure and chain scission occurs throughout the network.[6, 7] As a network undergoes bulk degradation, the random breaking of the polymer backbone weakens the network, resulting in a decrease in mechanical properties.

The initial compressive moduli was calculated to be 207 ± 18 MPa (t= 0) for PBF relative to 122 ± 18 MPa (t= 0) for PPF crosslinked networks (Figure 4.6, left). Interestingly, after 24 hrs, the PBF crosslinked networks maintain their decreased moduli, whereas the PPF networks displayed an increase in mechanical properties throughout the duration of the experiment (Figure 4.6, right). This phenomenon has been previously reported for crosslinked PPF networks[27, 28] and was attributed to the incubation in elevated temperatures which allow for further crosslinking of network.[29] Perhaps this observation can be supported by the crosslinking efficiency results for our PPF networks (Table 4.1).

3.2.2.2. Dimensional Analysis

Mass loss is a later indicator of degradation as polymer chains are only able to leave the network once enough ester bonds have been broken thoughout the network to release small degradation products. Both PPF and PBF display a similar trend in weight loss with in the first 24 hrs of incubation, with ~20 % mass loss (g). However, after 24 hrs, the mass of PBF crosslinked networks starts to decline at a faster rate compared to PPF. The final mass loss observed after 60 hrs are presented in Figure 4.7.

In addition to mass loss, sample height and diameter were monitored thoughout the study and fractional changes were calculated. There was little to no difference seen in dimension over time for both PPF and PBF crosslinked networks (Figure 4.8). The lack of dimensional changes indicates that crosslinked PPF and PBF networks are undergoing bulk erosin.[6] Furthermore, these results suggest that

crosslinked scaffolds upon implantation *in vivo* would not have significant network changes in physical structure.

Water absorption was also evaluated, PBF displayed a higher percentage of water uptake compared to PPF throughout the 60 hr study (Figure 4.9). This observation supports our hypothesis that the inclusion of the methylene unit ($-CH_2$) in PBF would allow for increased water ingress over PPF networks crosslinked in the same manner, as there is a significant increase in PBF as compared to PPF at each degradation time point.

4. Conclusions

Photo crosslinked poly(propylene fumarate) (PPF) and poly(butylene fumarate) (PBF) networks were evaluated by calculating double bond reduction (consumption) due to crosslinking by heat capacity, Cp (DSC) and changes in absorbance as correlated to concentration of double bonds (FT-IR). In addition, high performance liquid chromatography (HPLC) was used to evaluate the presence of fumaric acid (FA) in crosslinked and un-crosslinked networks. In addition, common crosslinking density techniques were employed to evaluate sol fraction and degree of network swelling. Crosslinked network performance was was evaluated by both changes in mechanical properties and mass loss by monitoring compressive moduli and mass. These results indicate that the inclusion of a methylene unit ($-CH_2$) within the glycol structure results in a fumarate-based polymer with mechanical properties suitable for orthopedic applications. Furthermore, the rate of degradation is increased relative to PPF without sacrificing those mechanical properties.

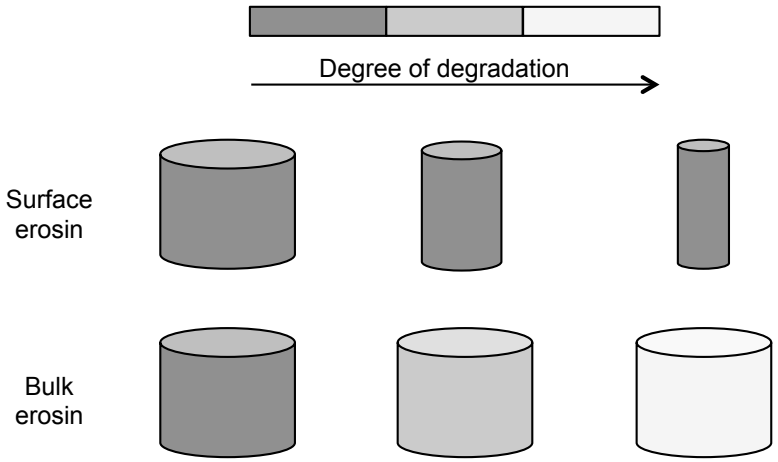

Figure 4.1. Schematic illustration of the effect of surface and bulk erosion on samples as a function of time (left to right). (Adapted from Gopferich, 1996, # 6)

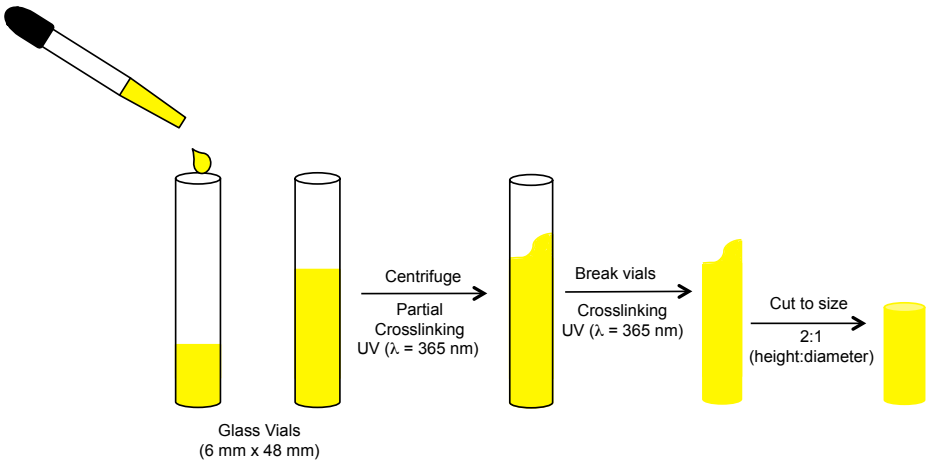

Figure 4.2. Schematic representing the glass mold filling/crosslinking procedure, producing crosslinked polymer samples to undergo evaluation via degradation.

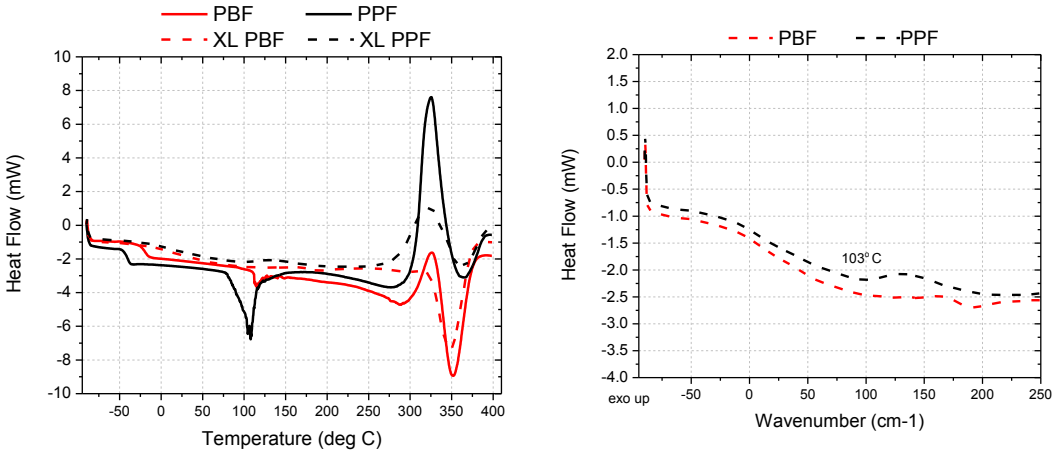

Figure 4.3. DSC thermographs from which heat capacities (Cp) were determined for uncrosslinked (—PBF and —PPF) and photocrosslinked (- -PBF and - -PPF) networks (left). Onset temperature of Cp for each crosslinked network is seen at ~100°C (right).

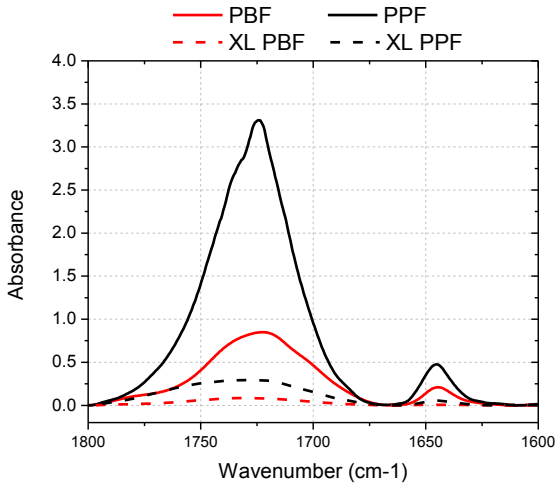

Figure 4.4. Representative FTIR spectra for uncrosslinked (—PBF and —PPF) and photocrosslinked (- -PBF and - -PPF) networks in the region of 1600-1800 cm^{-1}. The fumarate (C=C, double bond) absorption occurs at ~1645 cm^{-1} (left).

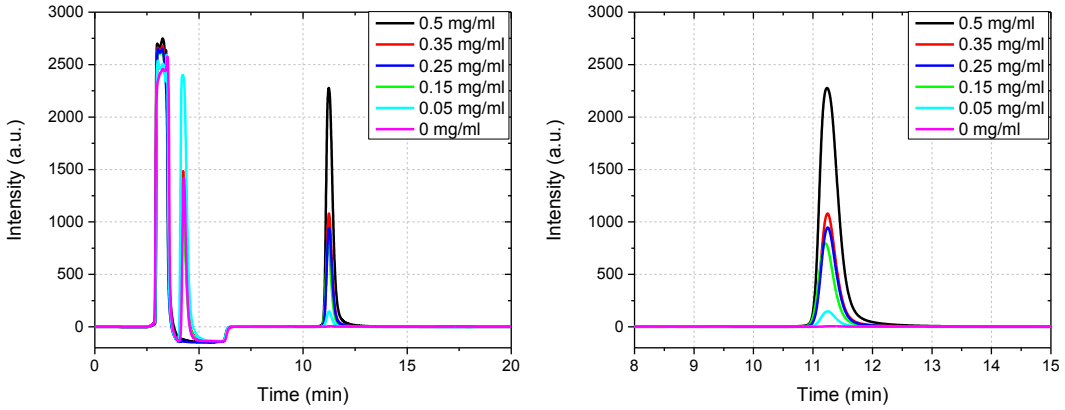

Figure 4.5. Representative calibration chromatograms of fumaric acid (FA) standards intensity as a function of retention time in 1N NaOH for the entire run time (left) and zoom in of peak attributed to FA (right).

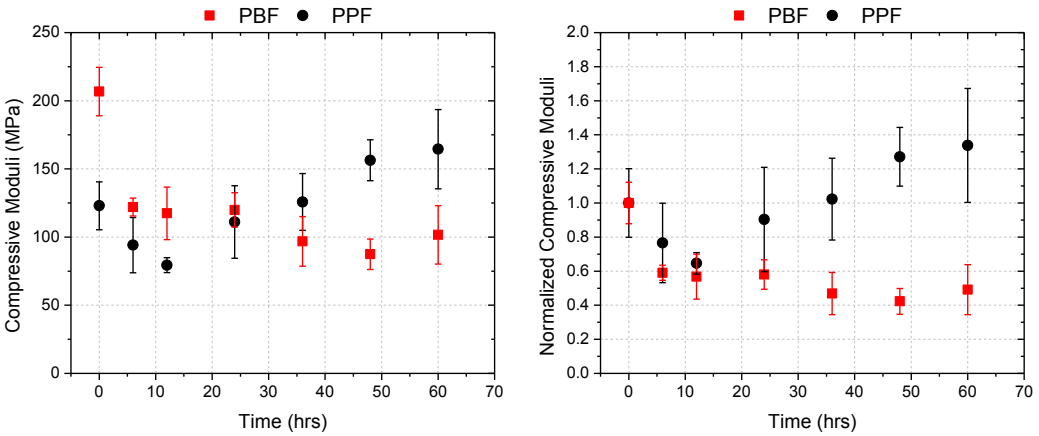

Figure 4.6. Compressive moduli (left) and normalized moduli (right) for PBF (■) compared to PPF (●) crosslinked networks as a function accelerated degradation time. Results represent mean ± standard deviation for n = 5.

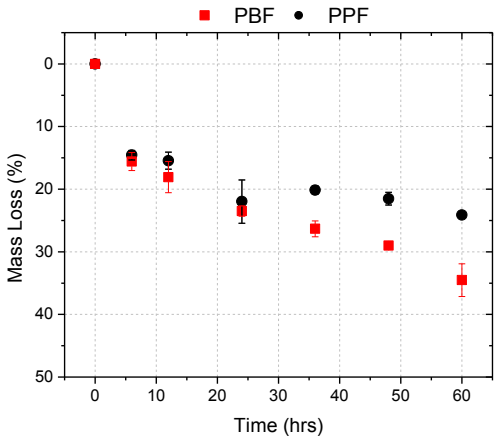

Figure 4.7. Percent change in specimen mass of PBF (■) compared to PPF (●) as a function accelerated degradation time. Results represent mean ± standard deviation for n = 5.

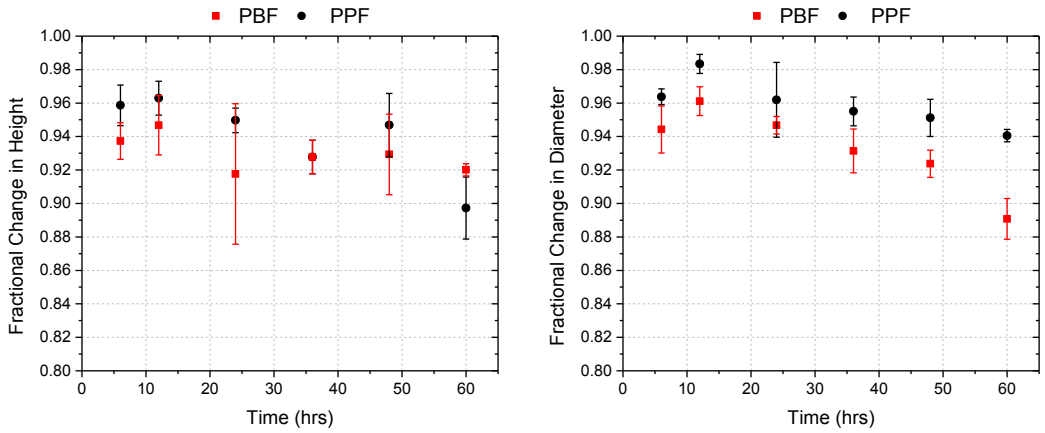

Figure 4.8. Fractional change in height (left) and diameter (right) for PBF (■) compared to PPF (■) as a function accelerated degradation time. Results represent mean ± standard deviation for n = 5.

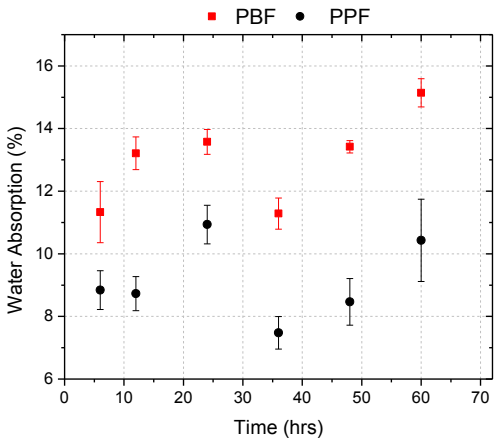

Figure 4.9. Water absorption, or % water uptake for PBF (■) compared to PPF (■) as a function accelerated degradation time. Results represent mean ± standard deviation for n = 5.

Table 4.1. Crosslinking Density of PPF and PBF networks. *Results are represent mean ± standard deviation for n = 3.

Characterization Method	PPF	PBF
DSC	84%	94%
FT-IR *	85 ± 3%	98 ± 2%
HPLC *	76 ± 3%	87 ± 1%

Table 4.2. Crosslinked PPF and PBF network characterization. Results represent mean ± standard deviation for n = 3.

	PPF	PBF
Sol Fraction	0.1 ± 0.0	0.04 ± 0.0
Swelling Degree	0.05 ± 0.0	0.02 ± 0.00

Chapter 5: Cytotoxicity Evaluation of Crosslinked Poly(Butylene Fumarate) Networks and their Osteoconductive Potential

1. Introduction

As the field of tissue engineering continues to evolve, researchers are working towards unique modifications of existing polymers or creation of novel polymer systems for biomedical applications.[1] Prior to use, all biomaterials must be tested in cellular environments, both *in vitro* and *in vivo*, to evaluate the cellular response to the material. Initial cell response can be evaluated through *in vitro* cytotoxity, a measurement of the materials toxic potential to cells.[2, 3] Cytotoxic potential is measured by the appearance of cell death or inhibition of cell proliferation.

Recently, we have synthesized the homo and copolymers of poly(butylene fumarate) (PBF) and poly(butylene fumarate)-*co*-(butylene maleate) (PBFcBM).[4-6] These new fumarate-based polymers are modeled after the biomaterial poly(propylene fumarate) (PPF), where propylene glycol (PG) is used instead of butylene glycol (BG). Poly (propylene fumarate) (PPF) crosslinked networks have undergone cytotoxity studies to evaluate its potential as a good biomaterial.[2] Biodegradability of PPF, through hydrolytic cleavage of the ester functionality in the polymer backbone, results in the generation of fumaric acid and propylene glycol.[7] In addition to being biodegradable, an ideal materials degradation products will easily be expelled from the body without resulting in an inflammatory response. Both fumaric acid and PG are capable of fulfilling this requirement and will easily be removed through metabolic pathways (Kreb's cycle). With this substitution of BG in place of PG, the degradation products will be fumaric acid and BG. Again, fumaric

acid will be expelled via the Kreb's cycle where as BG is likely to be metabolized primarily in the liver due to the high concentrations of alcohol and aldehyde dehydrogenase.[8] The biocompatibility of BG should also not cause issues as it has been approved and used as an additive in cosmetics[9] and food[10], as well as treatment for ethylene glycol poisoning in dogs.[11]

In addition to a material for potential orthopedic applications being cytocompatible, the material must support and allow for the attachment, proliferation, differentiation and the ability of the cells to lay down extra cellular matrix (ECM) on the scaffold material.[12] This task, like biocompatibility/cytotoxicity, can be screened *in vitro* through evaluation of cell-material interactions. To this end, mesenchemyl stem cells (MSCs) have been utilized in the area of bone tissue engineering (BTE) to evaluate interactions of cells with the scaffold.[13, 14] MSCs, a multipotent self-renewing stem cell is a progenitor of adipogenic (fat), chondrogenic (heart) and osteogenic (bone) lineages.[15-17] These cells within their native stem cell niche (bone marrow) are capable of receiving chemical, biological and mechanical stimuli which allows differentiation of the MSCs. This process of osteogenisis can be mimicked *in vitro* by adding supplements to the culture medium.

Osteogenic differentiation of MSCs is induced *in vitro* by the presence of dexamethasome (Dex), ascorbic acid (Asc) and β-glycerol phosphate (β-GP). Each of these supplements serve a specific purpose in differentiation of MSCs to the bone forming osteoblastic cells, they are: 1) the expression of a mineralized matrix by the synthetic glucocorticoid Dex, 2) supplying a cofactor for the hydroxylation of proline and lysine residues in collagen and finally 3) a source of inorganic phosphate in β-

GP, which is also needed in matrix mineralization and enzymatically hydrolyzed by alkaline phosphatase (ALP).[18]

Osteogenesis occurs in stages this is depicted in Figure 5.1 and can be categorized into 3 stages. First, days 1-4 in culture there is a peak in cells seen with early cell differentiation from days 5-11 of the protein expression of ALP. Secondly, early deposition of collagen I provides a matrix for mineral deposition to be deposited. Lastly, days 14 – 28 result in high expression of osetocalcin and osteopotin.[19]

In this chapter we evaluate the cytotoxicity of the newly synthesized PBF, as described in Chapter 3 from maleic anhydride. In addition evaluation of the new fumarate-based material is assessed for its osteoconductive potential by osteogenic differentiation of MSCs *in vitro*, monitoring ALP expression and mineralization.

2. Materials and Methods

2.1 Chemicals and Reagents

Maleic anhydride (briquettes 99%, MA) 1,3-butanediol (Reagent Plus®, 99%, BD), phenylbis(2,4,6-trimethylbenzoyl)-phosphine oxide (97%, BAPO), dexamethasome (minimum 98%, Dex), L-ascorbic acid (cell culture tested, Asc), β–glycerophosphate disodium salt hydrate (BioUltra, β-GP), cetylpyridinium chloride (USP specked, CPC), alizarin red S (ARS) and sodium phosphate dibasic (BioXtra ≥ 99.0%,Na_2HPO_4) were purchased from Sigma. Tris buffer (10X, Tris) and triton X-100 were purchased from EMD Millipore. 2-amino-2-methyl-1-propanol (99%,

2A2M1P) was purchased from Acros.. Silicon vacuum grease was obtained from Dow Corning. All chemicals were used as received from suppliers.

2.2 Cell Culture

The murine osteoblastic cell line (MC3T3-E1) was purchased from ATCC (Manassas, VA). Fetal bovine serum (FBS), αMEM, penicillin/streptomycin (10,000 units/ml penicillin; 10,000 units/ml streptomycin, P/S), trypsin/EDTA (0.25% (w/v)) and fungizone (250mcg/ml amphotocin B in saline, 205 mcg/ml sodium deoxycholate) were purchased from ThermoScientific. Rat bone marrow derived mesenchemyl stem cells (MSCs), DMEM (GlutaMax® medium), MSC qualified fetal bovine serum (MSC-FBS), αMEM (GlutaMax® ribnucleosides and deosyribonucleosides medium), TrypLE™ express disassociation enzyme and trypan blue (0.4 %) were purchased from LifeTechnologies. Tissue culture polystyrene (TCPS) 75cm^2 Flasks (75-T) and 96 well plates were purchased from Corning. Non-TCPS 96 well plates were purchased from BD Falcon. LIVE/DEAD® Viabilty/Cytotoxicity (L/D) kit for mammalian cells was purchased from Invitrogen®. Cell Titer 96® AQueous One Solution Cell Proliferation Assay (MTS) was purchased from Promega®. Both assays were used in accordance to manufacturer's protocol.

2.3 Equipment

Cells were incubated under standard culturing conditions using a CO_2 incubator (NAPCO series, 800 DA, ThermoSci). A sterile environment for tissue culture was maintained using a class II type A2 biological safety cabinet (Labguard).

Cell spinning was performed using a Isotemp 110 centrifuge (Fisher). Cell counting was carried using a hemocytometer (Hyclone®, ThermoSci). Cell imaging was carried out using a NIKON Eclipse TS100 equipped with camera and Spot imaging software. Absorbance readings were collected using a plate reader (SpectraMax M5) and data was processed using Microsoft® Excel. Thin films of polymeric networks were created using a drawdown machine (Gardco Automatic Drawdown Machine,Otto).

2.3 Cell Culture

2.3.1 Cell Line: Mouse Osteoblastic Fibroblasts (MC3T3-E1)

A murine osteoblastic cell line, MC3T3-E1 were received from ATCC®, thawed and established according to manufacturer's specifications. Cells were cultured in 75-T tissue cultured polystyrene (TCPS) flask using αMEM supplemented with 10% (v/v) fetal bovine serum (FBS), 1% (v/v) penicillin/streptomycin and 1 % (v/v) fungizone at 37°C with 5% CO_2 with 95% relative humidity (RH).

Passaging of MC3T3-E1 (typically 3-5 days) was carried out when cell coverage of the 75-T flask was at 70-80%. Briefly, medium was aspirated followed by lifting of the cells under 37°C incubation with 2 ml of 0.25% (w/v) trypsin/EDTA for 3-5 minutes. Fresh medium was added (~5 ml) to the cell/trypsin solution and the resulting cell suspension was spun via centrifugation at 2000 rpm for 5 minutes. Upon retrieval of the cell pellet ~2 ml of fresh media was added and the cells were counted via a hemocytometer. Trypan blue (1:1 v/v) solution was used in order to

discriminate between live and dead cells. Following counting, a stock solution of cells was prepared.

2.3.2 Primary Cell: Rat Bone Marrow Derived Mesenchymal Stem Cells (MSC)

Rat (Sprague Dawley) mesenchymal stem cells (MSC) were purchased from LifeTechnologies thawed, and established according to manufacturer's specifications. Cells were cultured at a minimum initial seeding density of 3,000 cells/cm^2 in a 75-T TCPS flask in DMEM GlutaMax® medium supplemented with 10% (v/v) MSC qualified fetal bovine serum (MSC-FBS) at 37°C with 5% CO_2 and 95% relative humidity (RH). Medium was changed every 2-3 days. Differentiation of MSCs was carried out in osteoblastic medium (OB) consisting of αMEM GlutaMax® supplemented with 10% (v/v) MSC-FBS, 10^{-8} M dexamethasone (Dex), 10 mM β−glycerophosphate (β−GP) and 50μg/ml ascorbic acid (Asc) at the same culturing conditions as undifferentiated MSCs.

Cell passaging of MSCs (typically 2-3 days) was carried out when cell coverage of the 75-T flask was at 70-80%. Briefly, medium was aspirated cells were incubated at 37°C with 5 ml of TrypLE™ disassociation enzyme for 3-5 minutes. Fresh medium (~5 ml) was added to the cell/TrypLE™ and the cell suspension was spun via centrifugation at 1100 rpm for 5 minutes. Upon retrieval of the cell pellet, ~2 ml of fresh media was added and the cells were counted via a hemocytometer. Trypan blue (1:1 v/v) solution was used in order to discriminate between live and dead cells. Following counting, a stock solution of cells was prepared.

2.4. Substrate Preparation

Polymers poly(propylene fumarate) (PPF) and poly(butylene fumarate) were previously synthesized as previously described. (Chapter 3) Thin films of each polymer were prepared using a solution of 3wt% BAPO/g of polymer in a minimal amount of chloroform ($CHCl_3$) was added, followed by remove of $CHCl_3$ *in vacuo*. The viscous solution was cast via a drawdown machine using a 18x3 rod, and allowed to sit for 2-5 minutes. After casting of the polymer (PPF or PBF) the film was then subjected to UV light (λ = 365nm, UV Fusion®) to crosslink the film (15 passes at belt speed of 10 and 25% lamp, followed by 5 passes at a belt speed of 5 and 50%UV). Upon crosslinking, 6mm discs (thickness = 0.12 mm) were punched out and collected using a biopsy punch. Samples were then attached to the non-TCPS well plate by adding a dap of grease to the bottom of the well prior to adding the film to the well.

2.5. Cytotoxicity Extraction Assay of Monomers, PBF and crosslinked PBF

Cytotoxicity is assessed in the form of an extraction assay, where evaluation is performed in order to assess the cytotoxicity potential of any leachable materials to be cytotoxic. The starting materials as well as resulting polymer and crosslinked network (MA, BD, BAPO, grease, PBF and crosslinked PBF) were each placed in individual wells in a 6 well TCPS well plate. Monomers were incubated at 1 mmol/mL media, while the grease and PBF were incubated at 2 cm^2/mL media under normal cell culture conditions for 24 hours. Prior to performing the extraction assay, MC3T3-E1 cells were harvested from 75-T flasks using 2 mL trypsin/EDTA

per flask. Cells were counted using a hemocytometer and a stock solution of cells was prepared to obtain a seeding density of 8,000 cells/cm^2. Cells were seeded in a 96 multiwell TCPS plate. Following 24 hr cell culture in regular medium, medium was aspirated and replaced with extracted media at 100, 10 and 1 % (v/v) for n = 5 at each dilution (Figure 5.2). Cell viability was tested using LIVE/DEAD® Viability/Cytotoxicity kit for mammalian cells per the manufacturers' specifications and cell images were obtained. The commercially available assay uses calcein AM and ethidium homodimer-1 to fluorescently stain live and dead cells, respectively. Calcein AM is cleaved by live cells, producing a cytoplasmic green fluorescence and ethidium homodimer-1 stains nucleic acids, allowing for those cells with compromised membranes to be stained red.[20]

2.6. Cell Attachment

Crosslinked films (PPF, PBF, PPFcPM and PBFcBM) (n=5) were washed with DPBS (5 ml, 2×) to remove any debris, followed by placement in a 96 non-tissue culture polystyrene (non-TCPS) well plate adhering the substrates to the well using a small dob of grease on the underside of the substrate. Cells, MC 3T3-E1, were cultured using the conditions stated in the cell culture section. Once cells were 80-90% confluent, they were lifted using trypsin/EDTA (2ml/75-T flask), counted using a hemocytometer, and diluted with culture media to obtain a seeding density of 25,000 cells/well. After 24 hrs of culture, attachment and cytocompatibility was evaluated through the use of brightfield imaging and LIVE/DEAD® Viability/Cytotoxicity kit for mammalian cells.

2.7. *Osteogenic Differentiation of MSCs*

2.7.1. Substrate Seeding with MSCs

After establishing and splitting the rat MSCs cells were counted using a hemocytometer and diluted with media in order to obtain a seeding density of 1,000 cells/cm^2.[21] Crosslinked films of PPF and PBF (each formulation had n= 75) were rinsed (3×) with DPBS to remove any debris, followed by adhering to a non-TCPS 96-well plate (using a dab of grease between the well plate and crosslinked polymer film). Once films were adhered to the wells, samples were sterilized by exposure to UV for 30 min, and finally rinsed with DPBS before seeding with MSCs. Cells underwent normal culturing conditions (37°C, 5% CO2 and 95 % RH) in DMEM GlutaMax® medium for 24 hours, after which the medium was aspirated and replaced with osteoblastic (OB) media which was replaced every 2 days for the duration of the study. Time points which were evaluated in this study were at 2, 4, 7, 11 and 14 days from the start of OB medium conditions (24 hours after seeding). In addition to the seeded substrates, control plates (minus substrates) of 96-well TCPS plates were also seeded with MSCs and treated as MSC/substrate plates.

2.7.2 Cell Viability and Proliferation

The colorimetric MTS assay was used to evaluate cell viability and proliferation. Briefly, 20μl of assay solution is directly added to the 100μl of cell/medium solution and incubated in the dark at 37°C for 4hrs. Upon completion of incubation the absorbance of each well was read at 490 nm. The absorbance

reading is a direct measurement of living cells, as the MTS tetrazolium salt is converted only to a soluble formazan product by those cells that are viable. Cells were evaluated after 2, 4, 7, 11 and 14 days in contact with OB medium.

2.7.3. Alkaline Phosphatase (ALP) Activity

The enzyme ALP is a cellular enzyme that can be measured in living cultures and is expressed early on in osteogenic differentiation.[22] The ALP protocol followed is specific to the Dirk Lab and is a compilation of previous established techniques.[23, 24] Briefly, the culture medium was aspirated and the wells were carefully washed 3× with 100 μl of DPBS. Cells were than lysed by adding 100ul of 1% (v/v) Triton X-100 to each well followed by incubation for 60 min while on ice. Upon completion of lysis, 30 μl of the lysate was transfer to new wells of a TCPS 96-well plate. To this lysate was added 50 μl of 2-amino-2methyl-1-propanol (2A2M1P) and 50 μl of 40mM 4-nitophenol phosphate hexahydrate (4-NPP) substrate was added. Absorbance readings were measured at 405 nm at 15, 30 and 60 minutes during incubation at room temperature (RT) and this reading is a resultant of the ability of ALP to convert the substrate (4-NPP) to p-nitrophenol (p-NP). A standard curve is also constructed using p-NP serial dilution. Samples were evaluated after 2, 4, 7 and 11 days in contact with OB medium.

2.7.4. Calcium Mineralization

The anthriquinone dye alizarin red S (ARS), is used to evaluate matrix deposited calcium mineral content by forming a complex via chelation. Mineral

deposition was evaluated and quantified following the protocol described by Gregory et al.[25] Briefly, culture medium was aspirated, wells were rinsed 3× with DPBS followed by fixation using ice cold 70% (v/v) ethanol (EtOH) for 1 hour. After fixation, 30 μl of 40 mM ARS staining solution (pH 4.1-4.2) was added to each well and incubated for a minimum of 30 minutes in the dark at room temperature (RT). Upon completion the ARS solution was aspirated and the wells were rinsed 5× with dH20 and 3× with PBS in order to ensure removal of non-specific ARS stain. Samples were briefly visualized under brightfield and than underwent a dye extraction in order to quantify the amount of staining and therefore calcium content. ARS was extracted from the cultures through the addition of 100μl 10% (w/v) cetylpyridinium chloride (CPC) in 10mM Na_2HPO_4 buffer for 1 hour at RT. Upon completion of incubation with CPC the solution was moved to a new TCPS plate and the absorbance was read at 550 nm. Samples were evaluated after 4, 7, 11 and 14 days in contact with OB medium.

3. Results and Discussion

3.1. Evaluation of Cytotoxicity

The potential utility of crosslinked PBF films as a tissue engineering scaffold material was further evaluated using the extraction cytotoxicity assay of the monomers, the polymer itself, and crosslinked polymer. These extraction assays are used to assess whether there were any leachable products that would be toxic to surrounding cells. Serial dilutions of extraction medium, or medium which had been exposed to either maleic anhydride, 1,3-butylene glycol (BG), PBF and crosslinked

PBF solid substrates (MA, BG, BAPO, PBF and crosslinked PBF) were used to carry out this assay.

Extracted media was mixed with culture media at levels of 100, 10, 1 and 0 μl (v/v) followed by incubation at cell culture conditions for 24 hours as outlined by Timmer *et al*.[2] Cells exposed to high concentrations of 1,3-butane diol (BD) appeared to have altered morphology of the cells when exposed to extraction media. This is likely a result that the BD was miscible with the extraction media and as a result the MC 3T3-E1 cells were exposed very high concentrations of BD over the entire 24 hour incubation period, unlike the other "extracted" media incubations. To further assess cell viability a LIVE/DEAD ® Viability/Cytotoxicity kit for mammalian cells was performed. All 24 hour cell incubations with the extracted media rendered only viable cells, indicated by green, and no non-viable cells were observed, stained red (Figure 5.3). Although MC3T3-E1 cells exposed to 100 μl of extracted BD media had a rounded morphology, upon fluorescent staining of the cells there were no dead cells observed within the sample (lack of red fluorescence) (Figure 5.3). The fewer number of cells observed in this extraction condition (exposure to BD) and lack of dead cells may indicated that the dead cells were washed away prior to staining.

The results indicate that there is nothing cytotoxic leaching out of the PBF, the crosslinked PBF or BD that is toxic to the cells. Cells were evaluated under brightfield and fluorescent imaging to assess cell morphology and spreading, as they are an indicator of cellular function on a surface. Comparison of cultured cells incubated with monomers and polymers to those which were cultured with 0 μl

extracted media show that the cell line MC-3T3 behave as they do on TCPS under normal culturing conditions (Figure 5.2).

3.2. Attachment of MC3T3-E1 to Crosslinked Polymer Substrates

In addition to the extraction assay with MC3T3-E1, attachment on crosslinked solid PBF films was examined. The murine cell line was seeded on the PBF films at a seeding density of 25,000 cells/well and cultured at cell culture conditions for 24 hours. Cells seeded on PBF substrates were than imaged using the fluorescence-based LIVE/DEAD® assay according to manufacturer's protocol in order to observe the cell viability, where viability is visualized based on membrane integrity. PBF synthesized from MA allow for cellular attachment (Figure 5.4). The crosslinked PBF films fluoresce due to incubation with the dyes used in the LIVE/DEAD® kit and create a background fluorescence, this is seen in the images taken with the Nikon TS100.

3.3. Attachment, Viability and Osteogenic Differentiation of MSCs

3.3.1. Attachment and Viability

Prior to the start of the 2 week study, seeding efficiency of MSCs on the crosslinked polymeric network of PPF and PBF was evaluated. Cells were seeded at 1,000 cells/ cm^2 followed by incubation at 37°C, 5% CO_2 and 95% RH for 24 hours. After 24 hrs, cells were fixed via 1% (v/v) formaldehyde and stained with 4',6-diamidino-2-phenylindole dihydrochloride (DAPI), a nuclear stain, to visualize cell location (Figure 5.5). Cell attachment to TCPS compared to crosslinked PPF and

PBF films is greater by ~1.5-2× higher as indicated in cell number at Day 2 (Figure 5.5). However each seeding environment, including PPF and PBF crosslinked films, provide a suitable environment for the anchorage-dependent MSC cells.

Cell viability, as assessed by the colormetric bioreduction of MTS tetrazolium salt to formazan, shows a similar trend across all samples. Figure 5.6 shows a peak in cell number at day 4, followed by a decline at day 7 – 14. A possible reason for this could be due to the inclusion of 10^{-8} M dexamethasome (Dex), although this synthetic glucocorticoid is required in osteoblastic media (OB) to promote mineralization, it has also been seen to have an apoptotic effects on MSC cultures.[26] In addition, contact inhibition has been reported to suppress cell proliferation and is surface area dependent.[27] This may be the cause of our decrease at seen at Day 7 following the rapid proliferation from Day 2 to Day 4 (Figure 5.6).

3.3.1. Evaluation of Alkaline Phosphatase (ALP) Activity

The enzyme-catalyzed reaction operates by removing a phosphate from the substrate (4-nitophenol phosphate hexahydrate, 4-NPP), generating free phosphate (P_i) and the chromophore p-nitrophenol (p-NP) (Figure 5.7). The yellow colored p-NP has a maximum absorption at 405 nm and Beer's Law can be used to calculate the ALP concentration:

$$\text{ALP Activity} = \left(\frac{(A_{60}\text{-}A_0)\ (1000)\ V_{rxn}}{T_{rxn}\ (\varepsilon)(l)\ V_{sample}} \right)$$

The modified equation, is used to calculate the concentration of enzyme (ALP) over the 60 minute kinetic study where the absorbance (A) is equal to the A at t = 60 min

minus A at t = 0 min, the reaction volume (V_{rxn}) is 130 μl (substrate + lysate + buffer), the sample volume (V_{sample}) is 30 μl (lysate), the extinction coefficient (e) at 405 nm for p-NP is 18.5 $mM^{-1}cm^{-1}$,[28] the path length (l) is 1 cm and the reaction time (T) is 60 minutes. This equation provides ALP activity in μmol/L*min, or IU/L and can than be divided by the cell number obtained via MTS to obtain activity of ALP in IU/L per cell.

As seen in Figure 5.7, the ALP activity in MSCs with osteoblastic media (OB) peak at Day 7 and than decreases by Day 11. This is in contrast to cells that are cultured on PPF and PBF, were a significant increase over the control is seen on Day 2, peaking earlier than those MSCs cultured on TCPS, followed by continuous decline observed from Day 4 – 11 (Figure 5.7). Previous studies indicate that initial osteoprogenitor cell proliferation is rapid, leading to an increased production of extracellular matrix (ECM), followed by a decrease in proliferation, as we observed in these results (Figure 5.5) as well as an upregulation of ALP expression.[27, 29] There are two controls of this assay, MSCs seeded on the TCPS 96-well as well as the MSCs seeded on PPF crosslinked films. Both PPF and PBF show a similar trend and expression of ALP, where there is a significant difference seen on the TCPS controls. It has previously been reported that the cell density has an effect on ALP expression[27], with a lower density displaying an enhanced expression. This could account for the observation of PPF and PBF having an increased ALP expression over TCPS as the initial cell attachment at Day 2 was ~20,000 and ~35,000 to 40,000, respectively (Figure 5.7).

3.3.1. Evaluation of Matrix Mineralization via Alizarin Red S (ARS)

Dexamethacsome (Dex) is used in osteoblastic media, as it is necessary to promote mineralization. Prior research has demonstrated that ALP expression will still be observed, but mineralization will not occur unless the media is supplemented with the synthetic glucocorticoid.[18] The ARS staining is extremely versatile in that it can be observed optically (qualitative) as well as extracted using cetylpyridinium chloride (CPC) and the absorbance read it 550 nm (quantitative). The ARS salt forms a complex through chelation with calcium that has been deposited as a result of osteogenic differentiation.[30]

Brightfield images demonstrate significant matrix mineralization as seen by red staining seen in representative images at Day 11 (Figure 5.8**)**. The calcium extracted by CPC per well is calculated and is reported as mg/well (Figure 5.9). The amount of matrix deposition on crosslinked PBF is similar to the control of crosslinked PPF, whereas both PPF and PBF are significantly higher than the matrix deposition on in the control wells of TCPS. The increase in matrix deposition on PPF and PBF over the control could be attributed to the increased proliferation seen in PPF and PBF samples (Figure 5.5 and 5.7) and the possible increase in ECM in these samples versus the control TCPS sample.

4. Conclusions

In this chapter we present the cellular response of the novel polymer poly(butylene fumarate) (PBF) as synthesized in Chapter 3. The cytotoxic potential was evaluated via a solution based extraction method (non-direct contact) and it was

shown that there were no leachable products that could provide potential cytotoxic effects. In addition to the attachment, proliferation and viability of the pre-osteoblastic murine cell line MC3T3-E1, bone marrow derived mesenchemyl stem cells (MSCs) were used to determine the osteoconductive (supporting bone formation) potential of PBF compared to the widely explored poly(propylene fumarate) (PPF). The results of this study reveal that PBF behaves similarly to PPF and *in vitro* culture conditions indicate that the new biomaterial will support attachment as well as serve as an osteoconductive platform for the use in bone tissue engineering applications.

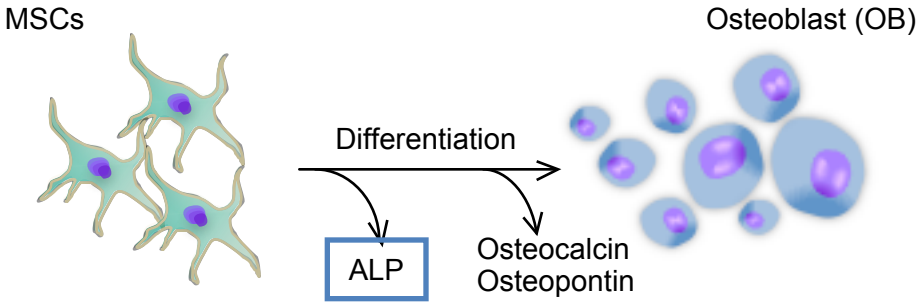

Figure 5.1. Schematic illustration of mesenchemyl (MSCs) undergoing osteogenic differentiation and the early signal (ALP) and later (osteocalcin and osteopotin) enzymes.

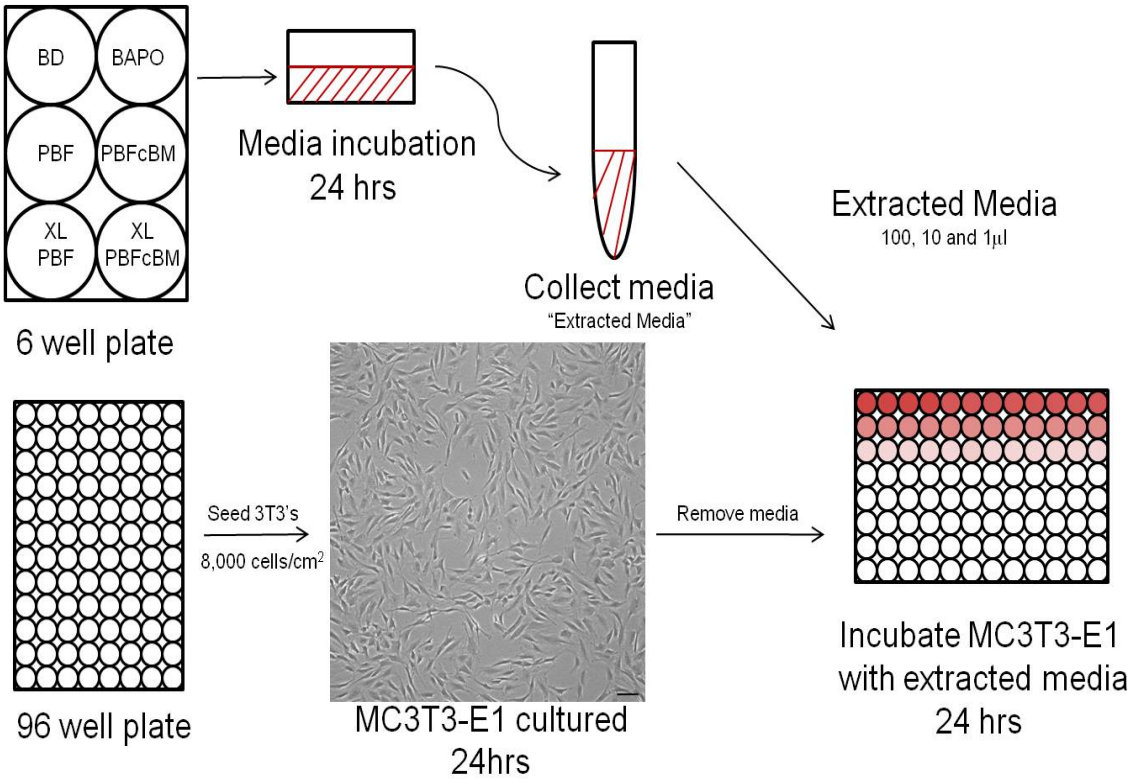

Figure 5.2. Schematic representing cytotoxicity protocol. Each of the monomers, polymers and crosslinked polymers were incubated in media under normal cell culture conditions. After 24 hrs, the media (extracted media) was removed and saved for later use. In parallel, MC3T3-E1 cells were seeded onto TCPS. At ~80 % confluence the cell culture media was removed and replaced with varying concentrations of the extracted media (100,10 and 0%).

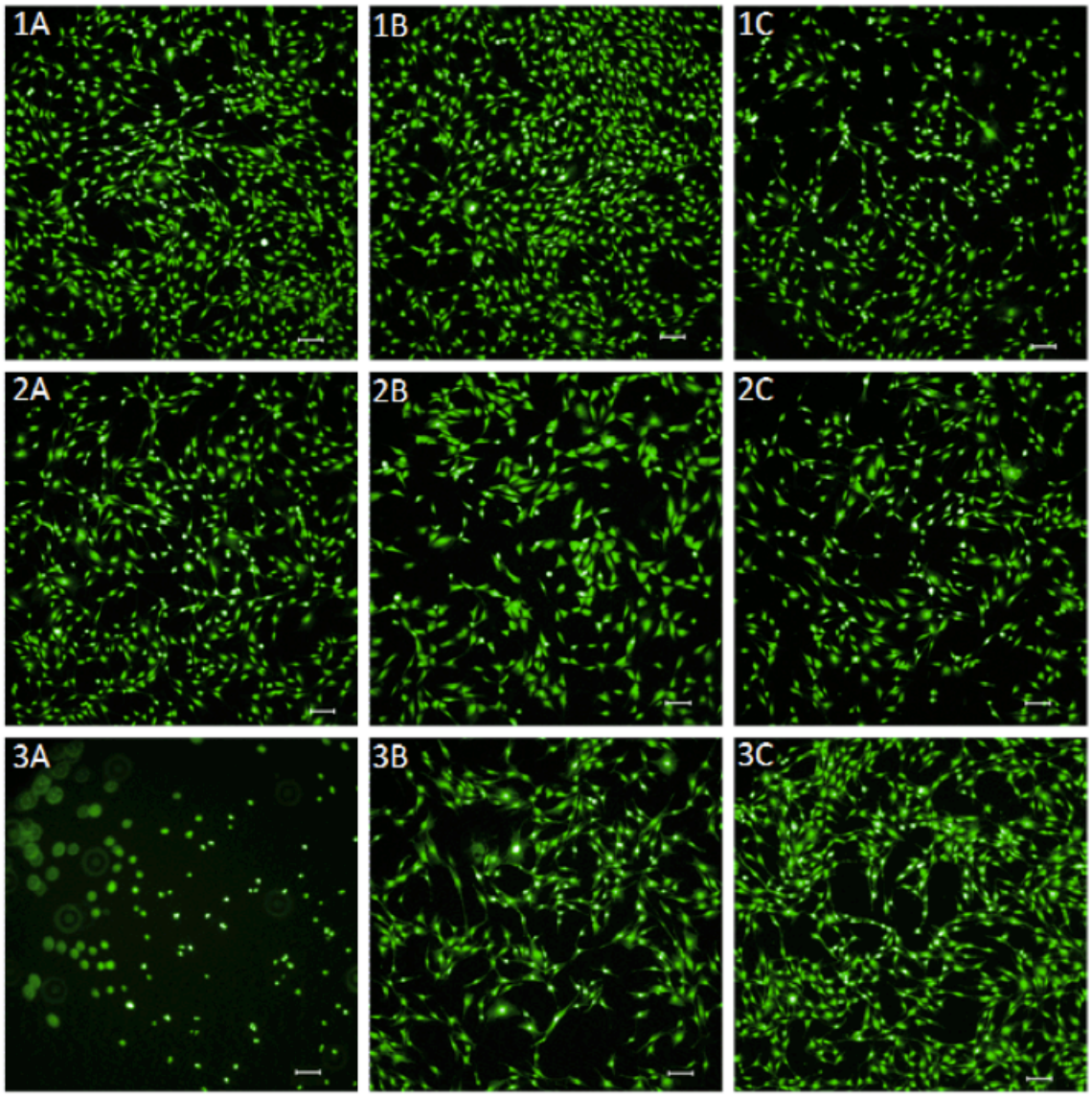

Figure 5.3. Viability assessment of MC3T3-E1 cells with extracted media post incubation imaged through the use of Epifluorescence (Invitrogen LIVE/DEAD®) where green represents viable cells and red represents dead cells, the image has been false colored to represent this. 1A-C) crosslinked PBF solid substrates, 100μl, 10μl and 1μl (respectively) 2A-C)PBF polymer, 100μl, 10μl and 1μl (respectively) and 3A-C) butanediol at 100μl, 10μl and 1μl (respectively). All scale bars are 100mm.

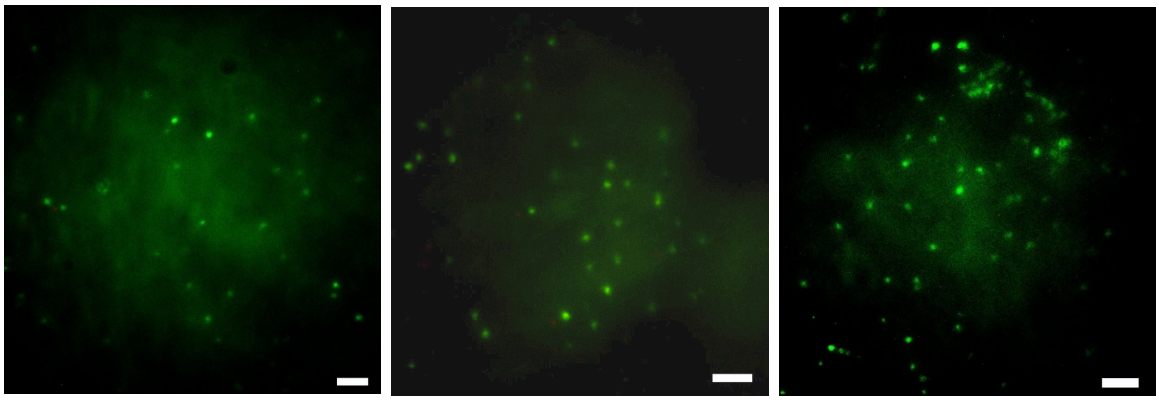

24 hrs 3 Days 5 days

Figure 5.4. MC3T3-E1 seeded on crosslinked solid PBF thin films, analysis performed by LIVE/DEAD® at 24 hrs, 3 and 5 days (left to right). Where green represents viable cells and red represents dead cells, the image has been false colored to represent this. Scale bar represents 100µm.

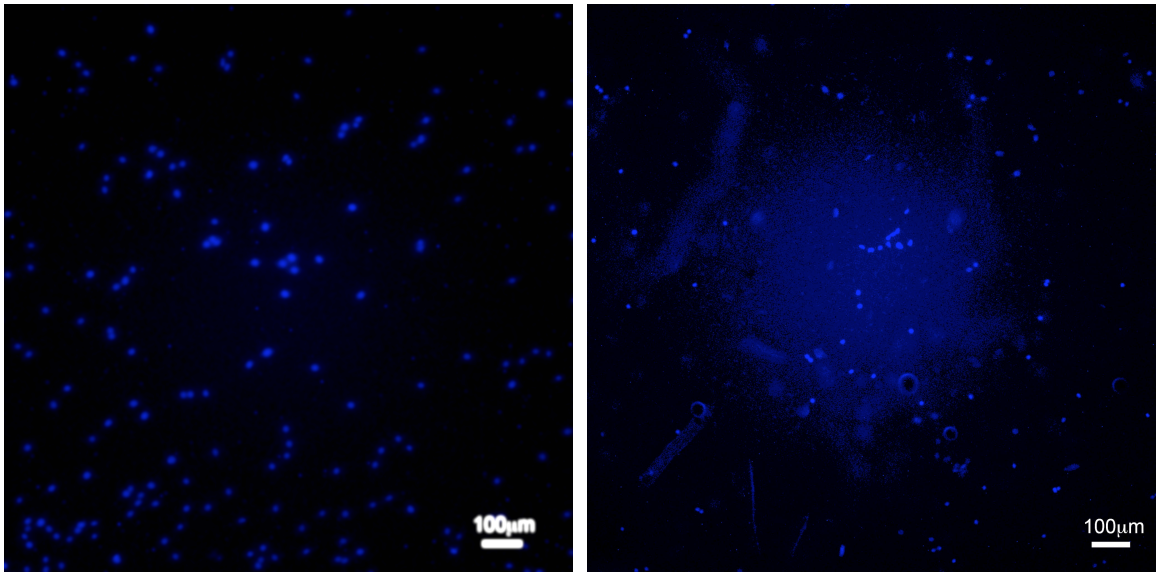

Figure 5.5. MSCs seeded on TCPS (left) and polymeric substrate (right) and incubated in culture for 24hrs, followed by staining with the nuclear stain DAPI to determine location. Cells are false colored blue and the scale bar is 100um.

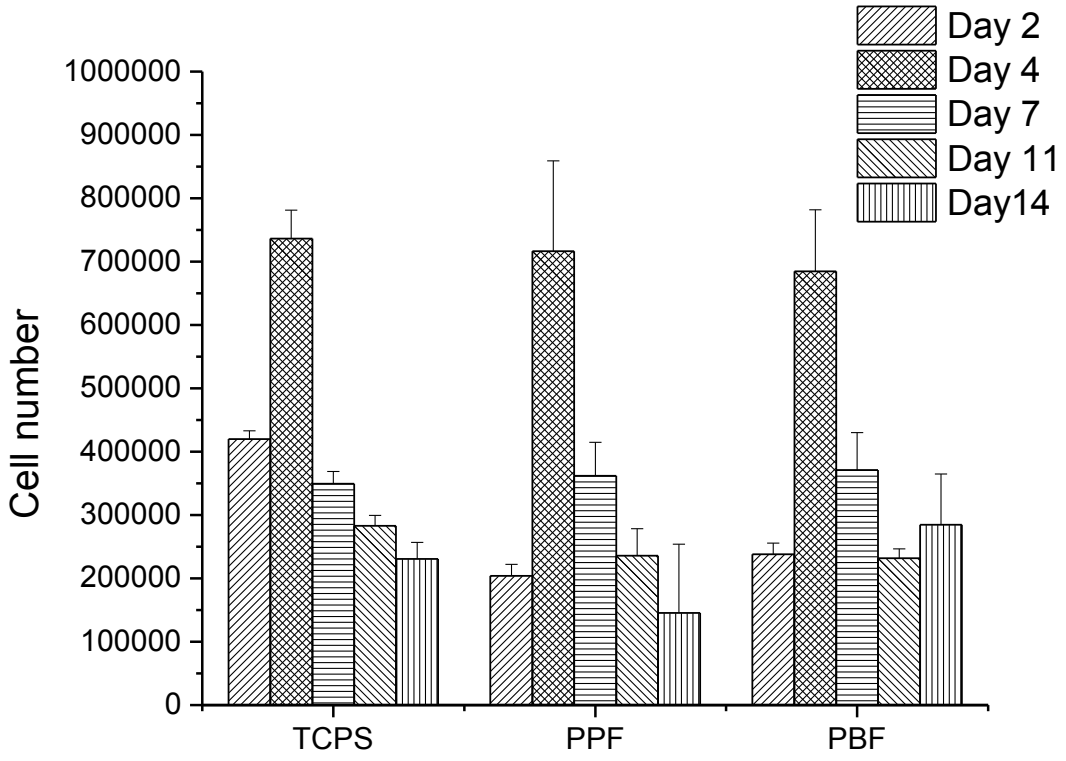

Figure 5.6. Cell viability as measured by the conversion of MTS tetrazolium to the soluble formazan product. The quantity of formazan is measured by the absorbance at 490 nm and is directly proportional to the living cells in culture.

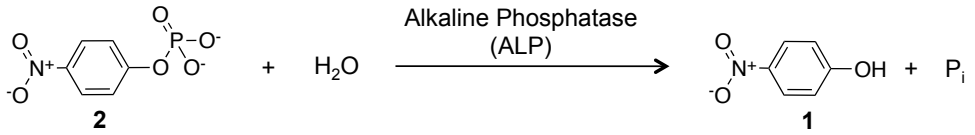

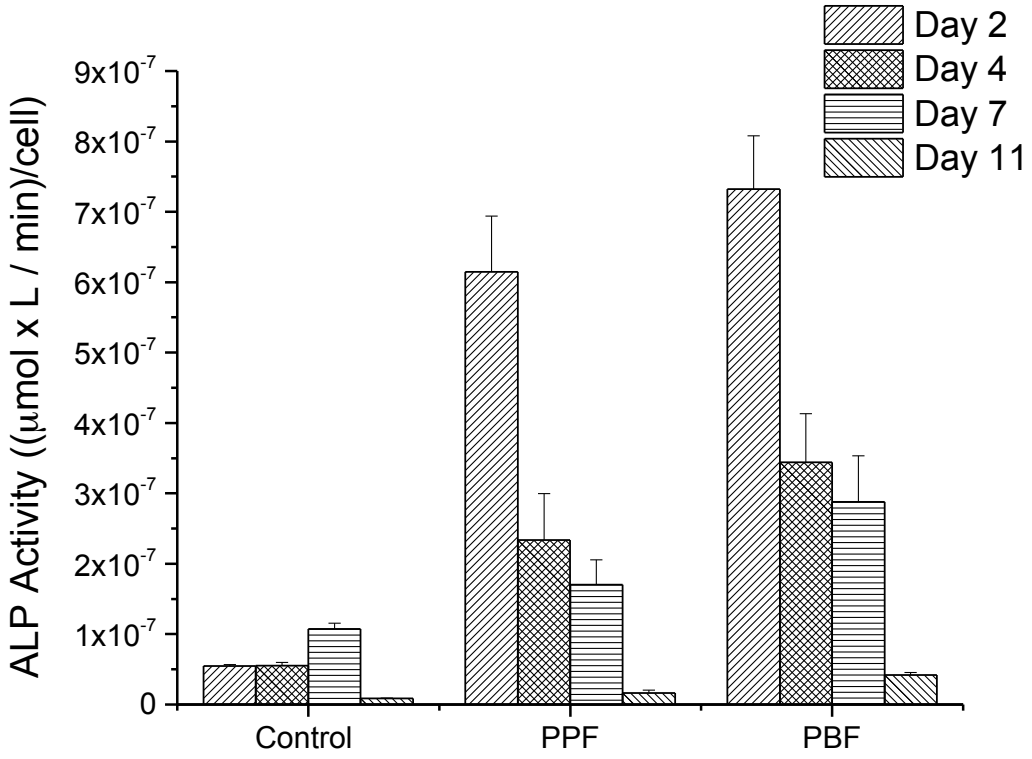

Figure 5.7. The enzymatic (ALP) driven assay removes a phosphate from the substrate 4-nitophenol phosphate hexahydrate (4-NNP, 2) to produce p-nitrophenol (p-NP,1) (Top scheme). The absorbance of chromophore p-NP at 405nm over a period of 60 minutes can be used to generate the ALP activity (bottom).

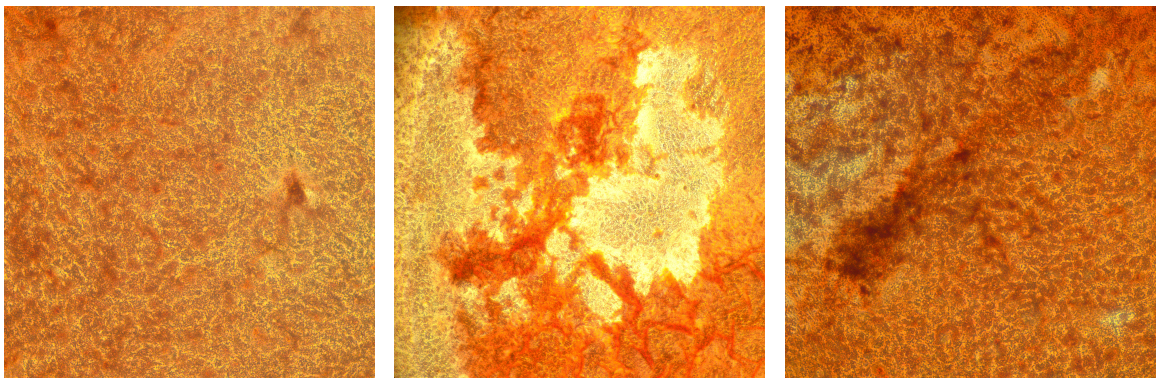

Figure 5.8. Representative brightfield images of ARS stained cultures from left to right, MSCs on TCPS, crosslinked PPF and crosslinked PBF substrates (pictured Day 11). Images at 20X.

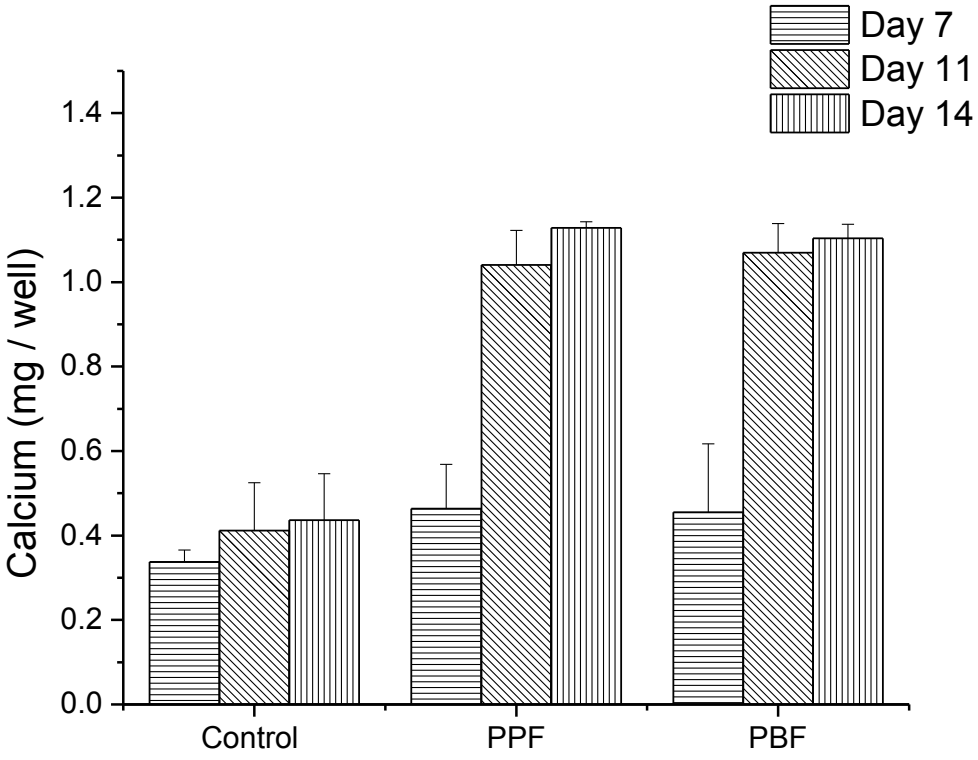

Figure 5.9. CPC extraction of ARS after briefly imaging is used to calculate matrix deposited calcium in mg per well.

Chapter 6. Method Development for Fabricating 3D Crosslinked Polymer Networks via Electrospining and Projection MicroStereolithography

1. Introduction

An important component of the tissue engineering (TE) paradigm lies in the construction and design of the scaffold. The scaffold serves as a 3D template for cell attachment, migration and proliferation as well as tissue formation.[1, 2] To be successful, a TE scaffold must possess these basic properties: 1) it must be biocompatible/biodegradable, 2) display degradation products which can easily be expelled from the body, 3) contain high porosity, 4) be comprised of interconnected pores, 5) display a microstructure to mimic the micro-environment, and finally 6) have suitable mechanical properties for the tissue being repaired/regenerated.[3, 4] Many processing techniques have been explored in for many different applications in the field of TE. In addition to the aforementioned minimum criteria of a TE scaffold, bone TE (BTE) applications require the scaffold to have a porosity ≥ 90%, display pore sizes of 200-400μm and have mechanical properties similar to the bone that is being repairied/regenerated (trabecular/cancellous and cortical bone).[4-8]

Currently, the only polymer system which meets the mechanical requirement is the fumarate-based unsaturated linear polyester poly(propylene fumarate) (PPF), poly(butylene fumarate) (PBF) and their copolymers, which have low glass transition (T_g) temperatures an can be crosslinked thermally or photochemically through the carbon-carbon double bone in the polymer backbone.[9] These material properties allows for various fabrication techniques to be implemented, those which are preformed prior to implantation or as an injectable system to be crosslinked *in situ*.[10]

Several techniques have been employed to fabricate 3D scaffolds of crosslinked PPF for tissue engineering applications including porogen or solvent leeching[8, 11], freeze-drying[12], poly HIPEs[13] and multiple stereolithography.[14-17 18] However, this chapter focuses on developing methods to produce 3D scaffolds of fumarate-based polymers that have not had success to date. These two methods are electrospinning and projection micro-stereolithography (PμSL).

Electrospinning, first introduced as early as 1934[19] regained popularity in the mid 90s.[20] In contrast to dry or melt spinning, electrospinning uses electrostatic forces to stretch a solution as it solidifies, allowing for continuous nano to micron sized films to be fabricated. Currently there are two standard electrospinning setups, vertical or horizontally fed, that consist of 4 major components.[21] As seen in Figure 6.1, the standard or generic setup, regardless of orientation, includes: 1) a syringe pump (to deliver the solution), 2) a spinneret (nozzle or needle where solution erupts from), 3) a DC high voltage source (to allow for solution charging) and 4) a grounded collection plate (for deposition of fibers). Many research groups have looked to alter the standard electrospinning set up to produce non-woven highly porous mats for use in TE applications. The resulting fiber size scale provides a scaffold that mimics that of the native extracellular matrix (ECM). Although electrospinning offers a very versatile and inexpensive fabrication technique for creating high surface area to volume scaffolds, there are current limitations and drawbacks that are associated with the technique. The generation rate of electrospun mats compared to the industrial fiber spinning technique speed of production is much less at ~30 m/min compared to 200-1500 m/min.[22] In addition, a

caveat to this system is that solid polymers are needed to create continuous solid fiber deposition. A few techniques to spin low glass transition (T_g) polymers have been developed and require a carrier polymer or a specialized spinneret to produce core-sheath fibers (low viscosity and/or liquid polymers encased by a sheath).

Stereolithography, first termed by Hull in 1986[23], is a general term used to describe printing of layers successively in order to render a three dimensional polymer structure with the assistance of a computer aided design (CAD). Many common terms used to describe this process of rapid prototyping (RP) have been coined, including three dimensional (3D) printing. The RP technique can generate complex 3D structures with finely controlled attributes (size, shape porosity and pore size), however the versatility comes at a cost. An alternative form of 3D printing with the ability to rapidly make micron sized features from photo-curable polymers that has recently been identified is projection micro-stereolithography (PμSL).[24] This technique uses the available UV light from a commercial LCD or DLP projector[25] to activate a highly effective photoinitiator. The printing can be repeated repeatedly when combined with a z-stage to create 3D structures. The cost of this setup is much less than the tradition $100-500K price tag associated with other RP techniques.

In this chapter we have developed methods in order to use the fabrication techniques of electrospinning and PμSL to created scaffold of fumarate-based polymers. Synthesis of low molecular weight oligomers from diethyl fumarate (DEF) and propylene glycol (PG) or glycerol have provided less viscous starting materials over the traditionally synthesized fumarate-based materials. Thereby overcoming

the limitation of PμSL and being able to pattern these fumarate-based oligomers in combination with the photoinitiator phenylbis(2,4,6-trimethylbenzoyl)-phosphine oxide (BAPO). Although electrospinning is a simple technique producing nanometer to micrometer diameter fibers, there are many variables which effect the resulting fibers.[26] However, traditionally synthesized fumarate-based materials with low T_g's have not seen success in spinning. Previously low T_g materials such as polybutadiene and acrylic copolymers have been spun through the us of a carrier polymer or post UV crosslinking after spinning.[27, 28] Our technique uses a one-step *in-situ* crosslinking of fumarate-based polymers and copolymers with BAPO, by including a UV lamp in the generic electrospinning setup.

2. Materials and Methods

2.1. Chemicals and Reagents

Propylene glycol (ReagentPlus®, 99% PG), glycerol(≥ 99%) and phenylbis(2,4,6-trimethylbenzoyl)-phosphine oxide (BAPO) were purchased from Aldrich. Diethyl fumarate (98%, DEF) and *p*-toluensulfonic acid (TsOH) were purchased from Acros Organics. All chemicals were used as received.

2.2 Equipment

Modified electrospining setup, consisting of syringe pump (KD scientific, model 100s), high voltage supply (Glassman High Voltage, Series EL), stainless steel blunt tip needles (SmallParts, SSB), grounded collection plate (Cu fitted with Al foil) and a hand held UV source (UVP, Blak-Ray longwave ultraviolet lamp, model

B100AP) was constructed in house. A modified projection microstereolithography (PμSL) setup was designed, consisting of a DLP Projector (Acer Model DSV008), a converging lens (Edmund Optics), motorized XY stage and 2 computers (Dell). Scanning electron microscopy (SEM) was carried out using a Zeiss Supera 55VP and a FEI DB235. Optical images of fabricated scaffolds were captured using an OmniScope.

2.3. Synthesis of Low Molecular Weight Polymers

Propylene glycol (PG) or glycerol, diethyl fumarate (DEF) (2 or 3 equivalents, respectively) and *p*-toluensulfonic acid were added to a 100 mL round bottom flask equipped with a stir bar and distillation head. The reaction mixture was heated to 250°C with stirring until the distillate was collected. Upon completion of the distillate collection the reaction was allowed to come to RT.

2.4. Polymer Processing Techniques

2.4.1. Electrospinning

2.4.1.1. General Procedure

All polymer solutions were delivered at a constant rate via a syringe pump through a syringe fitted with a stainless steel blunt tip needle. The needle was charged through a high voltage supply, and the resulting polymer fibers were collected on a grounded target (6 x 6 in). A UV source (λ =365 nm) was used to crosslink the polymer in situ (Figure 6.2).

2.4.1.2. Electrospining of Poly(Propylene Fumarate) (PPF) and Poly(Butylene Fumarate) PBF

A 2-mL plastic syringe [inner diameter (ID) = 4.64mm] equipped with a 20 gauge (g) x 1.5 in. stainless steel blunt tip needle was used to deliver solutions of polymer dissolved in chloroform (40, 50, and 60 wt %) at a volumetric flow rate of 0.2 mL/hr and a voltage difference of 1 kV/cm from needle tip to collection plate.

2.4.2. Projection MicroStereolithography (PμSL)

2.4.2.1. General Procedure

The PμSL apparatus is comprised of 1) a computer containing the corresponding PowerPoint® slide of black and white images to serve as the "mask" for printing the specified geometries, 2) a DLP projector, 3) a converging lens with 15 cm focal distance and finally 4) a stage which a silicon chip is placed to serve as a substrate to print the structure on to (Figure 6.3).

2.4.2.2. Patterning of LMW Polymers via PmSL

The initiator (phenylbis(2,4,6-trimethylbenzoyl)-phosphine oxide (BAPO)) was dissolved into the liquid monomer (3 wt%). The polymer solution was placed in a 150-mL beaker and the stainless steel platform was lowered into the solution. A series of black and white images were created in PowerPoint®, this creates the "mask" to use for patterning (Figure 6.4). Upon completion of the first crosslinked layer, a stepper controls lowered the newly formed polymer structure into a beaker to expose a new uncrosslinked polymer layer. With successive exposures, a 3D

structure was produced. The structure was than removed from the stainless steel stage and rinsed with water, followed by continued crosslinking via exposure to a UV source (λ=356 nm).

3. Results and Discussion

3.1. Electrospinning of Low T_g Polymers

Previously, PPF has been fabricated into highly porous structures with large surface to volume ratios by the Minkos and Yazemski groups by sovent casting/salt leaching and high internal phase emulsion (HIPEs).[29] Here, we present the fabrication of high surface area to volume scaffold fabricated through the established electrospinning technique. Electrospinning is also a very favorable and attractive technique for fabricating scaffolds for TE applications as it produces a network of fibers that mimic the biologically relevant extracellular matrix (ECM) environment *in vivo*. Traditionally low T_g as well as low viscosity polymers have been spun through the use of a carrier polymer[30-32] and the use of a coaxial needle to incorporate the "hard to spin" material as the core in a core/sheath design.[33, 34]

Initial attempts to electrospin PPFcPM were performed by making polymer/chloroform ($CHCl_3$) solutions of 40, 50 and 60 wt% in order to determine what concentration was needed in order to spin continuous fibers at 1kV/cm. Regardless of the polymer solution spun, fibrous mats were not produced when the low glass transition (T_g) polymer was spun. Instead there was a polymer self-calendaring effect that was observed (Figure6.5). Attempts to reduce the self-calendaring effect were seen in reduction of the flow rate from 0.5 ml/hr to 0.1 ml/hr,

however the polymers flow at room temperature (RT) due to the low T_g still was observed via scanning electron microscopy (SEM) still revealed self-calendaring.

Final attempts to produce a 3D fibrous network that did not self-calendar made use of the fact that the polymer can be crosslinked with the use of a photoinitiator. However, pre-crosslinking the polymer initiator solution prior to spinning was not possible as it would no longer be soluble in solvent and therefore could not be spun. PPF has previously been crosslinked using acyl phosphine oxides as the photoinitiators, as they are known to undergo a rapid alpha cleavage. Either benzyl or BAPO were incorporated at 3 wt% (g/polymer) into the PPFcPM at the 40, 50 and 60 wt% polymer/CHCl3 solution. Both solutions (benzyl/PPFcPM or BAPO/PPFcPM) were spun using the same aforementioned parameters and elctrospinning set up, with the addition of a hand held UV lamp (l= 365nm). Previously electrospun mats have been crosslinked via a post processing step, collection of fibers is done followed by crosslinking.[28] In contrast, a UV source allowed for crosslinking *in situ* due to the location of the lamp as the fibers were being spun as well as a post 15 min exposure after fiber collection.

The benzyl/PPFcPM solution still produced self-calendaring fibers, presumably this was due to the generation of to few radicals being produced during fiber formation. In contrast, the BAPO/PPFcPM solution was able to form a fibrous mat. Although a mat was formed, after 0.1 ml was delivered the crosslinked polymer formed pillars (Figure 6.6). It was determined that the pillar formation was a result of increased viscosity due to partial crosslinking of the spinning solution as a result of the UV light being reflected off the aluminum foil on the collection pate back to the

syringe. To combat the problem of increasing solution viscosity, the syringe was shielded and in turn a non-calendared crosslinked PPFcPM mat was produced free of pillars (Figure 6.7).Using ImageJ®, 30 random fibers in the SEM image were measured and averaged to determine the average fiber size to be 6.94 ± 3.64 μm.

Upon modifying the general electrospinning setup, with the addition of an *in situ* crosslinking capability, it was extended to spinning of PBF and PBFcBM. Briefly, the 3wt% BAPO/ g polymer in a 75 wt% $CHCl_3$ solution was spun using the same parameters as the PPFcPM mat production (0.1 ml/hr and 1kV/cm). Again, the butylene fumarate-based polymer of PBF produced a crosslinked porous mat with an average fiber size of 1.08 ± 1.1 um (Figure 6.8).

3.1. Patterning via PμSL

3.1.1. Synthesis

Previously synthesized fumarate-based polymers, poly(butylene fumarate) (PBF), poly(butylene fumarate)-*co*-(butylene maleate) (PBFcBM) as well as those from propylene glycol (PPF and PPFcPM) were synthesized from the ring opening polymerization (ROP) of maleic anhydride (MA), detailed in Chapter 3. These polymers were used to carry out the electrospinning experiments discussed here in, however the viscosity advantage that is desired in electrospinning is not favorable for carrying out projection microstereolithography (PμSL). Therefore, to overcome this, short chain fumarate-based monomers were synthesized by an acid catalyzed condensation reaction from propylene glycol and diethyl fumarate (DEF) (Scheme 6.1 A) and glycerol and DEF (Scheme 6.1 B). Both monomers were synthesized in

high yields.

3.1.2. Patterning of Fumarate-Based Monomers via PmSL

Prior to patterning with PμSL, solutions of monomer and BAPO were combined in order to determine the feasibility and utility for use and the ability to be patterned with PμSL using the BAPO initiator system. Here success was seen if the monomer/BAPO solution could be crosslinked (λ = 365 nm) in a reasonable time (≤ 5 minutes). Upon verification that the newly synthesized monomers would be suitable, solutions of BAPO/ monomer were stirred until all of the BAPO was in solution. Patterning was accomplished using PμSL, however with slight modifications to the PμSL setup described originally by Fang et al[24] was altered. Specifically, the 45-degree mirror was removed in order to remove trapezoidal distortions seen from the projector and enable larger areas to be projected directly into the solution. The differences in the PμSL systems can be seen in Figure 6.3, but the basic components of the apparatus are the same and is comprised of computer to display the PowerPoint slides, which served as exposure masks, an LCD data projector, magnifying glass (3×), beaker with photo-activated monomer solution and a z-stage with additional computer/controls.

The goal to using these fumarate-based monomers with the inexpensive PμSL technique is to produce 3D scaffolds for tissue engineering (TE) applications. Initial 3D structures were created using PowerPoint slides with a regular array of circles. After the first layer was printed, the array was off-set by half a period and reprinted. Repeating this process resulted in a 3D structure with interconnected

pores. The monomer/initiator solution was crosslinked for 90 seconds with each slice projection, and the stage was lowered by 50 μm after completed layer exposure. The 3D structure was removed from the stainless steel stage and rinsed with water. UV flood exposure continued to ensure the 3D structure was fully crosslinked. The structure was than evaluated via optical microscopy. The optical images were analyzed with the NIH ImageJ® software to determine the pore size of ~960 ± 1 μm (Figure 6.4).

4. Conclusions

Two fabrication techniques, electrospinning and projection microstereolithography (PμSL), have been utilized to produce random fibrous porous mats and 3D porous structures, respectively. Two new fumarate-based monomers were synthesized via the reaction of excess diethyl fumarate (DEF) with either 1,2-propylene glycol or glycerol. These monomers were of sufficiently low viscosity that they enabled easy patterning via a modified PμSL apparatus. Compared to other printing techniques, the PμSL approach offers an inexpensive, mask-less system for printing any low viscosity monomer or oligomer that can be polymerized or crosslinked via a photoinitiator.

Electrospinning of fumarate-based polymers, PPF and PBF, containing a highly active photoinitiator (BAPO) produced nano- and micro fibrous mats with *in situ* UV crosslinking. The technique should be applicable to all polymers with a T_g lower than room temperature, containing a photo crosslinkable functional group.

Scheme 6.1. Synthesis of acid catalyzed condensation reaction to produce fumarate-based monomers, from A) propylene glycol (2) and DEF (1) and B) glycerol (3) and DEF.

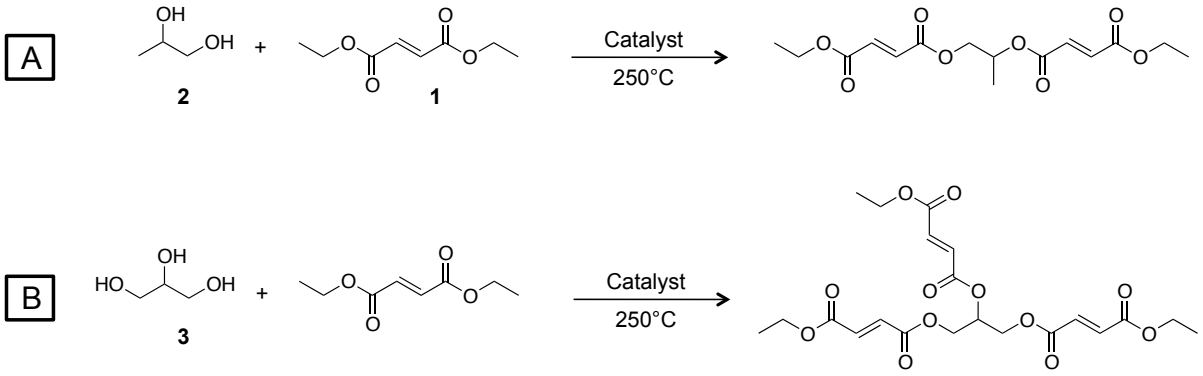

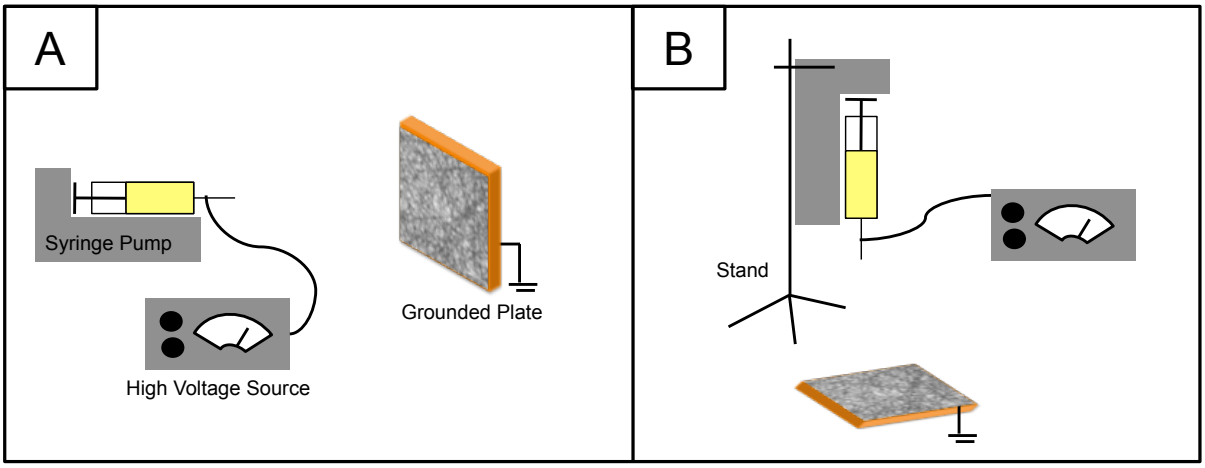

Figure 6.1. Schematic illustration of the two generic electrospinning setups, horizontally fed (A) and vertically fed (B). Both setups consists of a 1) syringe pump, 2) spinneret, 3) DC high voltage source and 4) copper grounded collection plate.

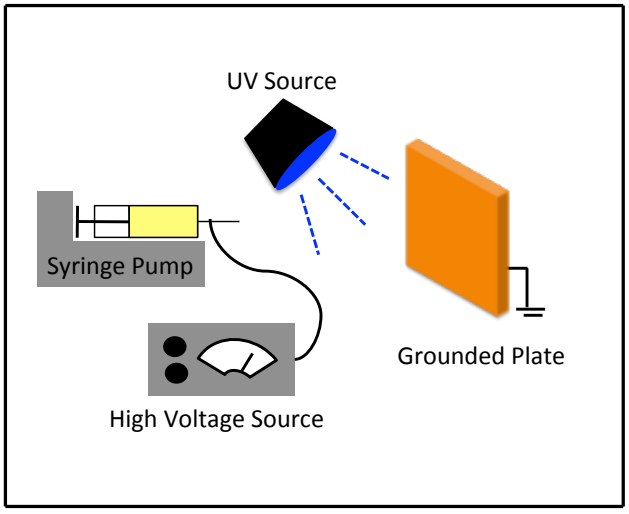

Figure 6.2. Schematic illustration of our in house modified electrospinning setup. Addition of a UV source allows for *in situ* crosslinking of a photoinitiator loaded polymer solution.

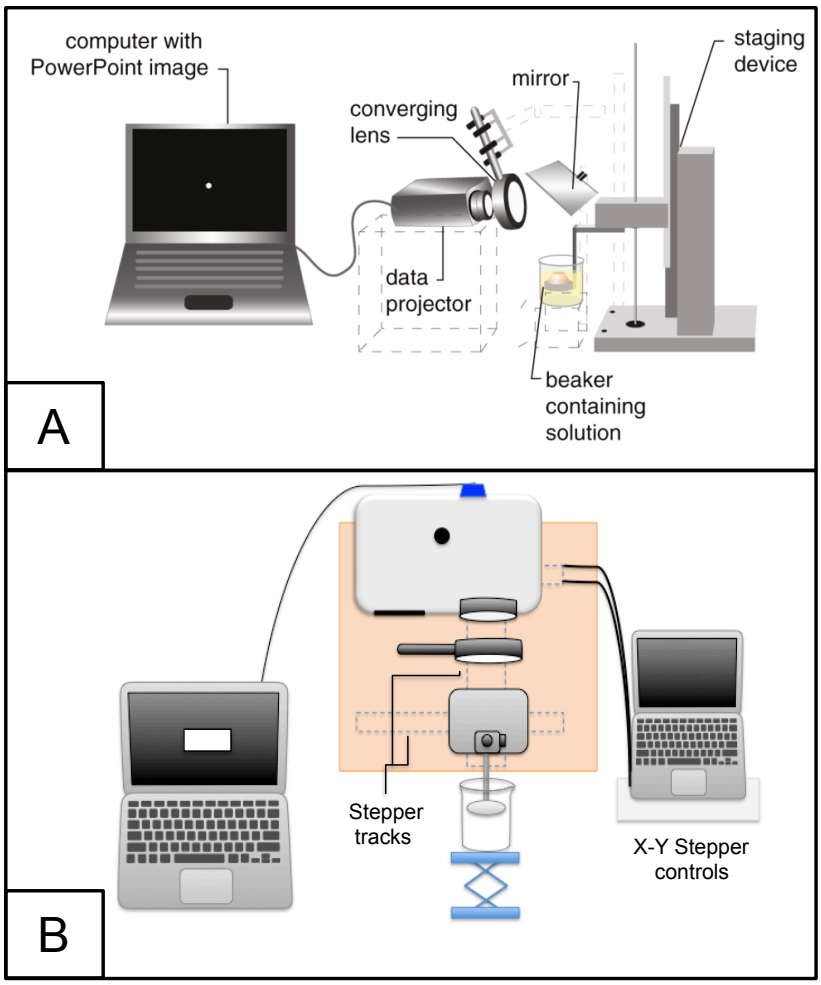

Figure 6.3. Schematic of projection microstereolithography (PμSL) comprised of a 1) computer to display Powerpoint® images (serving as the mask), 2) DLP projector, 3) converging lens, 4) 45 degree mirror (reflect image into crosslinking solution), 5) staging device and 6) beaker containing crosslinking solution (A). (Muskin, 2010, #24) The modified setup has removed the mirror, by changing orientation in printing and moving to an automated staging device (B).

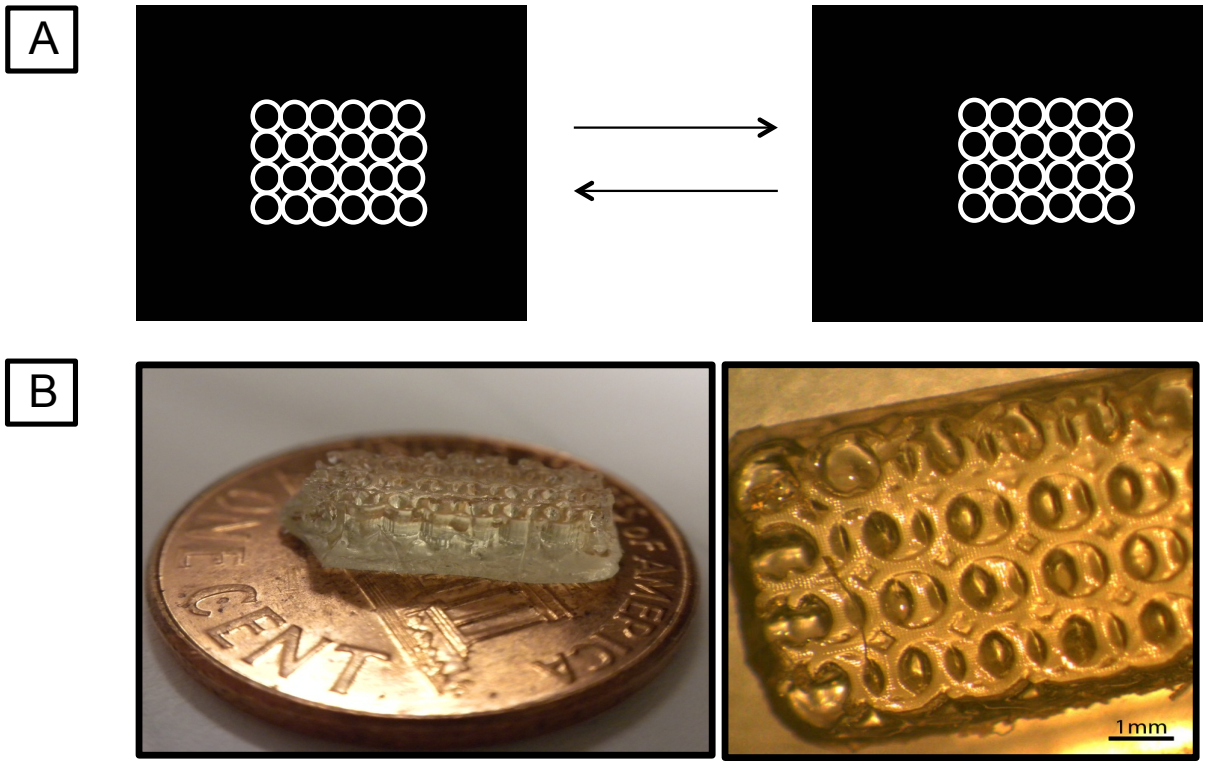

Figure 6.4. Masks (series of black and white images) created in PowerPoint® to create a crosslinked 3D structure (A). Porous fumarate-based PmSL printed substrate (B, left) and corresponding optical image (B, right). Scale bar 1 mm.

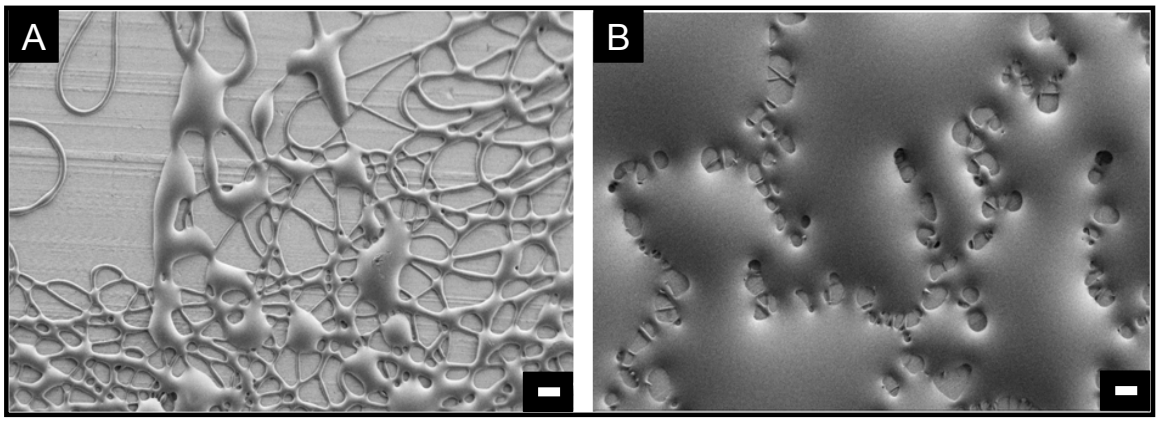

Figure 6.5. Effect of polymer deposition (time) on collection plate during electrospinning, as more fibers are deposited a self-calendaring effect is observed. This is visualized in the resulting SEM images A (less dense) and B (more dense). Scale bar is 20 μm.

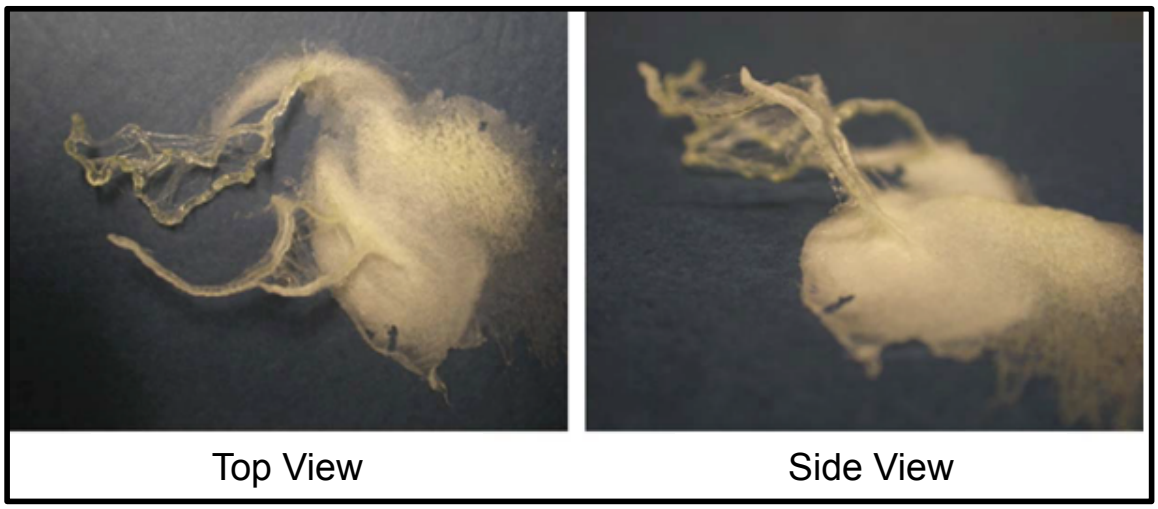

Figure 6.6. Pillar formation observed as a result of UV light reflecting back to the syringe, effecting the viscosity of the solution overtime and thereby depositing polymer on the same area of the collection plate throughout the collection period.

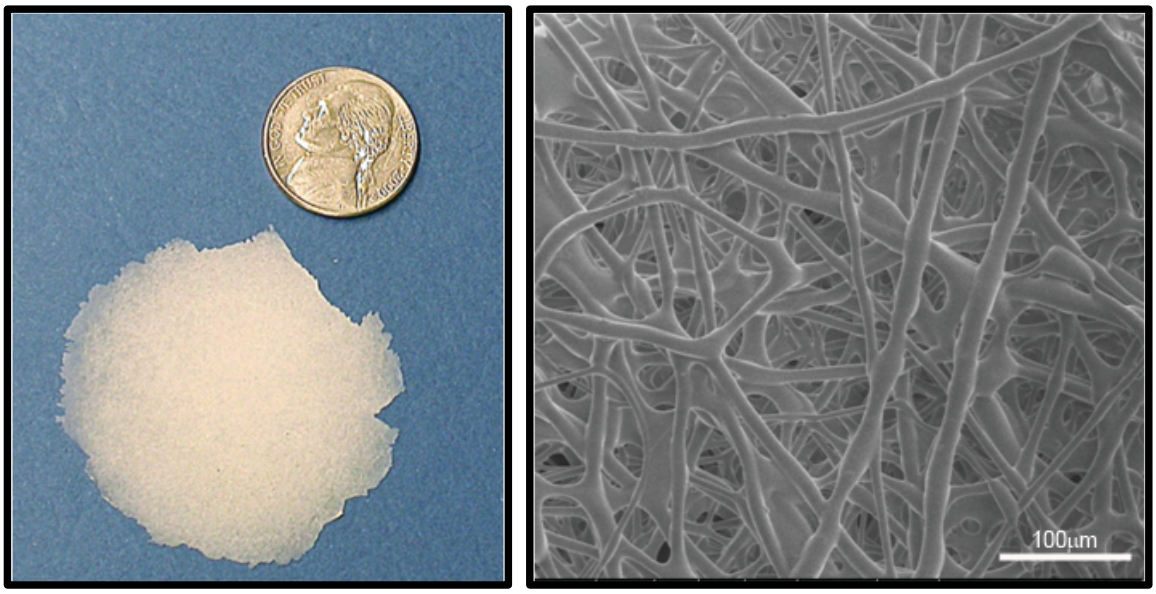

Figure 6.7. As spun electrospun mat (left) and accompanying SEM image (right) of the fiber composition seen in left hand image. Scale bar is 100 μm.

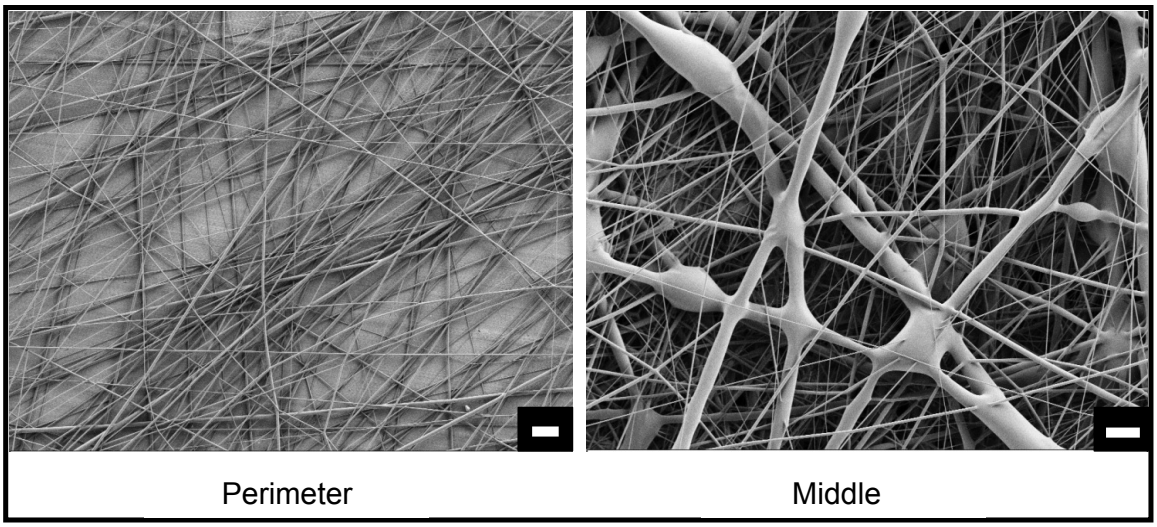

Figure 6.8. As spun PBF mats, areas of less dense fiber collection are seen around the perimeter (left) and the middle of the mat (right) displays an area of dense fiber collection. Scale bar is 10 and 20 μm (left to right).

Chapter 7.

Part I. Potential Neural Interface Material Printed via Projection Micro-StereoLithography

Part II. Printed Poly(Dimethyl Siloxane) Substrates with Controlled Pore Size: Studying Flap Revascularization in and Ischemic Mouse Model

Part I. Potential Neural Interface Material Printed via Projection Micro-StereoLithography

1. Introduction

In 1995 it was reported that at least 50,000 nerve repair procedures were preformed in the United States (US) and in 2002 that number was 250,000.[1, 2] These reported values only include those peripheral (PN) injuries which can be repaired and does account for PN injuries that are beyond repair using current clinical procedures and requires amputation of the limb. Unfortunately, the number of non repairable PN injuries is much higher, with about 1.7 million people in the US reported to be living with limb loss.[3] The current treatment for limb loss is to supply the patient with a static limb, which can decrease an individuals motor or sensory perception.[4]

The clinical need is driving the movement from a non static limb to a neuroprosthetis, or limb which interfaces with the patients nervous system. Many advancements have recently occurred in robotics[5], which has now shifted the research focus to lie on coupling the prosthesis with the nervous system through peripheral nerve interfaces (PNI).[3, 6] Neural interface devices operate at the intersection of the peripheral nervous system and an external system. These interfaces can be used to monitor nerve signals or provide inputs to allow amputees the ability to control prosthetic devices the same way they would control parts of their own body, by using direct neural signals.

Several approaches to developing PNIs, which are aimed to control prosthetic devices as well as augment nerve regeneration, have been evaluated in a research setting and can be categorized into 3 basic categories, 1) cuff 2) penetrating and 3)

regenerative.[6] Cuff electrodes are comprised of an insulating sleeve around the nerve, electrically simulating the superficial fascicles of the nerve. Therefore the lack of contact and spatial selectivity is a limitation of the cuff design.[6, 7] The lack of contact seen with the cuff design is dealt with in the penetrating electrode design, where electrodes are pushed into the nerve and the "needle like" design can have many contacting electrodes built in.[8] However, like the cuff electrode there are drawbacks, the material selection for penetrating electrodes has been limited to high modulus materials such as silicon.[6, 9, 10] Lastly, regenerative or sieve electrodes are applied to the proximal stump of the damaged PN, guiding nerve regeneration to the distal end. This design, as the name implies, is thin polymeric insulating (such as kapton) which has many holes machined into the film. These holes are than plated and provide contacts to the regenerated PN, the conduit (spanning from proximal to distal end of the PN) has conductive tracks which are wired to external connection sites.[6, 9, 11] However the materials used for these electrodes have moduli on the order of GPa and the elastic moduli of a PN is ~0.45 MPa.[12]

Due to the incompatible material mismatch, limited device lifetime and the need to develop a more compatible PNI.[12] Our research focus has looked at using polymers like polybutylene fumarate (PBF) and polydimethylsiloxane (PDMS), both have lower modulus of elasticity relative to previously used silicon, glass, or metal. As well as material selection, fabrication is carried out via the inexpensive techniques of electrospinning[13] and DLP® based projection microstereolithography (PμSL)[14] as described in chapter 6 to produce a flexible, porous conducting polymeric patch design (Figure 7.1)

2. Materials and Methods

2.1. Chemicals and Reagents

Polybutylene fumarate (PBF) was synthesized according to previously reported procedures, and as described in Chapter 3.[15] Phenylbis(2,4,6-trimethylbenzoyl)phosphine oxide (BAPO), 97% and tetrahydrofuran (THF) were purchased from Sigma. Nitric acid was purchased from Fisher Scientific. Methacryloxypropyl terminated polydimethylsiloxane (PDMS-MA) and hydroxyl terminated polydimethyl siloxane (PDMS-OH) were purchased from Gelest. All chemicals were used as received from suppliers.

2.2 Equipment

A syringe pump (KD scientific,model 100s), stainless steel blunt-tip needles (Small Parts) and a high voltage source (Glassman High Voltage, Series EL) were used in the general electrospinning setup. Scanning electron microscopy (SEM) was carried out using a Zeiss Supera 55VP and aFEI DB235. Optical images were obtained using an Amiscope® microscope and images were analyzed using NIH software ImageJ®.

2.3. Polymer Synthesis

2.3.1. Polydimethylsiloxane Sol-gel

Silanol terminated polydimethylsiloxane (PDMS-OH), tetrahydrofuran (THF), tetraethyl orthosilcate(TEOS) and nitric acid were mixed to prepare a PDMS-solgel solution, following a previous established protocol.[16] Briefly,

PDMS-OH was condensed with TEOS using an acidic catalyst (nitric acid) in a THF solution at 80 °C for 40 min, producing a viscous PDMS sol-gel solution. This was the precursor solution used for electrospinning.

2.3.2. Poly(butylene fumarate) (PBF)

PBF was prepared as described previously, detailed in Chapter 3 from ring opening polymerization (ROP) from maleic anhydride (MA) and 1,3-butanediol (BD).

2.4. Polymer Processing

2.4.1. General Electrospinning Procedure

All polymer solutions were delivered at a constant rate via a syringe pump through a syringe fitted with a stainless steel blunt tip needle. The needle was charged through a high voltage supply, and the resulting polymer fibers were collected on a grounded target (6 x 6 in^2 Cu plate fitted with Al foil). The grounded target was equipped with a resistive Minco® heater. A UV source (UVP, Blak-Ray long wave ultraviolet lamp, model B100AP, λ = 365 nm) was used to crosslink *in situ*.

2.4.1.1. Electrospinning PDMS Sol-gel

A 15% PDMS sol-gel dissolved in THF was delivered at a constant rate of 15 mL/hr, via a syringe pump through a 2 mL plastic syringe (inner diameter = 4.64 mm) fitted with a 1.5 inch 20 gauge stainless steel blunt tip needle (Small

Parts, Inc.). The needle was charged at 20kV and the resulting polymer fibers were collected on the grounded target, fitted with a Minco® resistive heater at a distance of 20 cm from the end of the tip to create an electric field of 1kV/cm. The Minco® heater allowed for the crosslinking condensation reaction to continue and form individual fibers (Figure 7.2).

2.4.1.2. Electrospinning PBF

A 3% (w/w) initiator (phenylbis(2,4,6-trimethylbenzoyl)phosphine oxide (BAPO)) 75% (w/w) PBF dissolved in chloroform ($CHCl_3$) was delivered at a constant rate of 0.1 mL/hr, via a syringe pump through a 2 mL plastic syringe (inner diameter = 4.64 mm) fitted with a 1.5 inch 20 gauge stainless steel blunt tip needle (Small Parts, Inc.). The needle was charged at 15 kV and the resulting polymer fibers were collected on the grounded target at a distance of 15 cm from the end of the tip to create an electric field of 1kV/cm. A UV source was used to crosslink polymer solution *in-situ* creating individual polymeric fibers (Figure 7.2).

2.4.2. General Projection Micro-StereoLithography (PμSL)

The PμSL apparatus is comprised of 1) a computer containing the corresponding PowerPoint® slide of black and white images to serve as the "mask" for printing the specified geometries, 2) a DLP projector (Acer Model DSV008), 3) a converging lens with 15cm focal distance (Edmund Optics) and finally 4) a stage which a silicon chip is placed to serve as a substrate to print the structure on to (Figure 7.3).

2.4.2.1. Printing Methacryloxyproply terminated Polydimethylsiloxane (*PDMS-MA)*

A solution of phenylbis(2,4,6-trimethylbenzoyl)-phophine oxide (BAPO) (.09g) was dissolved in 900μl of chloroform which was than added to 3g PDMS-MA and mixed. A silicon chip was then placed on the stage of the PμSL apparatus where the PDMS/BAPO solution (600 μl) was added and allowed to self level before exposure to light from the projector (2 min). After allowing the solution to level, it was exposed for 60 seconds followed by a developing step. The structure was than crosslinked further (5 min) under UV (Black-Ray®, λ= 365 nm).

2.5. Printed PDMS-MA substrate evaluation

2.5.1. PμSL Setup verification

A projection mask was drawn in PowerPoint® with a varying size circles (0.1 to 0.02 inch), which was reduced by optics. In order to determine the smallest feature size that could be obtained with the constructed set-up. In conjugation with varying hole size, the developer used was also evaluated for efficiency. Optical images were taken of each printed substrate using DinoScope® followed by analysis using ImageJ software® (NIH).

2.5.2. Dynamic Mechanical Analysis (DMA)

Substrates were printed using a projection mask to produce PDMS strips (thickness ~0.8 mm, width ~ 0.08 mm), the strips where tested by holding the samples at physiological temperature (37°C) under controlled force (3 N/min to 18N). The modulus was determined by using Microsoft Excel® to determine the slope within the linear region.

2.6. Animals Specimen

This study used 8-month-old retired breeder Sprague-Dawley male rats (Charles River Laboratories, Wilmington, Mass.) that were housed individually in a pathogen-free animal facility accredited by the Association for Assessment and Accreditation of Laboratory Animal Care and the National Institutes of Health. All procedures were approved by the Institutional Animal Care and Use Committee (IACUC) of the University of Texas MD Anderson Cancer Center. Animals had free access to food and water and were housed in individual cages in rooms that were maintained at 21 °C, with 12-h light and dark periods.

2.6.1. Scaffold Implantation Procedure

A rat hind-limb, peroneal nerve model was used in all experimental implantation procedures. PBF and PDMS implants were sterilized using ethylene oxide several days prior to the implantation procedure. For all surgical procedures, rats were given an anesthetic cocktail (64 mg/mL ketamine HCl, 3.6 mg/mL xylazine, and 0.07 mg/mL atropine sulfate), which was injected

intramuscularly. Isoflurane 0.5–2% was used as a supplementary perioperative anesthetic as required. After anesthesia was induced, the animal's left thigh was shaved, prepped with Betadine solution, and then draped sterilely. The peroneal nerve was accessed by making a diagonal skin incision 25 mm proximal to the knee. The overlying muscle was split parallel to the muscle fibers to reveal the peroneal nerve. The nerve was cleaned of its perinerual tissue for a short distance before dividing the nerve perpendicular to the axis of the nerve. The material tobe implanted was hydrated with saline in a Petri dish at the start of the procedure. The material was trimmed to the approximate diameter of the nerve under an operating microscope and then implanted between the cut ends of the peroneal nerve. The ends of the nerve were sutured together using 11-0 nylon suture. Small segments of 4-0 polypropylene suture were cut and one placed under the nerve about a centimeter above and below the implant to facilitate locating the implant at the time of implant-nerve harvest (Figure 7.4).

2.6.2. Implant-Nerve Harvest Procedure and Histology

Three weeks after surgery, all rats were euthanized with CO_2 asphyxiation according to IACUC protocol. The left and right thighs were shaved. Using the operating microscope, the implant-nerve specimens were located and harvested by cutting the nerve 1-1.5 cm above and below the implant and placed in formalin for histology. All specimens were fixed in paraffin blocks and cut with a microtome at 8 micons thickness. Specimens were placed on glass slides and stained with either hematoxylin and eosin (H&E) or Hirano-Zimmerman stains

before being read by an unbiased veterinary pathologist.

3. Results and Discussion

3.1. Electrospun Porous Mats

Non-woven porous mats of poly(butylene fumarate) (PBF) and poly(dimethyl siloxane) PDMS were created using modified electrospinning set-ups in our laboratory. PDMS was spun using a dilute stock solution of the starting PDMS sol-gel and crosslinked thermally with the use of a Minco® resistive heater, which enabled the material to be heated to high temperatures (~250 °C) when contact was made on the grounded stationary collection plate.

Successful electrospinning of PBF was accomplished following the methodology described in Chapter 6, allowing for *in situ* crosslinking to occur as it is spun and collected on the grounded collection plate. Evaluation of the mat morphology was carried out using scanning electron microscopy (SEM) (Figure 7.5). Mat thickness was measured to be ~100 μm and ~300 μm for the PDMS and PBF mats, respectively.

3.1.1. Electrospun (Espun) Mat Implantation and Evaluation

Our collaborators at MD Anderson Cancer Center (MDACC) (Gregory Reece and Patrick Lin) implanted both the PBF and PDMS espun mats in a rat hind-limb peroneal nerve model. Once the materials were implanted, the rats were housed and maintained for three weeks, after which the animals were sacrificed and the PDMS and PBF mats were transected from the specimen for

further evaluation.

Histological evaluation of the implant (espun mat)/ nerve interface included hematoxalin and eosin (H&E) and Hirano-Zimmerman staining. Both staining procedures require paraffin embedding of the extracted implant/nerve sample, PBF espun material is more brittle than that of PDMS and while samples were being prepared some breakage was observed. The H&E staining of the PBF mat/nerve interface (Figure 7.6) showed this PBF mat breakage as well as limited infiltration in the relatively thick espun mat as compared to the Hirano-Zimmerman stained PDMS mat/nerve interface (Figure 7.7). Due to the poor infiltration of the electrospun scaffolds and alternative technique was sought out.

3.2. Projection Micro-StereoLihography (PμSL):Set Up and Verification

Initial material performance, as evaluated by the electrospun implants, sparked interest in moving forward with PDMS as the implant material. The moduli of PDMS can range from 1.76 – 13.9 MPa[17] and has a much lower moduli compared to other materials being evaluated as peripheral nerve interfaces (PNI). However the PDMS sol-gel precursor solution used in electrospinning was not suitable to be printed by the inexpensive technique of PμSL. The need for a different PDMS precursor solution was due to the caveat that the PDMS precursor solution must contain a double bond to allow for patterning. To address this requirement, we identified a methacryloxypropyl terminated polydimethylsiloxane (PDMS-MA) which contains two terminal methacrylate units and therefore can be crosslinked photchemically with BAPO.

Our in-house PμSL setup was assembled as previous described by Fang et al[14], with the slight modification of removing the reflecting mirror and projecting the image directly into the crosslinkable solution, which allowed for removal of the trapezoidal effects seen from the projector itself (Figure 7.3). This system includes a computer and LCD/DLP projector which was used to display a MicrosoftPowerpoint® (ppt) presentation containing an image of regular pores, which inturn allows the user to dictate the resulting substrate composition, including porosity.

In order to identify the appropriate crosslinking and developing parameters which were necessary for the PDMS-MA system a mask was made with 5 different circle sizes, ranging from a diameter of 0.1 inches to as small as .02 inches (2540 – 508 μm) (Figure 7.8). Using this mask and the PuSL procedure was carried out as described in the methods section, the polymer was exposed for 45 seconds and then developed in various solvents. These solvents included toluene, hexanes, dichloroethane (DCE), water and a combination of solvents as a post crosslinking development step were evaluated. All of the resulting substrates were than optically imaged (Figure 7.8) and using Image J® the minimum pore size was determined to be 79 μm from the development step involving a brief rinse with toluene, followed by a water rinse. This resulted in a 6.4 × reduction in size from the image created by the projection mask.

3.2.1. PμSL Patterned Substrate Implantation and Evaluation

Once the PDMS-MA patterning parameters were established, patterned

strips 8 mm x 8 mm (width x thickness) were patterned and the moduli of the printed PDMS was calculated to be 9.13 ± 2.17 MPa by DMA. Next, patterning of a continuous porous thin film substrate was carried out and implanted into the same rat hind-limb pereonal nerve model as the espun PDMS sol-gel mat (Figure 7.4). The rats were maintained again for 3 weeks, upon completion the rats were sacrificed and the patterned PDMS substrate/nerve area of interest was extracted for H&E staining. Optical images of the implant/nerve area show nerve growth through the holes of the substrate, proximal to distal (Figure 7.9) relative to the less porous espun PDMS material that was first implanted.

4. Conclusions

Both inexpensive techniques of electrospinning (espin) and projection micro-stereolithography (PμSL) have been employed to create porous networks to study feasibility for a material to meet the requirements for peripheral nerve interfaces (PNI). Both PBF and PDMS were evaluated as potential materials at the start with initial expermiments on espun mats, promise in PDMS was seen as it was more flexible over the stiffer PBF espun mat. Using PDMS as the material offers a better material nerve moduli match over the mismatched materials that are currently used in PNI (Silicon).

Greater nerve infiltration was seen with the controlled porosity PDMS materials that were patterned through the use of PμSL using photo crosslinkable PDMS-MA. Initial *in vivo* studies in the rat hind-limb peroneal nerve model have indicated the potential to use a PDMS patterned membrane as a suitable

interface material. Movement towards an electrically active PDMS is currently being explored. This includes producing PDMS PμSL patterned substrates with the inclusion of multi-walled carbon nano-tubes (MWCNTs), carbon black and many other fillers/additives.

Scheme 7.1. Synthetic routes to produce PDMS-sol gel from silanol terminated PDMS (1), TEOS (2) and nitric acid (H^+) (A) and crosslinking of PDMS methacrylate terminated (PDMS-MA) by BAPO for PμSL (B).

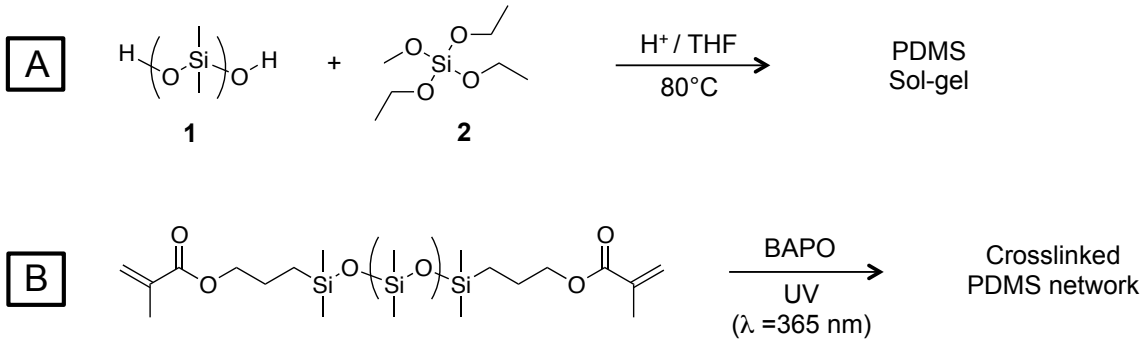

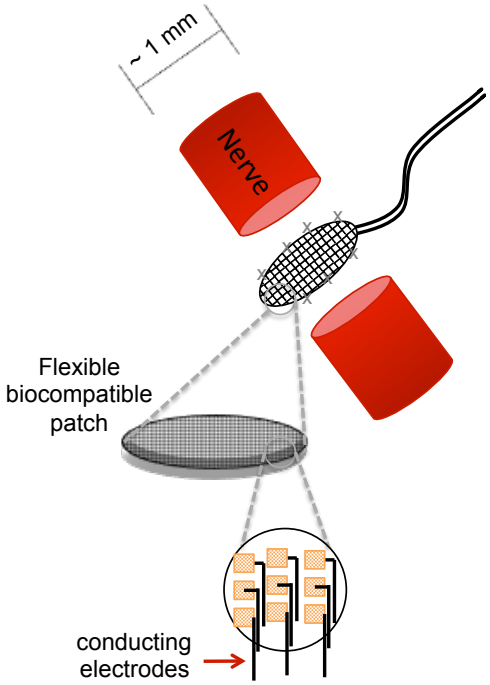

Figure 7.1. Schematic representing polymeric patch design. The patch will be inserted in the nerve (between distal and proximal ends), consisting of pores, conducting electrodes and wires to feedback signals.

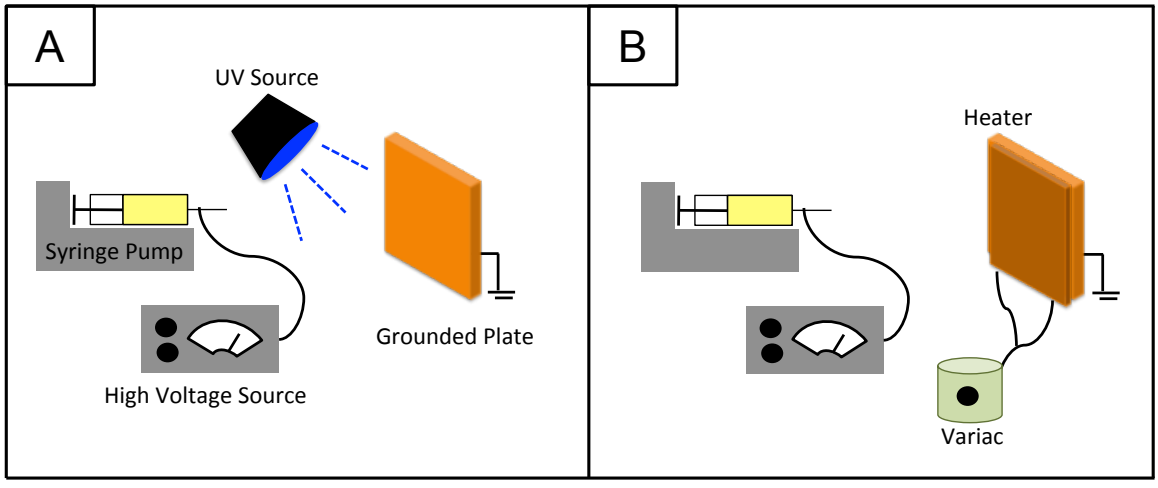

Figure 7.2. Schematic of modified electrospinning setups. Each setup is comprised of a 1) syringe pump, 2) high voltage source and 3) grounded collection plate. To spin PBF a UV source is added in-line to crosslink the photoinitator/polymer solution *in situ* (A) and to spin PDMS-sol a Minco® heater and variac are added to the general setup (B).

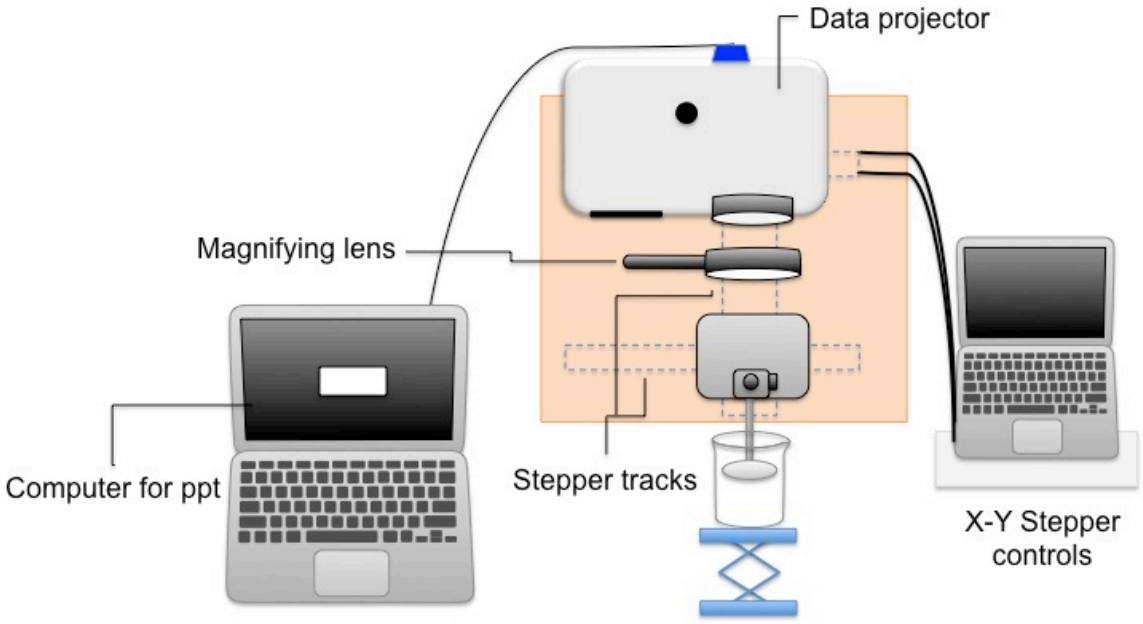

Figure 7.3. Schematic of projection microstereolithography (PmSL) setup. The system is comprised of a 1) computer, 2) DLP projector, 3) converging lens and finally a 4) stage.

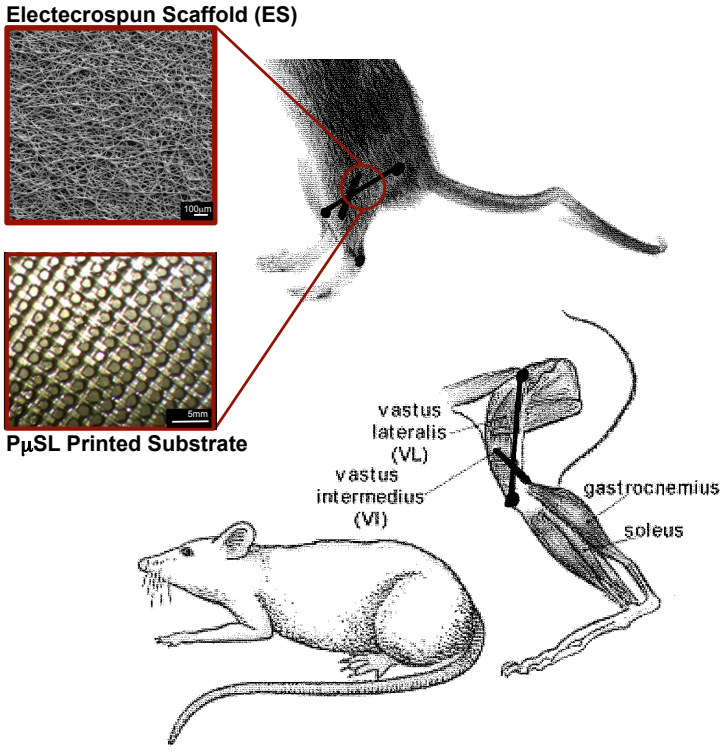

Figure 7.4. Schematic of rat hind-limb peroneal nerve model and implant procedure. Where the material, either electrospun scaffolds (PDMS or PBF) or PμSL substrates (PDMS) were implanted.

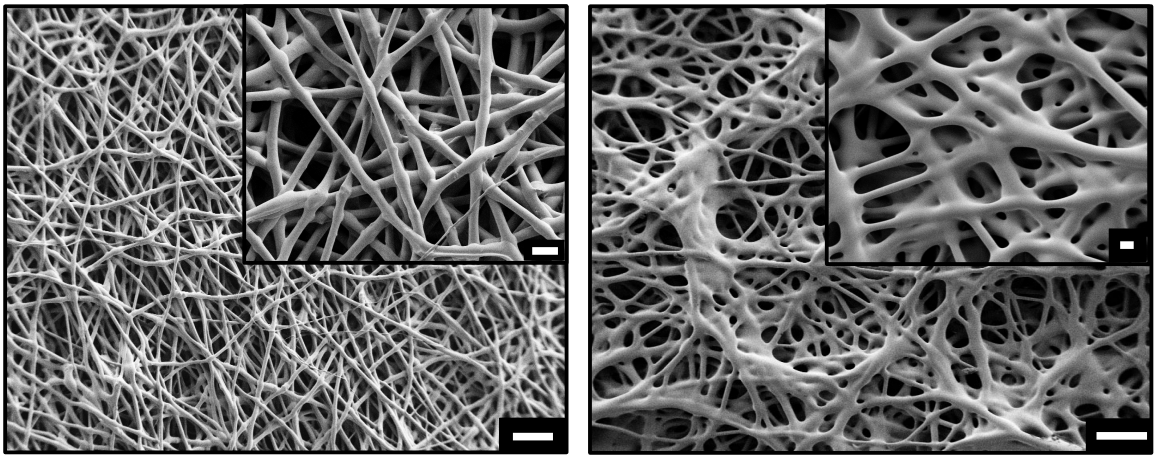

Figure 7.5. As spun PDMS sol-gel (left) and PBF (right) electrospun mats. Scale bar is 100μm and inset 20μm,

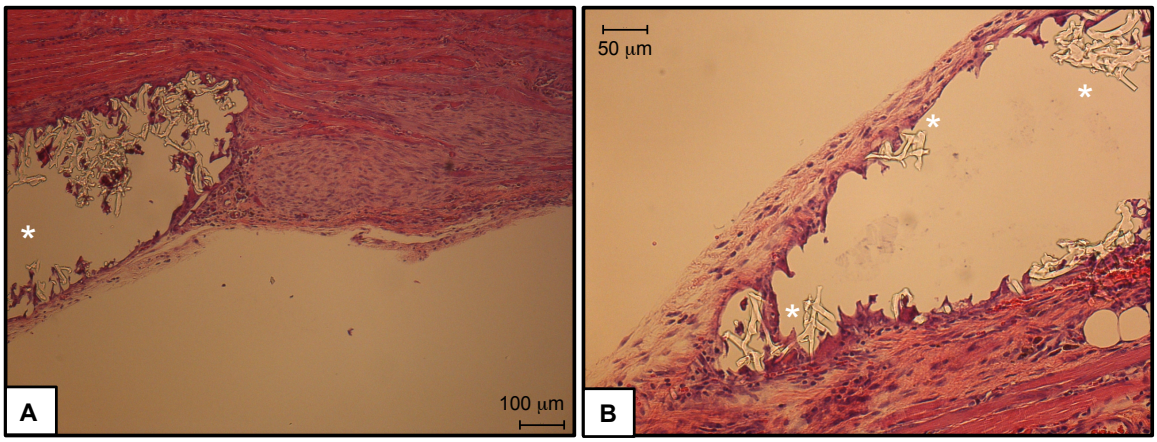

Figure 7.6. H&E staining of PBF implant/nerve interface. The PBF implant (*), was fractured during histological prep and is seen in the magnified image (B). Scale bar is 100 and 50 μm, respectively.

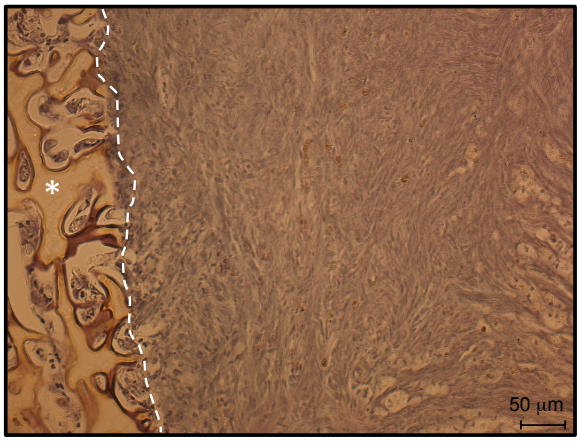

Figure 7.7. Hirano Zimmerman staining of PDMS implant/nerve interface. Implant (*) and the nerve implant boundary (- -) can be visualized. Scale bar is 50 μm.

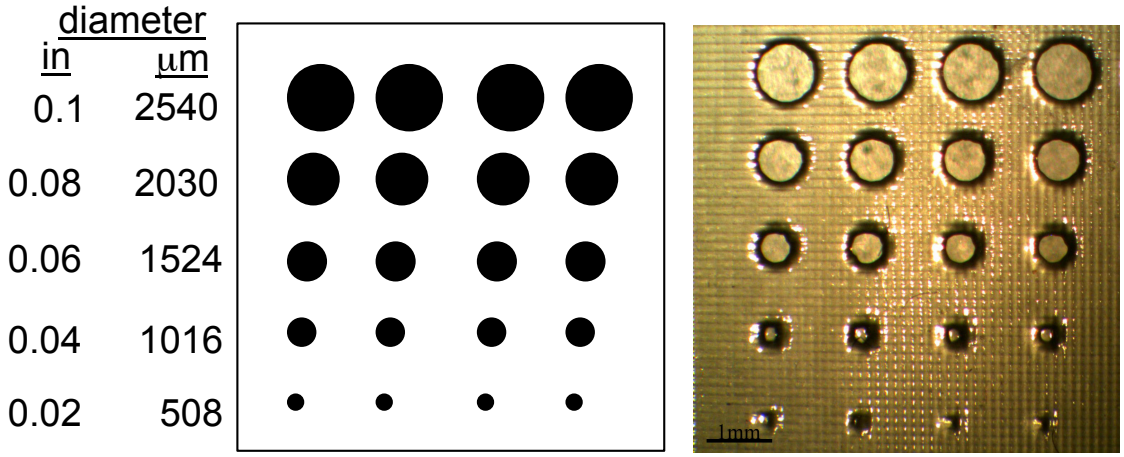

Figure 7.8. Schematic of the mask created in PowerPoint® to generate circles of 5 different diameters (2540 – 508 μm) (left) and an optical image of the resulting crosslinked PDMS-MA network. Scale bar 1 mm.

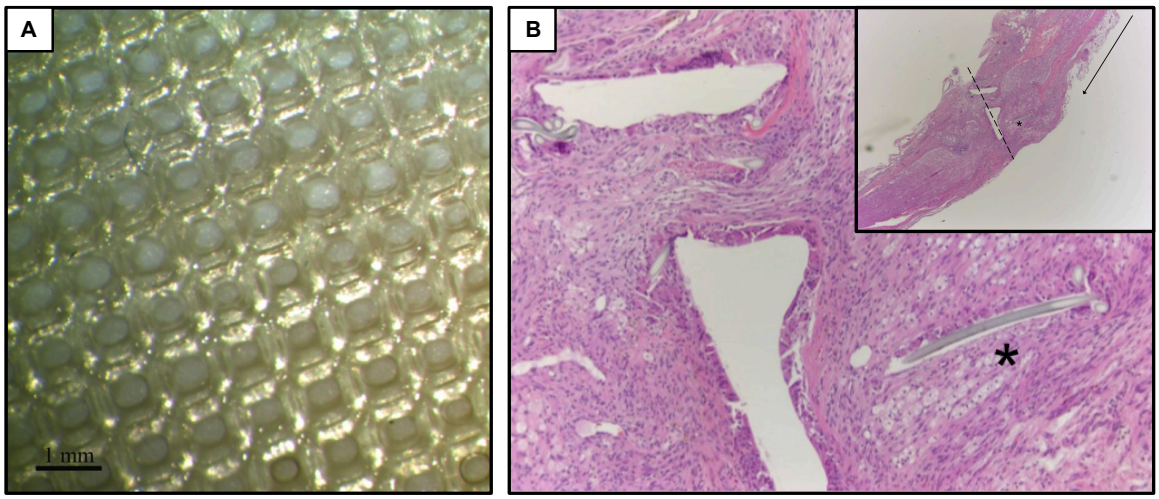

Figure 7.9. Optical image of porous PDMS PmSL printed sheet (A), and H&E histology after 21 days in the rat peroneal nerve (B), where the inset is a low magnification image of the nerve-implantation site (nerve fibers (+), nylon suture (*), plane of implant (- -) and proximal to distal (↙)). Scale bar 1 mm.

Part II: Printed Poly(Dimethyl Siloxane) Substrates with Controlled Pore Size: Studying Flap Revascularization in and Ischemic Mouse Model

1. Introduction

Angiogenesis, or the generation of new blood vessels from existing vasculature, is crucial for the realization of functional engineered tissues. As new tissues grow, the (resident or involved or active) cell populations must have immediate access to a blood supply for the delivery of nutrients and removal of waste products. Therefore, the success of a tissue engineering construct is dependent not only its ability to assist in the generation of the tissue of interest, but must also always (support) the neo-tissue with a healthy vascular network.[1, 2]

The need for a strategy to promote revascularization is apparent and researchers have begun to explore scaffolding parameters for this task. Scaffold parameters such as overall void volume as well as pore shape, size, and tortuosity are a few of the variables examined to date.[3] With each of these variables potentially influencing the overall angiogenic potential of a scaffold, it can be a daunting task to optimize the scaffolding geometry.

To study angiogenesis, murine (mouse) models are the most common wound healing models as mice are inexpensive to house.[4] Despite differences in epithelial architecture between human and mouse skin, the model is versatile and provides an effective genetic manipulation platform.[5, 6] Among the mouse skin models available, ischemic models offer significant advances over other models in studying and elucidating signaling roles in angiogenesis and vasculogenisis (vessel formation from circulating endothelial progenitor cells) due to the increased influx of cytokines and elevated protease levels. [7, 8]

A frequently used model, the myocutaneous flap model (flap consisting of skin and muscle), has been developed to produce an ischemic gradient. Ischemia is a potent stimulus for new blood vessel formation, establishing capillary growth and restoring the appropriate oxidative conditions.[9] Recently, this reproducible ischemic model has been employed at UNM by our collaborator Dr. Thomas Howdieshell to investigate a non-invasive technique to monitor revascularization.[10] This technique, full-field laser perfusion imaging (FLPI), allows for mapping of flow fields and produces a speckled high contrast image of blood flow within the flap.[11, 12] It has been demonstrated that if a material is not placed between the skin flap and underlying tissue, revascularization will occur.[10] However, if a nonporous implant is introduced, there is a inhibitory effect on engraftment and revascularization, and the distal flap will show signs of ischemic necrosis. Thereby providing an *in vivo* model which can be used to "tease" out the effects of a materials ability to promote angiogenesis.

Since there are many structural parameters to examine, we have decided to look at the bioinert material polydimethylsiloxane (PDMS), as it is similar to silicone used in the previous study and will not undergo degradation. In order to control the implant geometry and composition, we have chosen to use the inexpensive rapid prototyping (RP) technique of projection microstereolithography (PμSL). As discussed in Chapter 6, PμSL uses computer-controlled light projection to spatially control solidification of a liquid photo-polymerizable resin.[13] Structural parameters such as pore size, configuration, and gradient density can be freely varied with little effort and cost.

Here in, we look at the effect of controlled pore size on flap revascularization. To carry out this goal, we have fabricated PDMS printed implants with and without pores for implantation in the myocutaneous flap model. We monitored the perfusion of the flap throughout the study period by the non-invasive FLPI technique, followed by histological testing of the flap/implant interface at the termination of the study.

2. Materials and Methods

2.1 Chemicals and Reagents

Phenylbis(2,4,6-trimethylbenzoyl)phosphine oxide (97%, BAPO) was purchased from Sigma. Methacryloxypropyl terminated polydimethylsiloxane (PDMS-MA) was purchased from Gelest. All chemicals were used as received.

2.2. Equipment

A projection microstereolithography system (PμSL) was built in-house as described in Chapter 6. Optical images were obtained using an Amiscope® microscope and images were analyzed using NIH software ImageJ®. Full-Field Laser Perfusion Imager (FLPI) was purchase from Moor Instruments (Essex, UK).

2.3. Printing Methacryloxyproply terminated Polydimethylsiloxane (*PDMS-MA)*

A solution of phenylbis(2,4,6-trimethylbenzoyl)-phophine oxide (BAPO) (0.09 g) was dissolved in 900 μl of chloroform which was then added to 3 g PDMS-MA and mixed. A silicon chip was then placed on the stage of the PμSL apparatus where

the PDMS/BAPO solution (600 mL) was added and allowed to self level before exposure to light from the projector (2 min). After allowing the solution to level, it was exposed for 60 seconds followed by a developing step. The structure was than crosslinked further (5 min) under UV (Black-Ray®, λ= 365nm).

2.4. Animals Specimen

This study used 8-12 week old C57BL6 mice (Jackson Laboratories, Bar Harbor, Maine) that were housed individually in a pathogen-free animal facility in accordance with the National Research Council's "Guide for the use and care of laboratory animals." All procedures were approved the University of New Mexico's animal review committee. Animals had free access to food and water and were housed in individual cages in rooms that were maintained at ambient temperature, with 12 hour light and dark periods.

2.4.1. Scaffold Implantation Procedure

A previously identified mouse myocutaneous flap model was used in all experimental implantation procedures.[10] Briefly, PDMS implants were sterilized using Sterrad® hydrogen peroxide autoclaving several days prior to the implantation procedure. For all surgical procedures, mice were given anesthesia in the form of Isofluorane®, which was administered via nose-cone inhalation and maintained throughout scaffold implantation. Upon induction and maintenance of anesthesia, back skin hair was removed via electronic clippers followed by surgically prepping with povidone-iodine and alcohol. Once prepped, a peninsular-shaped flap was

created surgically (approximately 3.0 cm in height by 1.5 cm in width, in a rectangular shape). The control mice (no implant, n = 3) were immediately sutured to close the flap. Mice (n = 6) to receive scaffolds underwent insertion of 3.0 x 1.5 cm trimmed implants of solid crosslinked PDMS sheets (S, n =3) or porous crosslinked PDMS (SP, n = 3) before closure of the flap.

2.4.2. Full-Field Laser Speckle Perfusion Imaging (FLPI)

At 0, 2, 5 and 10 days after surgery, each mouse underwent Isoflourane® anesthesia, and each mouse (control, S, or SP) underwent FLPI perfusion analysis at 20 cm camera distance in low resolution/high speed setting at a display rate of 25 Hz, time constant of 0.1 s, and camera exposure time of 20 ms, and images were collected and recorded electronically. Perfusion is determined as an arbitrary unit, PU, based on calibration to a reference flux measurement of polystyrene beads in water undergoing thermal Brownian motion.[12]

2.4.3. Implant-Tissue Harvest and Histology

10 days after surgery, all mice were euthanized with CO_2 asphyxiation followed by cervical dislocation according to the institutional animal review board protocol. The entire flap was excised (ie. implant included) for examination. All flaps harvested were transected into cranial and dorsal sections that corresponded to FLPI orientation carried out at the previous time points (0, 2, 5 and 10 days). Specimens were then fixed in IHC Zinc fixative (BD Biosciences, San Jose, CA) overnight followed by paraffin embedding and cut to 5 micron thick slices by

microtome. Histologic sections were imaged by hematoxylin and eosin (H&E) staining (morphology), CD-31 immunohistochemistry (vessel density), and F4/80 immunohistochemistry (macrophage density and location). Our collaborator, Dr. Thomas Howdieshell of UNM Health Sciences Department of Surgery, then photographed and analyzed the images of each specimen for morphology, microvascular density, and macrophage localization.

3. Results and Discussion

3.1. Substrate Fabrication

Previous work by McGuire and Howdieshell, investigated importance of flap engraftment for revascularization by looking at an ischemic cranial-based myocutaneous flap model with and without silicone sheets inserted. (JSurg ref) As medical grade silicone (MedSi) was used in the previous flap study, methacryloxyproply terminated polydimethylsiloxane (PDMS-MA) was chosen for its similar material properties as well as our previous experiencing printing patterned PDMS-MA thin films via projection microstereolithography (PμSL).[14] Substrates of PDMS with (SP) and without (S) pores were patterned using our in-house PμSL setup described in Chapter 6. Masks to create S and SP substrates of 1.5 x 3.0 cm (width x length) was created in PowerPoint ® followed by patterning of PDMS-MA. The methacrylate unites of PDMS-MA were crosslinked using the photoinitiator phenylbis(2,4,6-trimethylbenzoyl)-phophine oxide (BAPO) and uncrosslinked PDMS-MA was removed by a toluene and water rinse. Thin films were patterned (n=6) with average thicknesses of 13.4 ± 0.1 μm (S) and 12.2 ± 0.1 μm (SP), which are similar

to the medSi thickness of 10.6 ± 0.1 μm. SP films had an average pore size of 271 ± 1 μm with horizontal spacing of 490 ± 1 μm and 602 ± 1 μm vertical spacing (7.10).

3.2. Scaffold Implantation and Evaluation

Upon completion of patterning S and SP substrates, creation of a myocutaneous flap model in C57BL6 mice was carried out. There were three models, including 1) flap only, 2) flap with underlying S inserted and 3) flap with underlying SP inserted (Figure 7.11). After substrate implantation, mice were subjected to full-field laser speckle perfusion imaging (FLPI) as well as at 2, 5 and 10 days while maintaining anesthesia. Throughout the study the flap area was also visually observed followed by termination of the study at day 10. On day 10 mice were sacrificed via CO_2 asphyxiation and the implant/flap was harvested and histology was preformed.

3.2.1. Laser Speckle Perfusion Imaging (FLPI)

This non-invasive and no contact technique provided a method to map flow fields of blood flow by illuminating the area of tissue with laser light, producing a high contrast speckle pattern. Perfusion was measured cranial to caudal, focusing on regions of interest (ROI) throughout the implant/flap area (cranial, central and caudal) (Figure 7.12). These ROI were selected in order to span the gradient ischemic flow that is introduced from this model.[10] Prior to flap creation, imaging showed uniform perfusion across all of the mice selected for this study at ~300-325 perfusion units (PU) (Figure 7.13). Upon closure specimens were again imaged and

the lack of perfusion can be visualized and compared to the control or pre flap creation and is seen as there was a decrease in PU's corresponding to post-operative measurements (Figure 7.13).

Gross visualization of the flap with S inserted showed caudalflap necrosis over the 10 day period (data not shown) that was also confirmed by speckle imaging. Looking at Figure 7.3 of the speckle imaging for S implant mice shows large areas of white at both day 5 and 10 (indicated by thin white arrows). This is in line with the visualization of caudal flap necrosis seen by the naked eye, as red indicates high perfusion and minimal perfusion is indicated by blue. In contrast, mice with SP implants showed no visual ulcers or necrotic signs and through FPLI high perfusion areas (red) were observed and there was a lack of minimal perfusion (blue) observed as compared to the non-porous S implants (Figure 7.12). Analysis of the ROI and plotting the perfusion at for each day (Figure 7.13) further confirms the difference in implant (S or SP) performance. In both specimen groups had a decrease in perfusion across all ROI's. However in the specimens with S implanted, the perfusion for all ROI's (cranial to caudal) increased at day 2 followed by a continued decrease seen at day 5 and day 10 in the central and caudal ROI's (Figure 7.13). This was not the case for SP specimens, Figure 7.13 shows significant increase in perfusion over the course of the study in a similar fashion to the control specimens.

3.2.2. Implant-Tissue Harvest and Histology

Excision of the flap-implant showed the effect of implant selection on

engraftment, further confirming the observations that were seen with the non-invasive FLPI results. Specimens with S implants show no flap engraftment, and the substrate is completely unattached to the flap upon removal. However, integration of the SP implants can be seen visually and the implant is attached to the flap tissue (data not shown). After excision of the full flap it was sectioned to directly correspond to the cranial, central and caudal ROI's that were assigned in the speckle imaging. Samples were then fixed and paraffin embedded (Tricore Labs, NM) followed by hematoxylin and eosin (H&E), CD-31 and F4-80 immunostaining.

Distal flap H&E of non-porous (S) reveled an attenuated panniclus carnosus muscle with evident necrosis of multiple muscle bundles due to persistent ischemia and lack of revascularization (Figure 7.14). In contrast, porous (SP) revealed viable panniclus carnosus muscle, with healthy dermis and epidermis of the growth through the pore (tissue peg). The tissue peg bridged the granulation tissue to the underlying muscle, several large blood vessels can be seen as well (Figure 7.14).

CD-31 immunostaining of the proximal flap of specimen with S implants showed large blood vessels and viable panniculus carnosus muscle (Figure 7.14). The proximal flap remains perfused by the specimens' segmental vessels with compensatory "arteriogenesis" attempting to provide perfusion of the distal flap, which remains ischemic. This ischemia is due to the lack of neovascularization of the recipient bed, which is being blocked by the S implant (Figure 7.14). However, with the SP implant specimens there was no lack of neovascularization as the tissue peg displayed multiple blood vessels in the panniculus muscle as well as in the dermis and epidermis (Figure 7.14).

Macrophage density and location, as stained by F4-80, revealed prominent monocyte infiltration in granulation tissue deep into the non-porous implanted sheet (Figure 7.14). Within the tissue peg of the SP specimen, monocyte infiltration was marked into the muscle and beyond into the perivascular locations (Figure 7.14).

4. Conclusions

We have fabricated PDMS thin films via the inexpensive technique of PμSL with or without pores. Using a myocutaneous mouse model we have shown that the pores (SP) implants allowed for better perfusion over the solid (S) implants. The SP implants also allowed for engraftment of the material to the flap. The combination of both the mycutaneous flap mouse model and fabrication technique of PμSL presents an inexpensive model to study de novo or induced vascularization in a mouse model, further leading to solving the translational problem of tissue integration and vascularization.

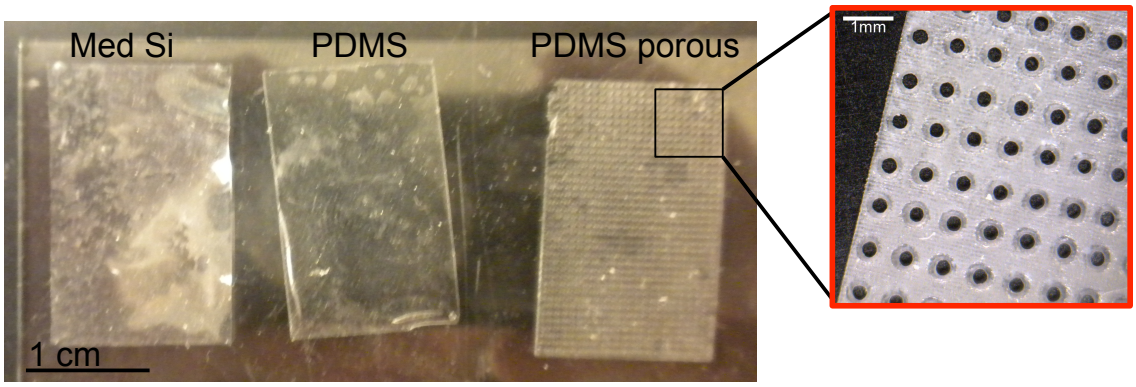

Figure 7.10. Image of 1.5 x 3.0 cm (length x width) of as received medical grade silicone (Med Si) and as printed PDMS non porous (S) and porous (SP). Optical image of SP pores are visible in the accompanying zoomed in image (far right). Scale bar 1 cm and 1 mm, respectively.

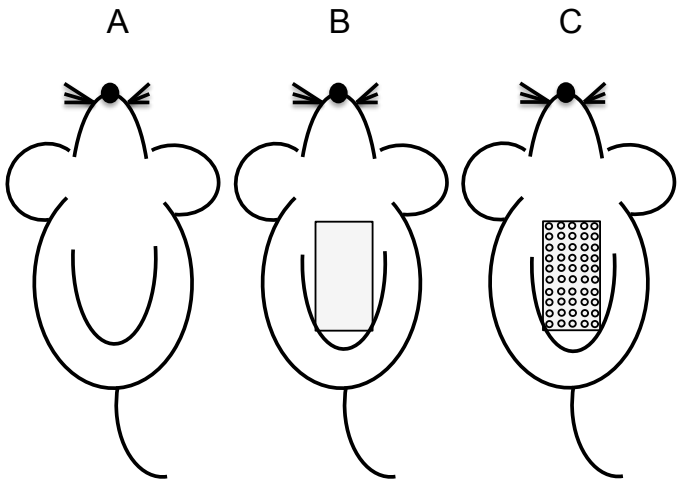

Figure 7.11. Schematic representation of myocutaneous flap surgical model and the proposed specimens in this study. The control mouse (incision only) (A), mice with S implanted (B) and SP implanted mice (C).

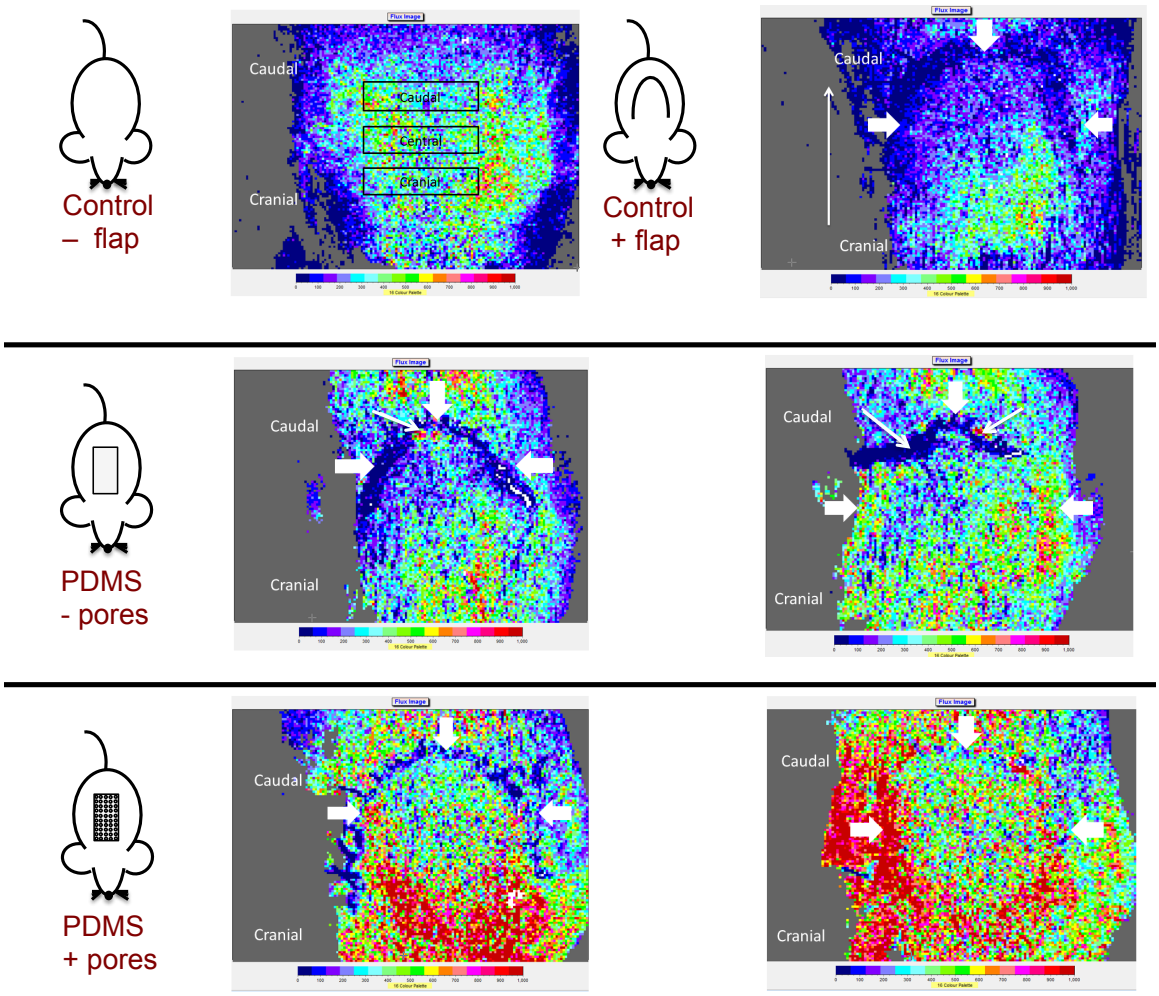

Figure 7.12. Representative images of laser speckle (FLPI) images as obatained at day 5 (left) and 7 (right)after implantation of the material (none, S and SP). The speckle pattern displays differences in perfusion, a high perfusion (red) can be distinguished from a low perfusion (blue). The flap incision boundary is represented by the thick white arrows (⇧) and areas were there is lack of perfusion (ie. necrotic or death of flap) are indicated by thin white arrows. All images are orientated from caudal to cranial and the accompanying specimen is displayed.

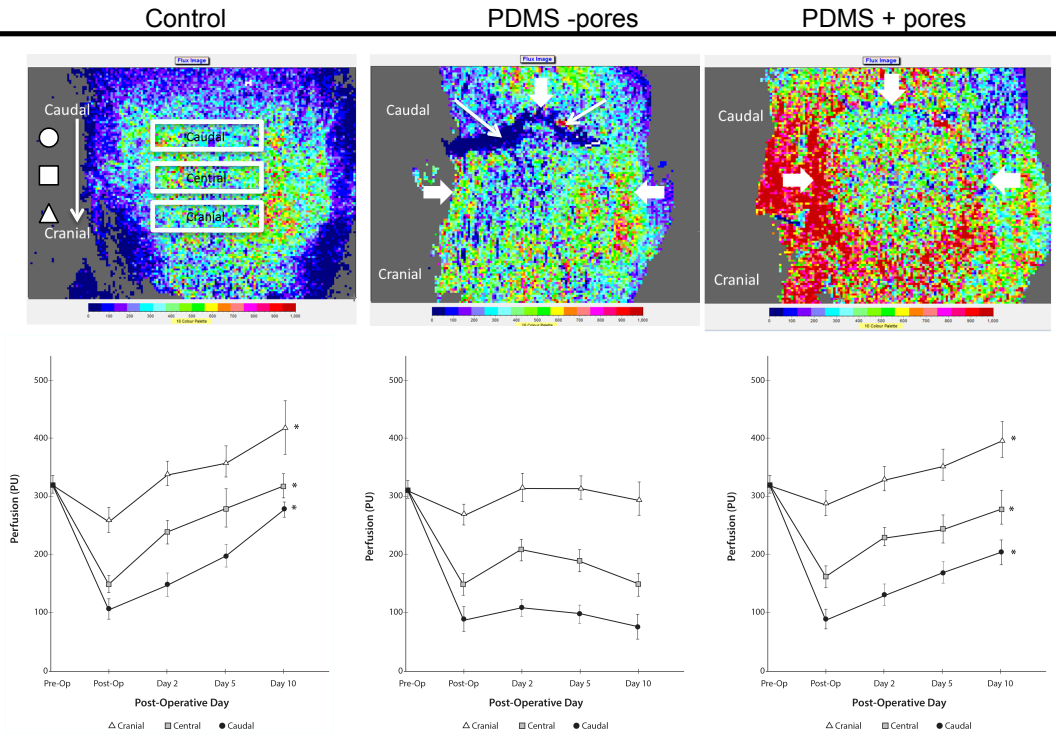

Figure 7.13. Perfusion (PU) can be quantified as a function of time by evaluating the predefined regions of interest (ROI). Representative FPLI images are shown above each perfusion chart.

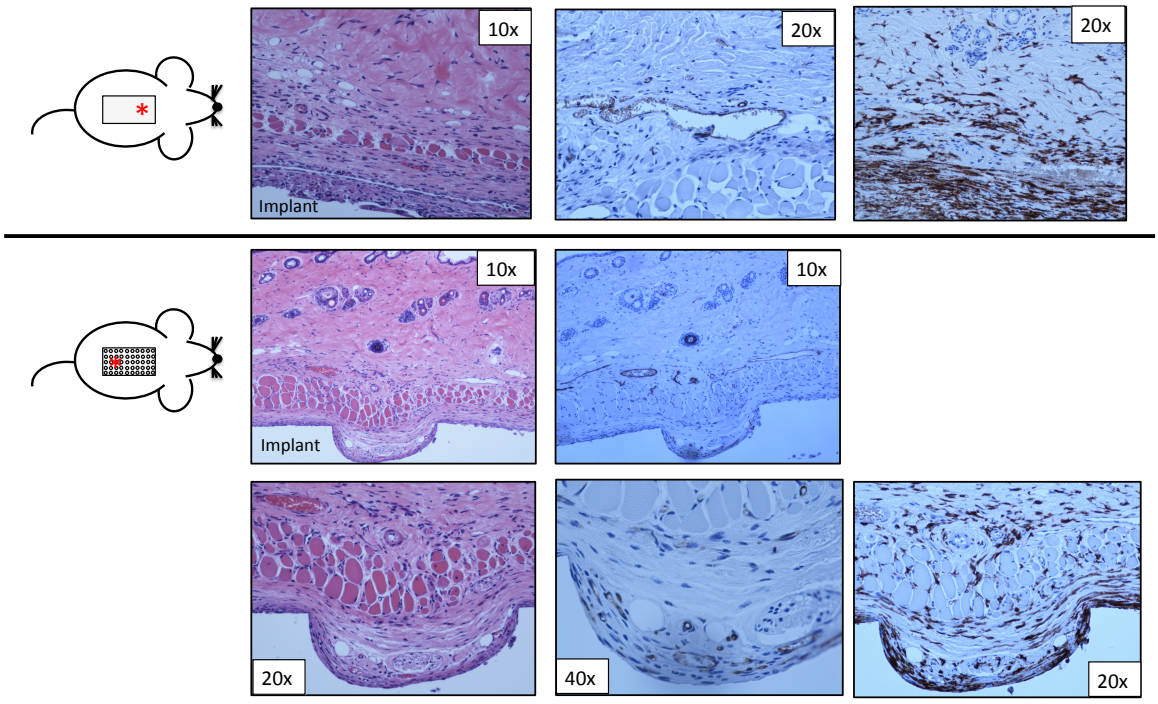

Figure 7.14. After specimens were sacrificed at Day 10 Samples were then fixed and paraffin embedded followed by hematoxylin and eosin (H&E) (left), CD-31 (middle) and F4-80 (right) immunostaining. Image view of location is represented by * on the corresponding mouse schematic.

Chapter 8. Summary and Future Directions

8.1. Summary

The overall objective of this research was to development and characterize a crosslinkable, biocompatible polymeric system with tunable degradation for use in the fabrication of scaffolds for bone tissue engineering applications. The first specific aim, synthesize and characterize a biodegradable polymer system, was accomplished by leveraging the extensive knowledge gained from the biomaterial poly(propylene fumarate) (PPF) since its first introduction in 1987 by Ibay *et al*.[1, 2] Two synthetic routes were identified and followed to form the homopolymer of poly(butylene fumarate) (PBF) and the copolymers poly(propylene fumarate)-*co*-(propylene maleate) (PPFcPM) and poly(butylene fumarate)-*co*-(butylene maleate) (PBFcBM). The first route, ring opening polymerization (ROP) of maleic anhydride (MA) at high temperatures produced all fumarate containing polymers (PBF). Low temperature routes limited the *cis-trans* isomerization of the maleate functionality to fumarate yielding the copolymers PPFcPM and PBFcBM.[3-5] With this method, however, the final polymer maleate to fumarate ratio was not controllable. Due to this limitation, a second route starting from acid chlorides (maleoyl chloride, MCl and fumaryl chloride, FCl) was developed and led to a controlled fumarate to maleate ratio by controlling the stoichiometry through monomer selection.

The second specific aim focused on PBF network characterization and *in vitro* degradation. Initial studies were carried out to determine the extent of crosslinning of photo crosslinked PPF and PBF networks. By using an efficient acyl phosphine

photoinitator, phenylbis(2,4,6-trimethylbenzoyl)-phophine oxide (BAPO), highly crosslinked networks were obtained. Accelerated degradation conditions confirmed our hypothesis that the extra methylene unit in the backbone of PBF would allow for an increased degradation rate over PPF without compromising the materials crosslinkablilty, processability and mechanical suitability.

The third specific aim, validating *in vitro* cytocompatibility and osteogenic differentiation of mesenchemyl stem cells (MSCs) on crosslinked networks of PBF relative to PPF was carried out using previously established methods as described by Timmer *et al*.[6] It was found that there were no cytotoxic effects from incubation with fumaric acid, however cells in constant contact with 1,3-butanediol displayed a reduced cell number. The data also indicated the crosslinked substrates did not have anything leachable that elicited a cytotoxic response on the murine osteoprogenitor cell line of MC3T3-E1. In addition, cellular attachment, proliferation, and osteoblastic differentitaion of mesenchymal stem cells on crosslinked PBF was found to be similar to that of previously examined PPF Osteogenic differentiation was monitored by evaluating the expression of the osteogenic marker alkaline phosphatase (ALP) and matrix calcium deposition.

Finally, the fourth specific aim, using inexpensive processing techniques to create 3D polymeric scaffolds, was accomplished through the development of new methodology for electrospinning and projection microstereolithography (PμSL). Developing an *in situ* crosslinking step to the general electrospinning technique allowed the ability for crosslinking of low glass transition (Tg) materials such as the fumarate-based polymers. Our results are the first to demonstrate rendering

ofcontinuous fibers of PPF to produce a high surface area to volume porous mat for tissue engineering applications. In addition, the inexpensive 3D printing technique of PμSL offers a more affordable alternative to the more costly stereolithography procedures. Both of these methodologies can be extended to similar classes of polymers in order to produce prefabricated scaffold for potential clinical applications in the field of not only bone tissue engineering, but tissue engineering in general.

8.2. Future Directions

8.2.1. Degradation

The inclusion of the methylene unit to produce poly(butylene fumarate) (PBF) resulted in an increase in the degradation rate over the widely studied poly(propylene fumarate) (PPF) when it was examined under accelerated degradation conditions. The other engineered polymer modification, the introduction of the maleate functionality in the polymer backbone, was examined in order to create a polymer with tunable degradation kinetics without sacrificing mechanical suitability of the crosslinked network. A feasibility study where poly(butylene fumarate)-*co*-(butylene maleate) (PBFcBM) containing 33 mol% maleate was subjected to physiological *in vitro* degredation conditions (1X PBS @ 37 °C) showed that the rate of ester hydrolysis was altered (**Figure XX**). The results of this study verified that the “kinks” introduced by the addition of the maleate would allow for an increased rate of degradation. Promising results obtained from the *in vitro* degradation of PBFcBM allowed for the development of the controlled synthesis of PBFcBM, as detailed in Chapter 4. Future studies will need to be carried out in

order to determine the direct effect of maleate concentration in the polymer backbone and its effect on rate of ester hydrolysis. All polymer formulations will be explored via *in vitro* and *in vivo* physiological degradation conditions to determine long term performance.

8.2.2. Three Dimensional (3D) Substrates

With our recent method development to electrospin low glass transition (T_g) fumarate-based polymers, the ability to produce biomimetic relevant high surface area to volume porous mats of nano to micron sized fibers can be produced via the inexpensive technique. Although the electrospinning process is an inexpensive fabrication technique for the production of 3D scaffolds for tissue engineering applications, there are many processing parameters that can be altered to effect the resulting mat morphology.[8] Due to this flexibility, further optimization of the methodology presented in Chapter 6 is required.

Although electrospinning can produce highly nano to micron sized fibers which are highly interconnected, the fiber density is a parameter that deserves attention. The ideal scaffold which has found success in BTE applications is greater than 90 % porous, but also has an optimal pore size of 100-350 μm.[9, 10] Strategies to increase the pore size of electrospun scaffolds (ES) have included increasing the fiber diameter to increase the overall void volume in the scaffolds. [11] However, the implementation of nanofibers has been shown to increase cell adhesion, proliferation and aide in differentiation of stem cells.[12] A composite mat of the fumarate-based polymers could be electrospun using a multimodal design that was suggested by

Soliman *et* al[9] to yield a mat with a largely dense fiber morphology with smaller densely distributed fibers dispersed throughout. Another strategy to alter porosity would be to include post modification techniques; the easiest of these being the use of a sacrificial polymer, one which would be cospun with our polymer and removed after the scaffold was fabricated. Those which have been used previously include poly(ethylene oxide) and gelatin, which are both soluble in aqueous conditions and can be removed without causing structural damage to the polymer of interest (ie. PPF or PBF).[13]

In addition to optimizing fiber diameter and porosity of the resulting electrospun scaffolds (ES), the mechanical properties need to be evaluated. Mechanical properties of the mat can be looked at under similar degradation conditions as the solid crosslinked samples, looking at dimensional changes as well as changes in moduli of the mat. Analysis of the as spun ES by themselves not only is an area of future exploration, but also the cell interaction with/on the electrospun mats to evaluate the mechanical properties as mesenchymal stem cells (MSCs) undergo osteogenic differentiation and bone is laid down on the ES material *in vitro*

Chapter 9. References

Chapter 1

1. Liao, X.; Lu, S.; Zhuo, Y.; Winter, C.; Xu, W.; Li, B.; Wang, Y., *Cellular and Molecular Bioengineering* **2011,** *4* (4), 579-590.

2. Post, T. M.; Cremers, S. C. L. M.; Kerbusch, T.; Danhof, M., *Clinical Pharmacokinetics* **2010,** *49* (2), 89-118.

3. Fong, E. L. S.; Watson, B. M.; Kasper, F. K.; Mikos, A. G., *Advanced Materials (Weinheim, Germany)* **2012,** *24* (36), 4995-5013.

4. Hutmacher, D. W., *Journal of Biomaterials Science, Polymer Edition* **2001,** *12* (1), 107-124.

5. Bone and Joint Decade Initiative. http://orthoinfo.aaos.org/main.cfm (accessed July 4, 2012).

6. Rentsch, C.; Rentsch, B.; Breier, A.; Spekl, K.; Jung, R.; Manthey, S.; Scharnweber, D.; Zwipp, H.; Biewener, A., *J. Biomed. Mater. Res., Part A* **2010,** *95A* (3), 964-972.

7. Yu, N. Y. C.; Schindeler, A.; Little, D. G.; Ruys, A. J., *J. Biomed. Mater. Res., Part B* **2010,** *93B* (1), 285-295.

8. You, Z.; Bi, X.; Fan, X.; Wang, Y., *Acta Biomaterialia* **2012,** *8* (2), 502-510.

9. Porter, J. R.; Ruckh, T. T.; Popat, K. C., *Biotechnol. Prog.* **2009,** *25* (6), 1539-1560.

10. Kalfas, I. H., *Neurosurgical focus* **2001,** *10* (4), E1.

11. Moore, W. R.; Graves, S. E.; Bain, G. I., *ANZ journal of surgery* **2001,** *71* (6), 354-61.

12. Arrington, E. D.; Smith, W. J.; Chambers, H. G.; Bucknell, A. L.; Davino, N. A., *Clinical orthopaedics and related research* **1996,** (329), 300-9.

13. Li, J.; Wang, H.-L., *Implant dentistry* **2008,** *17* (4), 389-401.

14. Langer, R., *Tissue engineering* **2007,** *13* (1), 1-2.

15. Langer, R.; Vacanti, J. P., *Science (Washington, DC, United States)* **1993,** *260* (5110), 920-6.

16. Liu, X.; Ma Peter, X., *Annals of biomedical engineering* **2004,** *32* (3), 477-86.

17. Yang, S.; Leong, K. F.; Du, Z.; Chua, C. K., *Tissue engineering* **2001,** *7* (6), 679-89.

18. Behravesh, E.; Yasko, A. W.; Engel, P. S.; Mikos, A. G., *Clinical orthopaedics and related research* **1999,** (367 Suppl), S118-29.

19. Hacker, M. C.; Mikos, A. G., *Foundations of Regenerative Medicine* **2010**, 336-367.

20. Barbanti Samuel, H.; Santos Arnaldo, R., Jr.; Zavaglia Cecilia, A. C.; Duek Eliana, A. R., *Journal of materials science. Materials in medicine* **2011,** *22* (10), 2377-85.

21. Danmark, S.; Finne-Wistrand, A.; Albertsson, A. C.; Patarroyo, M.; Mustafa, K., *Biomedical materials (Bristol, England)* **2012,** *7* (3), 035011.

22. Liu, H.; Slamovich Elliott, B.; Webster Thomas, J., *International journal of nanomedicine* **2006,** *1* (4), 541-5.

23. Reichert Johannes, C.; Wullschleger Martin, E.; Cipitria, A.; Lienau, J.; Cheng Tan, K.; Schutz Michael, A.; Duda Georg, N.; Noth, U.; Eulert, J.; Hutmacher Dietmar, W., *International orthopaedics* **2011,** *35* (8), 1229-36.

24. Dormer, N. H.; Qiu, Y.; Lydick, A. M.; Allen, N. D.; Mohan, N.; Berkland, C. J.; Detamore, M. S., *Tissue Engineering, Part A* **2012,** *18* (7 and 8), 757-767.

25. Fu, H.; Zhou, X.; Gui, Y.; Zheng, Y.; Pan, J., *Zhonghua Shiyan Waike Zazhi* **2012,** *29* (2), 286-288.

26. Kim, J.; McBride, S.; Tellis, B.; Alvarez-Urena, P.; Song, Y.-H.; Dean, D. D.; Sylvia, V. L.; Elgendy, H.; Ong, J.; Hollinger, J. O., *Biofabrication* **2012,** *4* (2), 025003/1-025003/11.

27. Nitya, G.; Nair, G. T.; Mony, U.; Chennazhi, K. P.; Nair, S. V., *Journal of Materials Science: Materials in Medicine* **2012,** *23* (7), 1749-1761.

28. Heller, J., *Handbook of Biodegradable Polymers* **2011**, 77-105.

29. Barr, J., *World Pharmaceutical Developments* **2001,** (2), 110-111.

30. Heller, J.; Ng, S. Y. Bioerodible poly(ortho esters) from dioxane-based di(ketene acetals), and block copolymers. 2002-298151 20040096506, 20021115., 2004.

31. Hasturk, H.; Kantarci, A.; Ghattas, M.; Schmidt, M.; Giordano, R. A.; Ashman, A.; Diekwisch, T. G.; Van Dyke, T., *Journal of Periodontology* **2011,** *82* (9), 1339-1352.

32. Muggli, D. S.; Burkoth, A. K.; Keyser, S. A.; Lee, H. R.; Anseth, K. S., *Macromolecules* **1998,** *31* (13), 4120-4125.

33. Poshusta, A. K.; Burdick, J. A.; Mortisen, D. J.; Padera, R. F.; Ruehlman, D.; Yaszemski, M. J.; Anseth, K. S., *Journal of Biomedical Materials Research, Part A* **2003,** *64A* (1), 62-69.

34. Shi, Q.; Zhong, S.; Chen, Y.; Whitaker, A., *Polym. Degrad. Stab.* **2010,** *95* (10), 1961-1968.

35. Adhikari, R.; Gunatillake, P. A.; Griffiths, I.; Tatai, L.; Wickramaratna, M.; Houshyar, S.; Moore, T.; Mayadunne, R. T. M.; Field, J.; McGee, M.; Carbone, T., *Biomaterials* **2008,** *29* (28), 3762-3770.

36. Bertoldi, S.; Fare, S.; Denegri, M.; Rossi, D.; Haugen, H. J.; Parolini, O.; Tanzi, M. C., *Journal of Materials Science: Materials in Medicine* **2010,** *21* (3), 1005-1011.

37. Bil, M.; Ryszkowska, J.; Wozniak, P.; Kurzydlowski, K. J.; Lewandowska-Szumiel, M., *Acta Biomaterialia* **2010,** *6* (7), 2501-2510.

38. Hafeman, A. E.; Li, B.; Yoshii, T.; Zienkiewicz, K.; Davidson, J. M.; Guelcher, S. A., *Pharmaceutical Research* **2008,** *25* (10), 2387-2399.

39. Khan, F.; Dahman, Y., *Designed Monomers and Polymers* **2012,** *15* (1), 1-29.

40. Sadr, N.; Pippenger, B. E.; Scherberich, A.; Wendt, D.; Mantero, S.; Martin, I.; Papadimitropoulos, A., *Biomaterials* **2012,** *33* (20), 5085-5093.

41. Sears, N.; Moglia, B.; Benhardt, H.; Cosgriff-Hernandez, E., *Transactions of the Annual Meeting of the Society for Biomaterials* **2010,** *32* (Annual Meeting of the Society for Biomaterials: Giving Life to a World of Materials, 2010, Volume 1), 389.

42. Hollinger, J. O.;, A. C.; Mark, D. E. *Biocompatible, biodegradable polymers for use in bone repair*; Army Inst. Dent. Res., Washington, DC, USA.: 1987; p 57 pp.

43. Ibay, A. C. *Synthesis of a moldable biodegradable bone repair material: characterization and in vivo evaluation of crosslinked poly(propylene fumarate)*; Army Inst. Dent. Res., Washington, DC, USA.: 1987; p 34 pp.

44. Ibay, A. C.; Whalley, C. E.; Miller, R. A.; Carr, H., Jr.; Battistone, G. C., *Polymeric Materials Science and Engineering* **1985,** *53*, 505-9.

45. Shung Albert, K.; Timmer Mark, D.; Jo, S.; Engel Paul, S.; Mikos Antonios, G., *Journal of biomaterials science. Polymer edition* **2002,** *13* (1), 95-108.

46. Kasper, F. K.; Tanahashi, K.; Fisher, J. P.; Mikos, A. G., *Nature Protocols* **2009,** *4* (4), 518-525.

47. Peter, S. J.; Suggs, L. J.; Yaszemski, M. J.; Engel, P. S.; Mikos, A. G., *Journal of biomaterials science. Polymer edition* **1999,** *10* (3), 363-73.

48. Domb, A. J.; Laurencin, C. T.; Israeli, O.; Gerhart, T. N.; Langer, R., *Journal of Polymer Science, Part A: Polymer Chemistry* **1990,** *28* (5), 973-85.

49. Frazier, D. D.; Lathi, V. K.; Gerhart, T. N.; Altobelli, D. E.; Hayes, W. C., *Mater. Res. Soc. Symp. Proc.* **1995,** *394* (Polymers in Medicine and Pharmacy), 15-19.

50. Timmer, M. D.; Ambrose, C. G.; Mikos, A. G., *J. Biomed. Mater. Res., Part A* **2003,** *66A* (4), 811-818.

51. Fisher, J. P.; Timmer, M. D.; Holland, T. A.; Dean, D.; Engel, P. S.; Mikos, A. G., *Biomacromolecules* **2003,** *4* (5), 1327-1334.

52. Fisher, J. P.; Dean, D.; Mikos, A. G., *Biomaterials* **2002,** *23* (22), 4333-4343.

53. Fisher, J. P.; Holland, T. A.; Dean, D.; Mikos, A. G., *Biomacromolecules* **2003,** *4* (5), 1335-1342.

54. Hedberg, E. L.; Kroese-Deutman, H. C.; Shih, C. K.; Crowther, R. S.; Carney, D. H.; Mikos, A. G.; Jansen, J. A., *Biomaterials* **2005,** *26* (22), 4616-4623.

55. Wang, K.; Wang, S., *Abstracts of Papers, 238th ACS National Meeting, Washington, DC, United States, August 16-20, 2009* **2009**, PMSE-362.

56. Wang, S.; Lu, L.; Gruetzmacher, J. A.; Currier, B. L.; Yaszemski, M. J., *Polymer Preprints (American Chemical Society, Division of Polymer Chemistry)* **2006,** *47* (1), 358-359.

57. Jo, S.; Shin, H.; Shung, A. K.; Fisher, J. P.; Mikos, A. G., *Macromolecules* **2001,** *34* (9), 2839-2844.

58. Temenoff, J. S.; Athanasiou, K. A.; LeBaron, R. G.; Mikos, A. G., *Journal of Biomedical Materials Research* **2002,** *59* (3), 429-437.

59. Bose, S.; Roy, M.; Bandyopadhyay, A., *Trends in Biotechnology* **2012,** *30* (10), 546-554.

60. Gunatillake, P. A.; Adhikari, R., *European Cells and Materials* **2003,** *5*, 1-16.

61. Jayabalan, M.; Shalumon, K. T.; Mitha, M. K., *Journal of materials science. Materials in medicine* **2009,** *20* (6), 1379-87.

62. Peter, S. J.; Lu, L.; Kim, D. J.; Mikos, A. G., *Biomaterials* **2000,** *21* (12), 1207-1213.

63. Hedberg, E. L.; Kroese-Deutman, H. C.; Shih, C. K.; Crowther, R. S.; Carney, D. H.; Mikos, A. G.; Jansen, J. A., *J. Biomed. Mater. Res., Part A* **2005,** *72A* (4), 343-353.

64. Lewandrowski, K.-U.; Bondre, S. P.; Gresser, J. D.; Wise, D. L.; Tomford, W. W.; Trantolo, D. J., *Bio-Medical Materials and Engineering* **1999,** *9* (5,6), 265-275.

65. Hedberg, E. L.; Mikos, A. G., *Mater. Res. Soc. Symp. Proc.* **2001,** *662* (Biomaterials for Drug Delivery and Tissue Engineering), NN3 7/1-NN3 7/5.

66. Payne, R. G.; McGonigle, J. S.; Yaszemski, M. J.; Yasko, A. W.; Mikos, A. G., *Biomaterials* **2002,** *23* (22), 4381-4387.

67. Timmer, M. D.; Carter, C.; Ambrose, C. G.; Mikos, A. G., *Biomaterials* **2003,** *24* (25), 4707-4714.

68. Ueda, H.; Hacker, M. C.; Haesslein, A.; Jo, S.; Ammon, D. M.; Borazjani, R. N.; Kunzler, J. F.; Salamone, J. C.; Mikos, A. G., *J. Biomed. Mater. Res., Part A* **2007,** *83A* (3), 656-666.

69. Fisher, J. P.; Holland, T. A.; Dean, D.; Mikos, A. G., *Mater. Res. Soc. Symp. Proc.* **2001,** *662* (Biomaterials for Drug Delivery and Tissue Engineering), LL5 5/1-LL5 5/7.

70. Hedberg, E. L.; Shih, C. K.; Lemoine, J. J.; Timmer, M. D.; Liebschner, M. A. K.; Jansen, J. A.; Mikos, A. G., *Biomaterials* **2005,** *26* (16), 3215-3225.

71. Rajagopalan, S.; Lu, L.; Yaszemski, M. J.; Robb, R. A., *J. Biomed. Mater. Res., Part A* **2005,** *75A* (4), 877-887.

72. Choi, J.-W.; Wicker, R.; Lee, S.-H.; Choi, K.-H.; Ha, C.-S.; Chung, I., *J. Mater. Process. Technol* **2009,** *209* (15-16), 5494-5503.

73. Lan, P. X.; Lee, J. W.; Seol, Y.-J.; Cho, D.-W., *J. Mater. Sci.: Mater. Med.* **2009,** *20* (1), 271-279.

74. Lee, J. W.; Ahn, G.; Kim, D. S.; Cho, D.-W., *Microelectron. Eng.* **2009,** *86* (4-6), 1465-1467.

75. Lee, K.-W.; Wang, S.; Fox, B. C.; Ritman, E. L.; Yaszemski, M. J.; Lu, L., *Biomacromolecules* **2007,** *8* (4), 1077-1084.

76. Christenson, E. M.; Soofi, W.; Holm, J. L.; Cameron, N. R.; Mikos, A. G., *Biomacromolecules* **2007,** *8* (12), 3806-3814.

77. Sultana, N., Fabrication Techniques and Properties of Scaffolds. In *Biodegradable Polymer-Based Scaffolds for Bone Tissue Engineering*, Springer Berlin Heidelberg: 2013; pp 19-42.

78. Greenwald, A. S.; Boden, S. D.; Goldberg, V. M.; Khan, Y.; Laurencin, C. T.; Rosier, R. N., *The Journal of bone and joint surgery. American volume* **2001,** *83-A Suppl 2 Pt 2*, 98-103.

Chapter 3

1. Fisher, J. P.; Timmer, M. D.; Holland, T. A.; Dean, D.; Engel, P. S.; Mikos, A. G., *Biomacromolecules* **2003,** *4* (5), 1327-1334.

2. Vehof, J. W. M.; Fisher, J. P.; Dean, D.; Van der Waerden, J.-P. C. M.; Spauwen, P. H. M.; Mikos, A. G.; Jansen, J. A., *J. Biomed. Mater. Res.* **2002,** *60* (2), 241-251.

3. Hollinger, J. O.; Ibay, A. C.; Mark, D. E. *Biocompatible, biodegradable polymers for use in bone repair*; Army Inst. Dent. Res., Washington, DC, USA.: 1987; p 57 pp.

4. Payne, R. G.; McGonigle, J. S.; Yaszemski, M. J.; Yasko, A. W.; Mikos, A. G., *Biomaterials* **2002,** *23* (22), 4373-4380.

5. Ibay, A. C.; Battistone, G. C.; Miller, R. A.; Carr, H., Jr., *Polym. Sci. Technol. (Plenum)* **1987,** *35* (Adv. Biomed. Polym.), 111-15.

6. Kharas, G. B.; Kamenetsky, M.; Simantirakis, J.; Beinlich, K. C.; Rizzo, A.-M. T.; Caywood, G. A.; Watson, K., *J. Appl. Polym. Sci.* **1997,** *66* (6), 1123-1137.

7. Shung, A. K.; Timmer, M. D.; Jo, S.; Engel, P. S.; Mikos, A. G., *J. Biomater. Sci., Polym. Ed.* **2002,** *13* (1), 95-108.

8. Peter, S. J.; Yaszemski, M. J.; Suggs, L. J.; Payne, R. G.; Langer, R.; Hayes, W. C.; Unroe, M. R.; Alemany, L. B.; Engel, P. S.; Mikos, A. G., *J. Biomater. Sci., Polym. Ed.* **1997,** *8* (11), 893-904.

9. Domb, A. J.; Laurencin, C. T.; Israeli, O.; Gerhart, T. N.; Langer, R., *J. Polym. Sci., Part A: Polym. Chem.* **1990,** *28* (5), 973-85.

10. Frazier, D. D.; Lathi, V. K.; Gerhart, T. N.; Altobelli, D. E.; Hayes, W. C., *Mater. Res. Soc. Symp. Proc.* **1995,** *394* (Polymers in Medicine and Pharmacy), 15-19.

11. Shung, A. K.; Timmer, M. D.; Jo, S.; Engel, P. S.; Mikos, A. G., *Journal of Biomaterials Science, Polymer Edition* **2002,** *13* (1), 95-108.

12. Peter, S. J.; Lu, L.; Kim, D. J.; Stamatas, G. N.; Miller, M. J.; Yaszemski, M. J.; Mikos, A. G., *J. Biomed. Mater. Res.* **2000,** *50* (3), 452-462.

13. Hedberg, E. L.; Kroese-Deutman, H. C.; Shih, C. K.; Crowther, R. S.; Carney, D. H.; Mikos, A. G.; Jansen, J. A., *J. Biomed. Mater. Res., Part A* **2005,** *72A* (4), 343-353.

14. Yaszemski, M. J.; Payne, R. G.; Hayes, W. C.; Langer, R.; Mikos, A. G., *Biomaterials* **1996,** *17* (22), 2127-2130.

15. Fisher, J. P.; Holland, T. A.; Dean, D.; Mikos, A. G., *Biomacromolecules* **2003,** *4* (5), 1335-1342.

16. Peter, S. J.; Nolley, J. A.; Widmer, M. S.; Merwin, J. E.; Yaszemski, M. J.; Yasko, A. W.; Engel, P. S.; Mikos, A. G., *Tissue Eng.* **1997,** *3* (2), 207-215.

17. Gueldry, S.; Bralet, J., *Metabolic brain disease* **1995,** *10* (4), 293-301.

18. Ibay, A. C. *Synthesis of a moldable biodegradable bone repair material: characterization and in vivo evaluation of crosslinked poly(propylene fumarate)*; Army Inst. Dent. Res., Washington, DC, USA.: 1987; p 34 pp.

19. Ibay, A. C.; Whalley, C. E.; Miller, R. A.; Carr, H., Jr.; Battistone, G. C., *Polymeric Materials Science and Engineering* **1985,** *53*, 505-9.

20. Jayabalan, M.; Shalumon, K. T.; Mitha, M. K.; Ganesan, K.; Epple, M., *Acta Biomater. 6* (3), 763-775.

21. Mistry, A. S.; Cheng, S. H.; Yeh, T.; Christenson, E.; Jansen, J. A.; Mikos, A. G., *J. Biomed. Mater. Res., Part A* **2009,** *89A* (1), 68-79.

22. Wang, K.; Wang, S., *Abstracts of Papers, 240th ACS National Meeting, Boston, MA, United States, August 22-26, 2010*, PMSE-282.

23. Mistry, A. S.; Cheng, S. H.; Yeh, T.; Christenson, E.; Jansen, J. A.; Mikos, A. G., *Journal of Biomedical Materials Research, Part A* **2009,** *89A* (1), 68-79.

24. *Federal Register* **1997,** *62* (92), 26225-26228.

25. Shelanski, M. V., *Cosmetics and Perfumery* **1974,** *89* (9), 96, 98.

26. Kasper, F. K.; Tanahashi, K.; Fisher, J. P.; Mikos, A. G., *Nature Protocols* **2009,** *4* (4), 518-525.

27. Shung Albert, K.; Timmer Mark, D.; Jo, S.; Engel Paul, S.; Mikos Antonios, G., *Journal of biomaterials science. Polymer edition* **2002,** *13* (1), 95-108.

28. Szmercsanyi, I. V.; Maros, L. K.; Zahran, A. A., *Journal of Applied Polymer Science* **1966,** *10* (4), 513-22.

29. Grobelny, J., *Polymer* **1995,** *36* (22), 4215-22.

30. Vlad, S.; Oprea, S.; Ciobanu, C.; Bulacovschi, V., *Revue Roumaine de Chimie* **2000,** *44* (7), 693-698.

Chapter 4

1. Das, D.; Zhang, Z.; Winkler, T.; Mour, M.; Guenter, C. I.; Morlock, M. M.; Machens, H.-G.; Schilling, A. F., *Advances in Biochemical Engineering/Biotechnology* **2012,** *126* (Tissue Engineering III), 317-333.

2. Mistry Amit, S.; Mikos Antonios, G., *Adv Biochem Eng Biotechnol* **2005,** *94*, 1-22.

3. Deshayes, S.; Kasko, A. M., *Journal of Polymer Science, Part A: Polymer Chemistry* **2013,** *51* (17), 3531-3566.

4. Lyu, S. P.; Untereker, D., *International Journal of Molecular Sciences* **2009,** *10* (9), 4033-4065.

5. Hofmann, D.; Entrialgo-Castano, M.; Kratz, K.; Lendlein, A., *Advanced Materials (Weinheim, Germany)* **2009,** *21* (32-33), 3237-3245.

6. Gopferich, A., *Biomaterials* **1996,** *17* (2), 103-14.

7. Gopferich, A.; Langer, R., *Macromolecules* **1993,** *26* (16), 4105-12.

8. von Burkersroda, F.; Schedl, L.; Gopferich, A., *Biomaterials* **2002,** *23* (21), 4221-4231.

9. Fisher, J. P.; Timmer, M. D.; Holland, T. A.; Dean, D.; Engel, P. S.; Mikos, A. G., *Biomacromolecules* **2003,** *4* (5), 1327-1334.

10. Peter, S. J.; Nolley, J. A.; Widmer, M. S.; Merwin, J. E.; Yaszemski, M. J.; Yasko, A. W.; Engel, P. S.; Mikos, A. G., *Tissue Engineering* **1997,** *3* (2), 207-215.

11. Cicotte, K. N.; Hedberg-Dirk, E. L.; Dirk, S. M., *Journal of Applied Polymer Science* **2010,** *117* (4), 1984-1991.

12. Wang, S.; Lu, L.; Yaszemski, M. J., *Biomacromolecules* **2006,** *7* (6), 1976-1982.

13. Hedberg, E. L.; Kroese-Deutman, H. C.; Shih, C. K.; Crowther, R. S.; Carney, D. H.; Mikos, A. G.; Jansen, J. A., *Journal of Biomedical Materials Research, Part A* **2005,** *72A* (4), 343-353.

14. Yang, S.; Leong, K. F.; Du, Z.; Chua, C. K., *Tissue Eng* **2001,** *7* (6), 679-89.

15. Jo, S.; Shin, H.; Shung, A. K.; Fisher, J. P.; Mikos, A. G., *Macromolecules* **2001,** *34* (9), 2839-2844.

16. Temenoff, J. S.; Athanasiou, K. A.; LeBaron, R. G.; Mikos, A. G., *Journal of Biomedical Materials Research* **2002,** *59* (3), 429-437.

17. Ifkovits, J. L.; Burdick, J. A., *Tissue Engineering* **2007,** *13* (10), 2369-2385.

18. Porter, J. R.; Ruckh, T. T.; Popat, K. C., *Biotechnol. Prog.* **2009,** *25* (6), 1539-1560.

19. Cicotte, K. N.; Dirk, S. M.; Hedberg-Dirk, E. L., *Materials Research Society Symposium Proceedings* **2010,** *1239* (Micro- and Nanoscale Processing of Biomaterials), No pp given, Paper #: 1239-VV05-02.

20. Mirzadeh, H.; Shokrolahi, F.; Daliri, M., *J. Biomed. Mater. Res., Part A* **2003,** *67A* (3), 727-732.

21. Vera-Graziano, R.; Hernandez-Sanchez, F.; Cauich-Rodriguez, J. V., *Journal of Applied Polymer Science* **1995,** *55* (9), 1317-27.

22. Buge, H. G.; Reich, P.; Steger, E., *Journal of Molecular Structure* **1976,** *35* (2), 175-9.

23. Enescu, C.; Shoichet Molly, S., *Journal of biomaterials science. Polymer edition* **2004,** *15* (2), 215-27.

24. Lam, C. X. F.; Savalani, M. M.; Teoh, S.-H.; Hutmacher, D. W., *Biomedical Materials (Bristol, United Kingdom)* **2008,** *3* (3), 034108/1-034108/15.

25. Nair, L. S.; Laurencin, C. T., *Progress in Polymer Science* **2007,** *32* (8-9), 762-798.

26. ASTM F1635-11. In *Standard Test Method for in vitro Degradation Testing of Hydrolytically Degradable Polymer Resins and Fabricated Forms for Surgical Implants*, ASTM International West Conshohocken, PA, 2006-2012.

27. Timmer, M. D.; Ambrose, C. G.; Mikos, A. G., *Biomaterials* **2002,** *24* (4), 571-577.

28. Yaszemski, M. J.; Payne, R. G.; Hayes, W. C.; Langer, R.; Mikos, A. G., *Biomaterials* **1996,** *17* (22), 2127-2130.

29. Timmer, M. D.; Horch, R. A.; Ambrose, C. G.; Mikos, A. G., *Journal of Biomaterials Science, Polymer Edition* **2003,** *14* (4), 369-382.

30. Vlad, S.; Oprea, S.; Ciobanu, C.; Bulacovschi, V., *Revue Roumaine de Chimie* **2000,** *44* (7), 693-698.

Chapter 5

1. Levenberg, S.; Langer, R., *Current Topics in Developmental Biology* **2004,** *61*, 113-134.

2. Timmer, M. D.; Shin, H.; Horch, R. A.; Ambrose, C. G.; Mikos, A. G., *Biomacromolecules* **2003,** *4* (4), 1026-1033.

3. Wang, M. O.; Etheridge, J. M.; Thompson, J. A.; Vorwald, C. E.; Dean, D.; Fisher, J. P., *Biomacromolecules* **2013,** *14* (5), 1321-1329.

4. Cicotte, K. N.; Dirk, S. M.; Hedberg-Dirk, E. L., *Materials Research Society Symposium Proceedings* **2010,** *1239* (Micro- and Nanoscale Processing of Biomaterials), No pp given, Paper #: 1239-VV05-02.

5. Cicotte, K. N.; Hedberg-Dirk, E. L.; Dirk, S. M., *Journal of Applied Polymer Science* **2010,** *117* (4), 1984-1991.

6. Hedberg-Dirk, E. L.; Cicotte, K. N.; Dirk, S. M., *Materials Research Society Symposium Proceedings* **2009,** *1235* (Engineering Biomaterials for Regenerative Medicine), No pp given, Paper #: 1235-RR06-08.

7. Kasper, F. K.; Tanahashi, K.; Fisher, J. P.; Mikos, A. G., *Nature Protocols* **2009,** *4* (4), 518-525.

8. Gueldry, S.; Bralet, J., *Metabolic brain disease* **1995,** *10* (4), 293-301.

9. Shelanski, M. V., *Cosmetics and Perfumery* **1974,** *89* (9), 96, 98.

10. *Federal Register* **1997,** *62* (92), 26225-26228.

11. Murphy, M. J.; Ray, A. C.; Jones, L. P.; Reagor, J. C., *American Journal of Veterinary Research* **1984,** *45* (11), 2293-5.

12. Bose, S.; Roy, M.; Bandyopadhyay, A., *Trends in Biotechnology* **2012,** *30* (10), 546-554.

13. Szpalski, C.; Barbaro, M.; Sagebin, F.; Warren, S. M., *Tissue Engineering, Part B: Reviews* **2012,** *18* (4), 258-269.

14. Salgado, A. J.; Coutinho, O. P.; Reis, R. L., *Macromolecular Bioscience* **2004,** *4* (8), 743-765.

15. Dominici, M.; Le Blanc, K.; Mueller, I.; Slaper-Cortenbach, I.; Marini, F.; Krause, D.; Deans, R.; Keating, A.; Prockop, D.; Horwitz, E., *Cytotherapy* **2006,** *8* (4), 315-7.

16. Augello, A.; De Bari, C., *Human Gene Therapy* **2010,** *21* (10), 1226-1238.

17. Kozhevnikova, M. N.; Mikaelyan, A. S.; Starostin, V. I., *Biology Bulletin (Wilmington, DE, United States)* **2008,** *35* (3), 223-232.

18. Vater, C.; Kasten, P.; Stiehler, M., *Acta Biomaterialia* **2011,** *7* (2), 463-477.

19. Birmingham, E.; Niebur, G. L.; McHugh, P. E.; Shaw, G.; Barry, F. P.; McNamara, L. M., *European Cells and Materials* **2012,** *23*, 13-27.

20. Probs), I. M., LIVE/DEAD(R) Viability/Cytotoxicity Kit (for mammalian cells). Catalog Numbe L-3224 ed.; Invitrogen, Ed. 2005; pp 1-7.

21. Invitrogen, GIBCO(R) Rat (SD) Mesenchymal Stem Cells rev date 120909 ed.; Invitrogen, Ed. 2009; Vol. Manual part no. A11561, pp 1-27.

22. Malaval, L.; Modrowski, D.; Gupta, A. K.; Aubin, J. E., *Journal of Cellular Physiology* **1994,** *158* (3), 555-72.

23. Bretaudiere, J. P.; Spillman, T., *Methods Enzym. Anal. (3rd Ed.)* **1984,** *4*, 75-82.

24. Takara, ALP Assay Kit. INC., T. B., Ed. 2001; pp 1-11.

25. Gregory, C. A.; Gunn, W. G.; Peister, A.; Prockop, D. J., *Analytical Biochemistry* **2004,** *329* (1), 77-84.

26. Song, I.-H.; Caplan Arnold, I.; Dennis James, E., *Journal of orthopaedic research : official publication of the Orthopaedic Research Society* **2009,** *27* (2), 216-21.

27. Kim, K.; Dean, D.; Mikos, A. G.; Fisher, J. P., *Biomacromolecules* **2009,** *10* (7), 1810-1817.

28. Sigma, Enzymatic Assay of alpha-galactosidase. Sigma, Ed. St. Louis, MI pp 1-3.

29. Lian, J. B.; Stein, G. S., *Critical reviews in oral biology and medicine : an official publication of the American Association of Oral Biologists* **1992,** *3* (3), 269-305.

30. Puchtler, H.; Meloan, S. N.; Terry, M. S., *Journal of Histochemistry and Cytochemistry* **1969,** *17* (2), 110-24.

Chapter 6

1. Deb, S., *Biomaterials Fabrication and Processing Handbook* **2008**, 457-481.

2. Yang, Y.; Cunha-Reis, C.; Bagnaninchi, P. O.; Aydin, H. M., *Biomaterials Fabrication and Processing Handbook* **2008**, 69-94.

3. Hollister, S. J., *Advanced Materials (Weinheim, Germany)* **2009,** *21* (32-33), 3330-3342.

4. Hutmacher, D. W., *Journal of Biomaterials Science, Polymer Edition* **2001,** *12* (1), 107-124.

5. Mikos, A. G.; Temenoff, J. S., *EJB Electronic Journal of Biotechnology [online computer file]* **2000,** *3* (2), No pp given.

6. Park, H.; Temenoff, J. S.; Mikos, A. G., *Topics in Bone Biology* **2007,** *3* (Engineering of Functional Skeletal Tissues), 55-68.

7. Yang, P. J.; Temenoff, J. S., *Tissue Engineering, Part B: Reviews* **2009,** *15* (2), 127-141.

8. Karageorgiou, V.; Kaplan, D., *Biomaterials* **2005,** *26* (27), 5474-5491.

9. Timmer, M. D.; Ambrose, C. G.; Mikos, A. G., *Journal of Biomedical Materials Research, Part A* **2003,** *66A* (4), 811-818.

10. Sabir, M. I.; Xu, X.; Li, L., *Journal of Materials Science* **2009,** *44* (21), 5713-5724.

11. Christenson, E. M.; Soofi, W.; Holm, J. L.; Cameron, N. R.; Mikos, A. G., *Biomacromolecules* **2007,** *8* (12), 3806-3814.

12. Hsu, Y. Y.; Gresser, J. D.; Trantolo, D. J.; Lyons, C. M.; Gangadharam, P. R.; Wise, D. L., *Journal of biomedical materials research* **1997,** *35* (1), 107-16.

13. Temenoff, J. S.; Mikos, A. G., *Biomaterials* **2000,** *21* (23), 2405-2412.

14. Lee, J.; Kim, B.; Lim, G.; Cho, D.-W., *Key Eng. Mater.* **2007,** *342-343* (Advanced Biomaterials VII), 141-144.

15. Buge, H. G.; Reich, P.; Steger, E., *Journal of Molecular Structure* **1976,** *35* (2), 175-9.

16. Cooke, M. N.; Fisher, J. P.; Dean, D.; Rimnac, C.; Mikos, A. G., *J. Biomed. Mater. Res., Part B* **2003,** *64B* (2), 65-69.

17. Sitharaman, B.; Shi, X.; Tran, L. A.; Spicer, P. P.; Rusakova, I.; Wilson, L. J.; Mikos, A. G., *Journal of Biomaterials Science, Polymer Edition* **2007,** *18* (6), 655-671.

18. Cooke Malcolm, N.; Fisher John, P.; Dean, D.; Rimnac, C.; Mikos Antonios, G., *Journal of biomedical materials research. Part B, Applied biomaterials* **2003,** *64* (2), 65-9.

19. Formhals, A. Apparatus for producing artificial fibers from fiber-forming liquids by an "electrical spinning" method. 1940-323036 2323025, 19400308., 1943.

20. Doshi, J.; Reneker, D. H., *Journal of Electrostatics* **1995,** *35* (2&3), 151-60.

21. Nair, L. S.; Bhattacharyya, S.; Laurencin, C. T., *Expert Opinion on Biological Therapy* **2004,** *4* (5), 659-668.

22. Khil, M.-S.; Bhattarai, S. R.; Kim, H.-Y.; Kim, S.-Z.; Lee, K.-H., *Journal of Biomedical Materials Research, Part B: Applied Biomaterials* **2005,** *72B* (1), 117-124.

23. Hull, C. W. Apparatus for production of three dimensional objects by stereolithography. Mar. 11, 1986 1986.

24. Muskin, J.; Ragusa, M.; Gelsthorpe, T., *Journal of Chemical Education* **2010,** *87* (5), 512-514.

25. Sun, C.; Fang, N.; Wu, D. M.; Zhang, X., *Sensors and Actuators, A: Physical* **2005,** *A121* (1), 113-120.

26. Huang, Z.-M.; Zhang, Y. Z.; Kotaki, M.; Ramakrishna, S., *Composites Science and Technology* **2003,** *63* (15), 2223-2253.

27. Cashion, M. P.; Brown, R. H.; Mohns, B. R.; Long, T. E., *Polymer Preprints (American Chemical Society, Division of Polymer Chemistry)* **2009,** *50* (2), 504-505.

28. Choi, S. S.; Hong, J. P.; Seo, Y. S.; Chung, S. M.; Nah, C., *Journal of Applied Polymer Science* **2006,** *101* (4), 2333-2337.

29. Lee, K.-W.; Wang, S.; Fox, B. C.; Ritman, E. L.; Yaszemski, M. J.; Lu, L., *Biomacromolecules* **2007,** *8* (4), 1077-1084.

30. Sweeney, A. D.; Pegg, C. E.; Ozer, R. R.; Chalker, J. M., *Abstracts of Papers, 245th ACS National Meeting & Exposition, New Orleans, LA, United States, April 7-11, 2013* **2013**, CHED-285.

31. Subianto, S.; Cavaliere, S.; Jones, D. J.; Roziere, J., *Journal of Polymer Science, Part A: Polymer Chemistry* **2013,** *51* (1), 118-128.

32. Celebioglu, A.; Uyar, T., *RSC Advances* **2013,** *3* (26), 10197-10201.

33. Viry, L.; Moulton, S. E.; Romeo, T.; Suhr, C.; Mawad, D.; Cook, M.; Wallace, G. G., *Journal of Materials Chemistry* **2012,** *22* (22), 11347-11353.

34. Xia, Y., *Abstracts of Papers, 232nd ACS National Meeting, San Francisco, CA, United States, Sept. 10-14, 2006* **2006**, PMSE-231.

Chapter 7: Part I

1. Wang, C.; Koh, H.; Ramakrishna, S.; Liao, S., *Electrospinning for Tissue Regeneration* **2011**, 168-201.

2. Dodla, M. C.; Bellamkonda, R. V., *Foundations of Regenerative Medicine* **2010**, 672-687.

3. Seifert Jennifer, L.; Desai, V.; Watson Robert, C.; Musa, T.; Kim, Y.-t.; Keefer Edward, W.; Romero Mario, I., *IEEE transactions on neural systems and rehabilitation engineering : a publication of the IEEE Engineering in Medicine and Biology Society* **2012,** *20* (2), 220-7.

4. Daly, W.; Yao, L.; Zeugolis, D.; Windebank, A.; Pandit, A., *Journal of the Royal Society, Interface* **2012,** *9* (67), 202-221.

5. Kameswaran, N.; Cullen, D. K.; Pfister Bryan, J.; Ranalli Nathan, J.; Huang Jason, H.; Zager Eric, L.; Smith Douglas, H., *Neurological research* **2008,** *30* (10), 1063-7.

6. FitzGerald James, J.; Lago, N.; Benmerah, S.; Serra, J.; Watling Christopher, P.; Cameron Ruth, E.; Tarte, E.; Lacour Stephanie, P.; McMahon Stephen, B.; Fawcett James, W., *Journal of neural engineering* **2012,** *9* (1), 016010.

7. Foldes Emily, L.; Ackermann, D. M.; Bhadra, N.; Kilgore Kevin, L.; Bhadra, N., *Journal of neuroscience methods* **2011,** *196* (1), 31-7.

8. Normann Richard, A., *Nature clinical practice. Neurology* **2007,** *3* (8), 444-52.

9. Rutten, W. L. C., *Annual Review of Biomedical Engineering* **2002,** *4*, 407-452.

10. Mensinger, A. F.; Highstein, S. M., *The Journal of comparative neurology* **1999,** *410* (4), 653-76.

11. Navarro, X.; Krueger Thilo, B.; Lago, N.; Micera, S.; Stieglitz, T.; Dario, P., *Journal of the peripheral nervous system : JPNS* **2005,** *10* (3), 229-58.

12. Rydevik, B. L.; Kwan, M. K.; Myers, R. R.; Brown, R. A.; Triggs, K. J.; Woo, S. L.; Garfin, S. R., *Journal of orthopaedic research : official publication of the Orthopaedic Research Society* **1990,** *8* (5), 694-701.

13. Cicotte, K. N.; Hedberg-Dirk, E. L.; Dirk, S. M., *Journal of Applied Polymer Science* **2010,** *117* (4), 1984-1991.

14. Muskin, J.; Ragusa, M.; Gelsthorpe, T., *Journal of Chemical Education* **2010,** *87* (5), 512-514.

15. Cicotte, K. N.; Dirk, S. M.; Hedberg-Dirk, E. L., *Materials Research Society Symposium Proceedings* **2010,** *1239* (Micro- and Nanoscale Processing of Biomaterials), No pp given, Paper #: 1239-VV05-02.

16. Kim, Y. B.; Cho, D.; Park, W. H., *Journal of Applied Polymer Science* **2009,** *114* (6), 3870-3874.

17. Schneider, F.; Draheim, J.; Kamberger, R.; Wallrabe, U., *Sensors and Actuators, A: Physical* **2009,** *151* (2), 95-99.

Chapter 7: Part II

1. Del Gaudio, C.; Baiguera, S.; Boieri, M.; Mazzanti, B.; Ribatti, D.; Bianco, A.; Macchiarini, P., *Biomaterials* **2013,** *34* (31), 7754-7765.

2. Bae, H.; Puranik, A. S.; Gauvin, R.; Edalat, F.; Carrillo-Conde, B.; Peppas, N. A.; Khademhosseini, A., *Science Translational Medicine* **2012,** *4* (160), 160ps23, 5 pp.

3. Baranski, J. D.; Chaturvedi, R. R.; Stevens, K. R.; Eyckmans, J.; Carvalho, B.; Solorzano, R. D.; Yang, M. T.; Miller, J. S.; Bhatia, S. N.; Chen, C. S., *Proceedings of the National Academy of Sciences of the United States of America* **2013,** *110* (19), 7586-7591, S7586/1-S7586/5.

4. Galiano Robert, D.; Michaels Joseph, t.; Dobryansky, M.; Levine Jamie, P.; Gurtner Geoffrey, C., *Wound repair and regeneration : official publication of the Wound Healing Society [and] the European Tissue Repair Society* **2004,** *12* (4), 485-92.

5. Harunari, N.; Zhu Kathy, Q.; Armendariz Rebecca, T.; Deubner, H.; Muangman, P.; Carrougher Gretchen, J.; Isik, F. F.; Gibran Nicole, S.; Engrav Loren, H., *Burns : journal of the International Society for Burn Injuries* **2006,** *32* (6), 669-77.

6. Ramos Maria Luiza, C.; Gragnani, A.; Ferreira Lydia, M., *Journal of burn care & research : official publication of the American Burn Association* **2008,** *29* (2), 363-8.

7. Wong, V. W.; Gurtner, G. C., *Experimental Dermatology* **2012,** *21* (10), 729-734.

8. Ceradini, D. J.; Kulkarni, A. R.; Callaghan, M. J.; Tepper, O. M.; Bastidas, N.; Kleinman, M. E.; Capla, J. M.; Galiano, R. D.; Levine, J. P.; Gurtner, G. C., *Nature Medicine (New York, NY, United States)* **2004,** *10* (8), 858-864.

9. Dorsett-Martin Wanda, A., *Wound repair and regeneration : official publication of the Wound Healing Society [and] the European Tissue Repair Society* **2004,** *12* (6), 591-9.

10. McGuire Paul, G.; Howdieshell Thomas, R., *The Journal of surgical research* **2010,** *164* (1), e201-12.

11. Du, Z.; Zan, T.; Li, H.; Li, Q., *Microvascular research* **2011,** *82* (3), 284-90.

12. Briers, J. D.; Webster, S., *Journal of biomedical optics* **1996,** *1* (2), 174-9.

13. Muskin, J.; Ragusa, M.; Gelsthorpe, T., *Journal of Chemical Education* **2010,** *87* (5), 512-514.

14. Dirk, S. M.; Cicotte, K. N.; Hedberg-Dirk, E. L.; Buerger, S.; Lin, P. P.; Reece, G., *MRS Online Proceedings Library* **2011,** *1418* (Gels and Biomedical Materials), No pp given.

Chapter 8

1. Hollinger, J. O.; Ibay, A. C.; Mark, D. E. *Biocompatible, biodegradable polymers for use in bone repair*; Army Inst. Dent. Res., Washington, DC, USA.: 1987; p 57 pp.

2. Ibay, A. C. *Synthesis of a moldable biodegradable bone repair material: characterization and in vivo evaluation of crosslinked poly(propylene fumarate)*; Army Inst. Dent. Res., Washington, DC, USA.: 1987; p 34 pp.

3. Cicotte, K. N.; Dirk, S. M.; Hedberg-Dirk, E. L., *Materials Research Society Symposium Proceedings* **2010,** *1239* (Micro- and Nanoscale Processing of Biomaterials), No pp given, Paper #: 1239-VV05-02.

4. Cicotte, K. N.; Hedberg-Dirk, E. L.; Dirk, S. M., *Journal of Applied Polymer Science* **2010,** *117* (4), 1984-1991.

5. Hedberg-Dirk, E. L.; Cicotte, K. N.; Dirk, S. M., *Materials Research Society Symposium Proceedings* **2009,** *1235* (Engineering Biomaterials for Regenerative Medicine), No pp given, Paper #: 1235-RR06-08.

6. Timmer, M. D.; Shin, H.; Horch, R. A.; Ambrose, C. G.; Mikos, A. G., *Biomacromolecules* **2003,** *4* (4), 1026-1033.

7. Timmer, M. D.; Ambrose, C. G.; Mikos, A. G., *Biomaterials* **2002,** *24* (4), 571-577.

8. Shin, S.-H.; Purevdorj, O.; Castano, O.; Planell, J. A.; Kim, H.-W., *Journal of Tissue Engineering* **2012**, 443530.

9. Soliman, S.; Pagliari, S.; Rinaldi, A.; Forte, G.; Fiaccavento, R.; Pagliari, F.; Franzese, O.; Minieri, M.; Di Nardo, P.; Licoccia, S.; Traversa, E., *Acta Biomaterialia* **2010,** *6* (4), 1227-1237.

10. Bose, S.; Roy, M.; Bandyopadhyay, A., *Trends in Biotechnology* **2012,** *30* (10), 546-554.

11. Eichhorn Stephen, J.; Sampson William, W., *Journal of the Royal Society, Interface / the Royal Society* **2005,** *2* (4), 309-18.

12. Badami Anand, S.; Kreke Michelle, R.; Thompson, M. S.; Riffle Judy, S.; Goldstein Aaron, S., *Biomaterials* **2006,** *27* (4), 596-606.

13. Rnjak-Kovacina, J.; Weiss, A. S., *Tissue Engineering, Part B: Reviews* **2011,** *17* (5), 365-372.